SAMPLE INTRODUCTION AND SOLVENT EFFECTS IN AN ARGON AND HELIUM MICROWAVE INDUCED PLASMA

by

Keith Alan McCleary

Dissertation submitted to the Faculty of the Virginia Polytechnic Institute and State University in partial fulfillment of the requirement for the degree of

Doctor of Philosophy

in

Chemistry

APPROVED:

Gary L. Long, Chairman

Mark R. Anderson

G. Alan Schick

Joseph S. Merola

George Sanzone

July 1992

Blacksburg, Virginia

SAMPLE INTRODUCTION AND SOLVENT EFFECTS IN AN ARGON AND HELIUM MICROWAVE INDUCED PLASMA

by

Keith Alan McCleary

Gary L. Long, Chairman

Chemistry

(Abstract)

Atomic emission spectrometry (AES) with a plasma has proven to be an important method for the analysis of metallic and nonmetallic species in a variety of matrices. Not only is atomic spectrometry useful for accurate and sensitive quantitative analysis, but it can be used as a means of unambiguous qualitative determinations.

The most common matrix for AES samples is liquid. Whether aqueous or organic in nature, the majority of samples are dissolved in some sort of solvent. Unfortunately, for most modes of sample introduction, a large portion of the solvent is simultaneously introduced to the plasma discharge along with the analyte species. The plasma is thus required not only to sufficiently excite the analyte, but also to desolvate and vaporize the solvent species. These processes tend to diminish the available energy of the plasma that is to be directed toward the analyte. The nature of the energy loss due to solvent

loading is not well understood and is the topic of debate for different systems.

It is the focus of this dissertation to determine the effect of solvent loading on the Highly Efficient Microwave Induced Plasma (HEMIP). The magnitude of solvent loading for Ar and He discharges using different sample introduction systems is determined. The solvent load is shown to have two separate constituents: aerosol and vapor. Each of these are shown to affect the plasma in different ways.

Two different sample introduction systems are evaluated for their respective solvent loadings: a cooled pneumatic nebulizer / double pass spray chamber and an ultrasonic nebulization system. These systems are compared under their normal operating conditions and for the two plasma support gases.

High solvent loads are shown to destabilize both the Ar and He microwave plasmas, decrease analytical sensitivity, and attenuate the energy of the plasma discharge. The conditions under which solvent loading is minimized do not have a significant effect on the operational characteristics of the sample introduction systems, but provide the optimal analytical sensitivity and limits of detection for the HEMIP.

ACKNOWLEDGEMENTS

The process of my education and growth has required the involvement of many individuals. To document this work without recognizing those people who have influenced my endeavors would be shameful.

It would have been impossible for me to pursue this work without the help of my parents and family. I owe a debt of gratitude to Mom and Dad, Jim and Judy McCleary, for encouraging me to aim high, and for the kind words and support needed to keep me sane and focused on the task at hand. My brother, Kirk, and nephew Jimmy, for some of the most engaging diversions required to keep the aforementioned sanity intact, my deepest thanks, and a promise to repay that kindness in some way.

To Dr. Gary Long, I offer thanks for the direction and guidance you extended me during my tenure here. Even across a distance of several thousand miles and through the tumult of an international war, you were able to find the words and ideas to keep me motivated. Drs. Mason, Anderson, Merola, Schick and Sanzone, your always constructive ideas and suggestions helped a great deal. Dr. Graybeal, I must thank you for always being able find a way to help financially. This is indeed a most excellent gift.

I am in the somewhat unusual position of having several other supervisors to acknowledge. Drs. Douglas Hausler,

Bruce Quimby, and Jim Sullivan, I thank you for allowing me to work with what I deem to be some of the finest scientists in the field today. The three of you made me realize the caliber of work that is done in the industrial sector.

There are many friends who made my stay at Virginia Tech so much more than academic. I wish to thank the plasmen, here and gone (Gerald Ducatte, Ward Mavura, Edwin Lancaster, Larry Perkins, and Curtis Motley) for the conversations, both scientific and decidedly unscientific. Paul Gregory, Mark Anderson, Alan Schick, Vince Remcho, and Greg Slack, you made this place much more fun than otherwise possible. This means a lot to me. Paul, my best man, even over a distance of 1200 miles, you took the time to keep me in touch with this place. I appreciate and value our friendship and hope that it will not end when we go our separate ways.

Finally, I need to thank a person who, albeit new to my life, has had the most profound effect on it. Ellen Slusher, you took the time to become my friend when few would have tried to break through the grouchy exterior. I learned from you the importance of laughter, and the need for love in a person's life. You taught me how ridiculous it was to let the circumstances I was in get me down. You have always been wonderful to me and this is a debt I plan to repay for the rest of my life.

TABLE OF CONTENTS

List of Figures

List of Tables

Chapter 1

Introduction

Atomic emission spectrometry (AES) has become a widely used tool for the determination of metals and nonmetals in a variety of sample matrices. Not only is this method useful for accurate and sensitive quantitative determinations, but it can also be employed for conclusive qualitative analysis.

Sample introduction for AES has been called the "Achilles' Heel" of the method [1]. The manner in which the sample is introduced into the atom cell, or plasma can be the controlling factor as to the ultimate credibility of the results. Many factors come into play when regarding the suitability of a sample introduction device: the total mass of solvent and solute which the system can deliver; the efficiency with which this is accomplished; the relative size of the droplets that the system produces; and to what extent, if any, the sample introduction system discriminates against the analyte in favor of the solvent.

The focus of this dissertation research is to determine the effect that solvent has on the operating characteristics and analytical sensitivity of a microwave induced plasma (MIP). The resonant cavity to be used is of the Highly Efficient Microwave Induced Plasma (HEMIP) [2]. To this end, two different sample introduction methods, cooled pneumatic and ultrasonic nebulization systems, will be

evaluated with respect to solvent loading. Solvent loading is operationally defined as the mass of solvent per unit gas volume that the sample introduction system provides to the atom cell.

To put this work into its proper perspective, a summary of the pertinent literature and a brief discussion of relevant introductory subjects will be presented. The topics to be covered are: microwave induced plasmas, sample introduction, and solvent loading.

Microwave Induced Plasmas. The invention of the TM_{010} resonant cavity by Charles Beenakker in 1976 [3] has equipped the spectroscopist with a functional source for MIP-AES. This source was capable of sustaining either an argon or helium plasma at atmospheric pressure and low (less than 200 W) power. Unfortunately, this cavity was plagued by power transfer problems and required the use of external tuning mechanisms. Also, this cavity was not capable of liquid sample introduction. Beenakker writes "owing to large water droplets reaching the plasma, stable analysis signals are not obtained" [3].

Researchers at the North Carolina State University, Matus, Boss, and Riddle, chose to address these problems [2]. Modifying the cavity to remove the external tuning devices, Matus *et al*, changed the coupling loop of the cavity to a capacitive device, which could be translated radially across the face of the plasma, tuning the plasma

internally. With this change, the cavity could now become tuned (the frequency of the generator equaled the resonant frequency of the cavity) and matched (the impedance of the cavity equaled the impedance of the generator, 50 ohms), generating a critically coupled state. Under these operating conditions greater than 95 % of the input power was channeled to the generation of a plasma discharge as opposed to reflecting back to the generator or heating the cavity. The cavity now was able to sustain a stable plasma with aqueous sample introduction. Boss termed this cavity the Highly Efficient Microwave Induced Plasma (HEMIP) [2]. The HEMIP has undergone much evaluation and modification by Long *et al* [4-7].

Sample Introduction. Figure 1 [8] shows the path that a sample must take from bulk solution to excited state species. For these experiments, solution transport is controlled by a peristaltic pump. Nebulization is the process of creating an aerosol from a liquid stream. Two different nebulization systems are used: pneumatic and ultrasonic. Aerosol transport is the intermediate step between nebulization and the plasma. The spray chambers used in this work help to reject the largest of the droplets produced by the nebulizers and channel the processed aerosol to the plasma torch. All processes in the boxed region are executed by the plasma for the pneumatic system case.

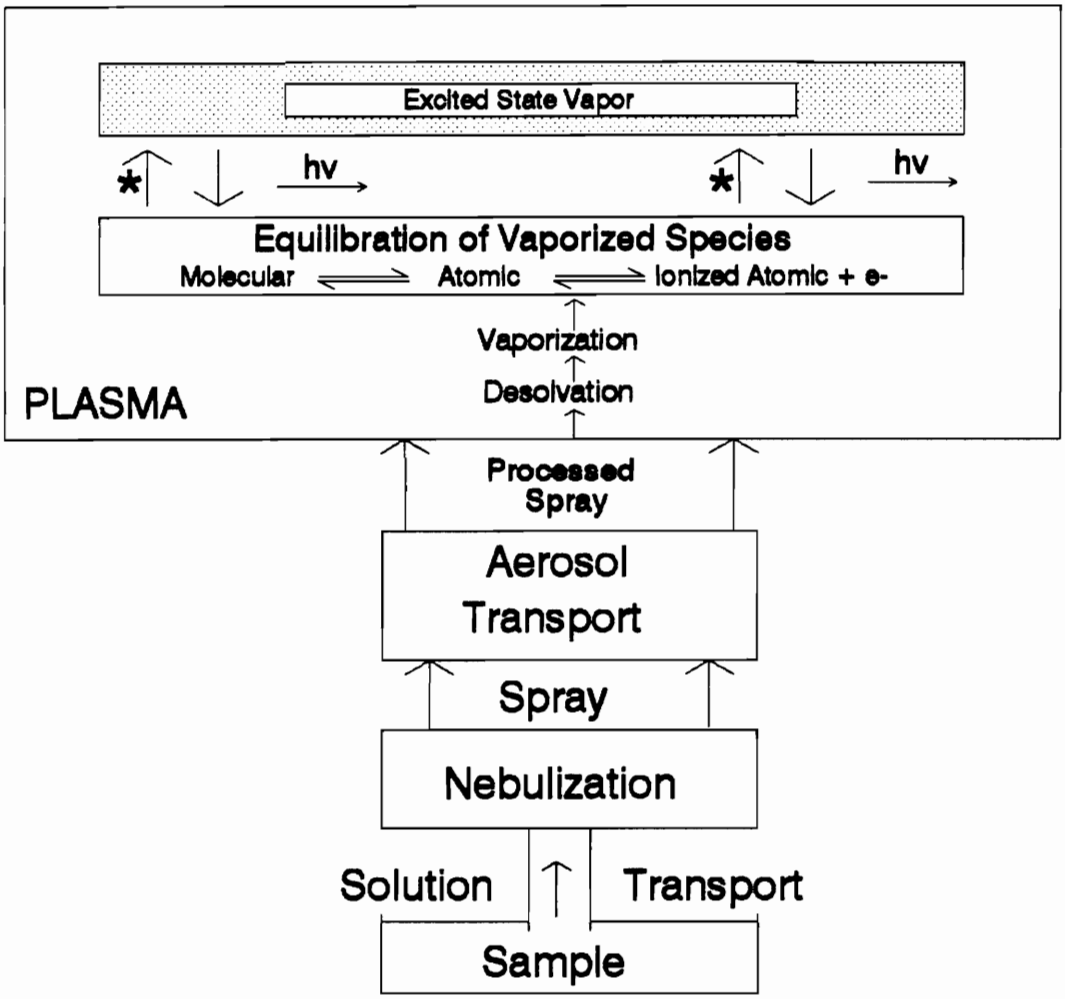

Figure 1. Sample Transport / Excitation Processes

Solvent Loading. Pneumatic nebulization coupled with a cylindrical, double pass spray chamber is one of the most common methods of sample introduction for solutions into analytical plasmas. This introduction method, unfortunately, is plagued by extremely low transport efficiencies. Although more efficient methods for sample introduction exist, such as ultrasonic nebulization, the plasma is limited in the quantity of sample and solvent that it can process into vapor phase species. In general, plasmas become unstable and exhibit poor analytical sensitivity when large quantities of solvent are introduced into the plasma discharge. This phenomenon is known as solvent loading [9-13].

To avoid solvent loading, the sample introduction system should attempt to minimize the quantity of solvent that is delivered to the plasma discharge. The elimination of the solvent, but at the same time maximizing the efficiency of analyte transport, has been accomplished through the use of thermostated spray chambers and/or condenser systems [14-16]. By heating the aerosol after nebulization, it is possible to hasten the desolvation process of the analyte aerosol. The solvent vapor is separated from the dry aerosol prior to introduction into the plasma torch with a cooled condenser. This approach is often employed with the ultrasonic nebulizer [17].

A variation of this arrangement for pneumatic nebulizer/spray chamber systems which has been examined in

our laboratory and others involves the cooling of the aerosol rather than the heating of it [9,10,18-21]. By lowering the temperature of the spray chamber, less evaporation of the aerosol occurs. With the vapor pressure of the solvent being less at reduced temperatures than at ambient conditions, a lesser quantity of solvent is presented to the discharge.

The role of solvent loading with respect to plasma atomic emission has been studied for the inductively coupled plasma (ICP) [9-12,22,23]. The ICP, a radio frquency generated discharge, is shown to be most greatly affected by large solvent aerosol droplets, which cause localized cooling of the discharge. This cooling effect tends to decrease the analytical sensitivity of the plasma.

The effect of solvent loading on a microwave induced plasma has, to date, not been studied. The work presented in this dissertation constitutes the first comprehensive study. The primary reason why this is the case is that the HEMIP is the first reported microwave cavity that is capable of sustaining a plasma discharge with direct aqueous sample introduction [24].

This work is organized according to the following overview. Chapter two is a description of the experimental apparatus employed in these studies. Chapter three is an introduction to the spectroscopic and diagnostic measurements used to delineate the effect of solvent loading

on the MIP. Chapter four examines the effect of solvent loading using a cooled spray chamber system with the HEMIP. Chapter five presents the results of studies completed employing the ultrasonic nebulization system with the HEMIP. The final chapter brings together the results of the previous chapters and draws conclusions.

The work presented in this dissertation examines the effect of solvent loading on the low powered HEMIP. Solvent loading is systematically measured for the different sample introduction systems. By monitoring the changes in analytical sensitivity, diagnostic temperatures, and emission profiles, conclusions can be made regarding the extent and the nature of the solvent loading effect.

Chapter 2

EXPERIMENTAL CONDITIONS

Reagents. The plasma gases, argon and helium, were analytical grade and purchased from Airco (Murray Hill, NJ). All solvents were analytical reagent or HPLC grade and obtained from Fisher Scientific (Raleigh, NC). The chemicals used were reagent grade and were dissolved in distilled and deionized water. Stock and Calibration solutions of 1000 ppm concentration were prepared according to standard procedures [25]. Volumetric dilutions were performed to yield required concentrations using class B glassware and digital pipets.

Experimental Apparatus. Table 1 lists the apparatus used in this project along with model and manufacturer information. More detailed descriptions of the configuration and use of the apparatus will follow.

Microwave Cavity. The microwave cavity used in this study is a modification of the Beenakker (TM_{010}) design and is illustrated in Figure 2. The modifications to the TM_{010} design were effected by Matus, Boss, and Riddle [2], and was labeled as the "Highly Efficient Microwave Induced Plasma" or HEMIP. The major change in the HEMIP cavity from the TM_{010} design is the use of a translatable antenna probe used to capacitively couple the microwave energy to the cavity. This differs from inductively coupled Beenakker design,

Table I. Instrumentation

COMPONENT	MODEL/SIZE	MANUFACTURER
Microwave Cavity	HEMIP	Lab Built
Microwave Generator	HI-2450	Holaday Industries Edina, MN
Discharge tube	Tangential	Lab Built
Coaxial Cable	RG-214	Times Fiber Co. Wallingford, CT
Monochromator	EU-700, 0.35 m	Heath Co. Benton Harbor, MI
PMT	R955	Hamamatsu Bridgewater, NJ
I/V	5002	EG & G Princeton, NJ
±15V, +5 V Power Supply	EU 601-11	Heath Co. Benton Harbor, MI
Lock-In Amplifier	501	EG & G PARC Princeton, NJ
Chopper	125 A	EG & G PARC Princeton, NJ
High Voltage Power Supply	204	Pacific Inst. Concord, CA
Lens	f/3, suprasil	Oriel Corp. Stratford, CT
Power Circulator	420B/IS	Micro-Now Inc. Skokie, IL
Power Meter	43	Bird Inst. Co. Cleveland, OH
Coolant Pump	G/D1	Haake GMBH West Germany

Table I. Instrumentation Continued

COMPONENT	MODEL/SIZE	MANUFACTURER
Nebulizer	Concentric TR-50-C2	J. C. Meinhard Santa Ana, CA
Spray Chambers	Cooled Scott Standard Scott	Lab Built Lab Built
Cooling Tube	Water Jacketed	Lab Built
Desolvation System	J-tube,Condenser	Lab Built
Cryogenic Flask	Lab Designed	Lab Built
Ultrasonic Nebulizer	UDX	Baird Co. Bedford, MA
Peristaltic Pump	Rabbit Minipuls 2	Rainin Co. Woburn, MA
Computer	IIe	Apple Computer Cupertino, CA
ADC Board	ADALAB	I.M.I. Pittsburgh, PA
Computer (II)	XT 286	IBM Co. Armonk NY
ADC Board (II)	Chrom-1 AT	Metrabyte Co. Taunton, MA
Data Acquisition Software	Lab Calc LCCP	Galactic Ind. Salem, NH
Rotammeters	MM3	Air Products Allentown, PA
Optical Rail	30 inch	Ealing Co. South Natick, MA
Translation Stages	430	Newport Co. Fountain Valley, CA

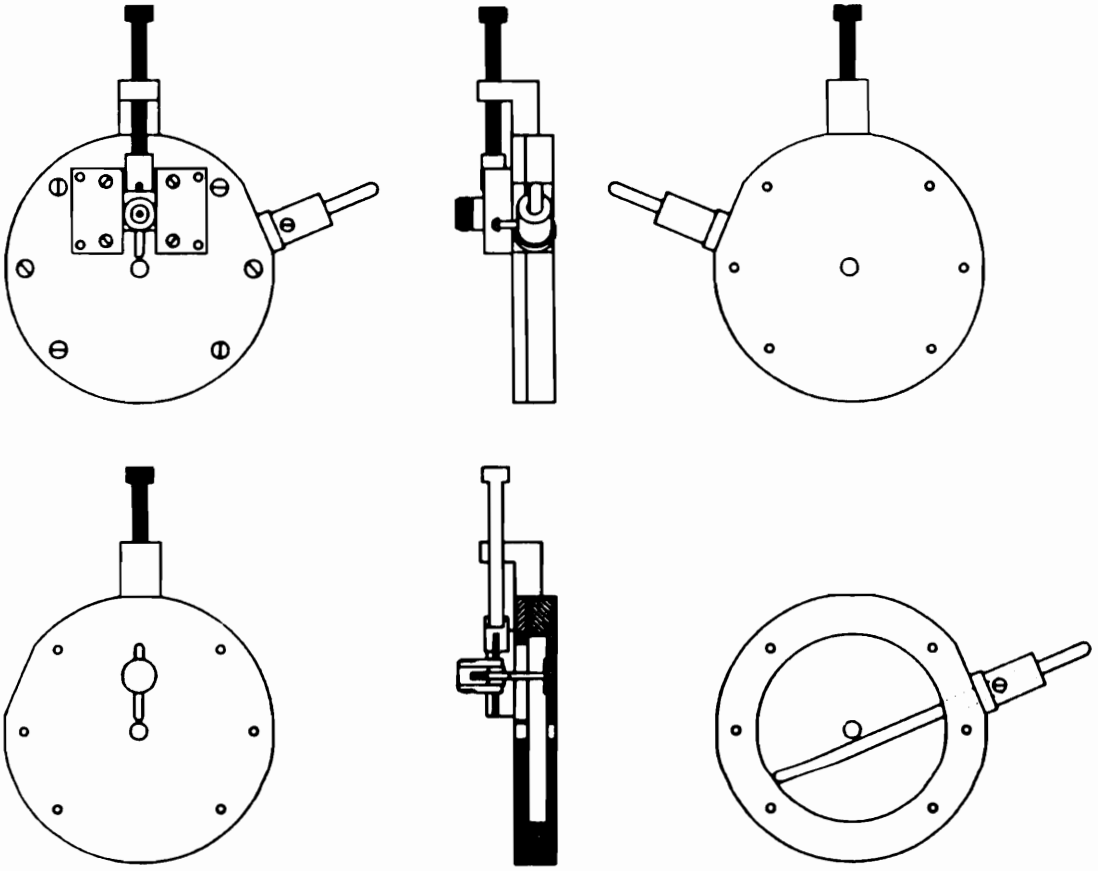

Figure 2 Highly Efficient
Microwave Induced Plasma Cavity

(Graphics courtesy of Mark Wingerd.)

which employs a fixed antenna that was radially inserted into the cavity and grounded to the bottom plate. This movable probe simplifies the tuning and impedance matching of the cavity to the microwave generator, and eliminates the need for the external tuning stubs required in inductively coupled designs.

The cylindrical cavity was machined from a 0.78 inch thick sheet of oxygen-free high conductivity (OFHC) copper. The interior depth of the cavity is 10.0 mm while the inner diameter is 89.1 mm. A hole 8 mm in diameter is drilled into the center of the cavity to allow insertion of the discharge tube. A quartz rod 6 mm in diameter extends into the cavity from a fitting in the side wall which allows the rod to be held at a chosen depth. This rod is used to tune the resonant frequency of the cavity to that of the microwave generator, 2450 MHz.

A removable cover plate was machined for the HEMIP cavity from OFHC copper to a thickness of 0.197 inches. This plate also has a 8 mm center hole, allowing the discharge tube to pass completely through the cavity. A 5 mm x 40 mm radial slot was machined into the plate to allow for the free translation of the antenna probe.

Attached to the cover plate is a set of brass guides on either side of the radial slot. These guides, along with a precision screw mechanism, allow for the radial positioning of the antenna probe. A cross-sectional diagram

of the cavity, Figure 3, shows this mechanism, along with that of the probe.

The antenna probe was constructed from a coaxial connector (UG 58 A/U type N) and a combination copper/stainless steel element. The mount for the connector was machined to a width of 0.875 inches, which allowed the connector to fit into the guides surrounding the radial slot. The probe element consisted of 10 gauge copper wire silver soldered to a 16 mm diameter stainless steel disk. This object was firmly "press-fit" to the center post of the N connector, allowing for the easy changing of probe elements. The probe was adjusted to a 96 % penetration depth. This depth was determined to provide maximum power transfer.

The combination of the quartz rod and antenna probe allows the microwave cavity to be tuned and matched to the generator. When this tuned and matched circumstance occurs, the cavity is said to be "critically coupled" [2], i.e. that all available power from the generator is delivered to the cavity, and hence the discharge, with maximum efficiency. Boss, *et al*, measured the power transfer efficiency to be greater than 95 % [2].

Microwave Torch. The torch (discharge tube) design used in this work has been developed in our laboratories at VPI and is shown in Figure 4. This tangential flow torch is similar to those used in ICP-AES and MIP-AES. The initial

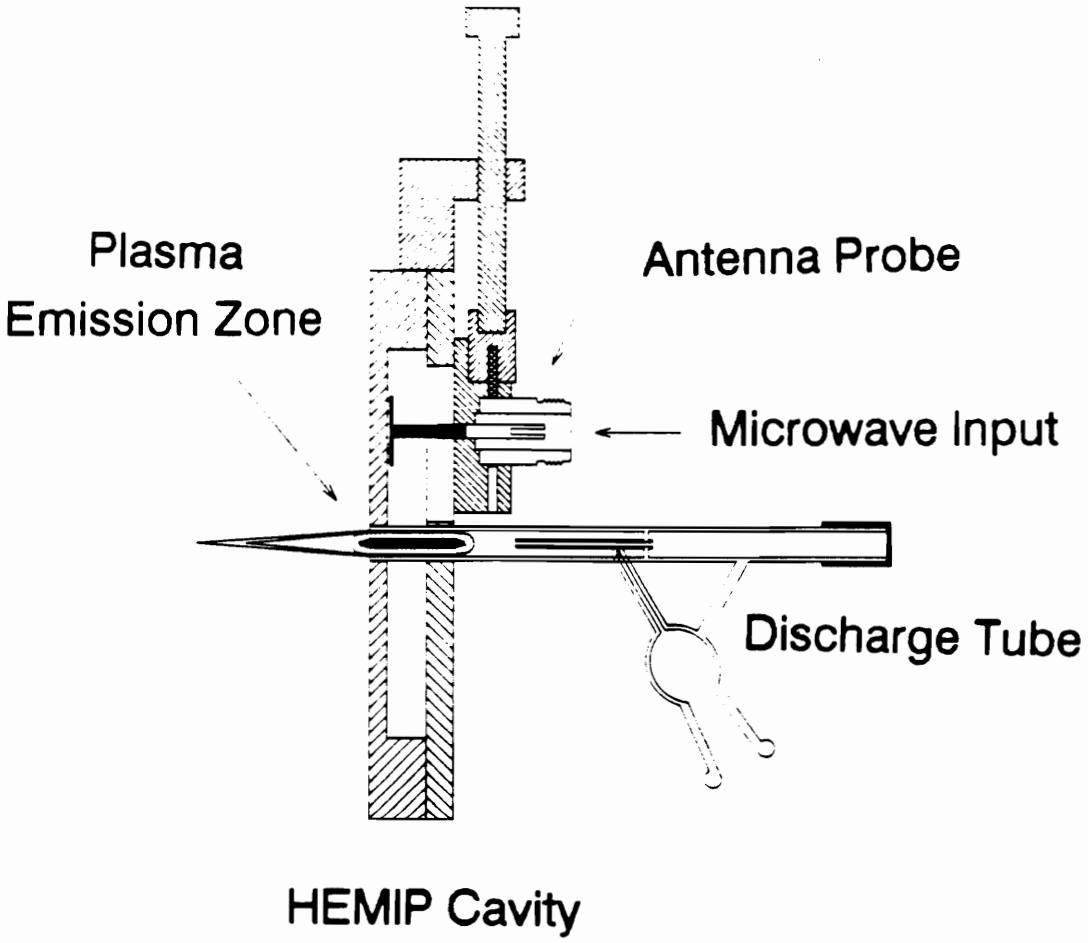

Figure 3 : Cross-sectional diagram of HEMIP and Torch

(Graphics courtesy of Mark Wingerd.)

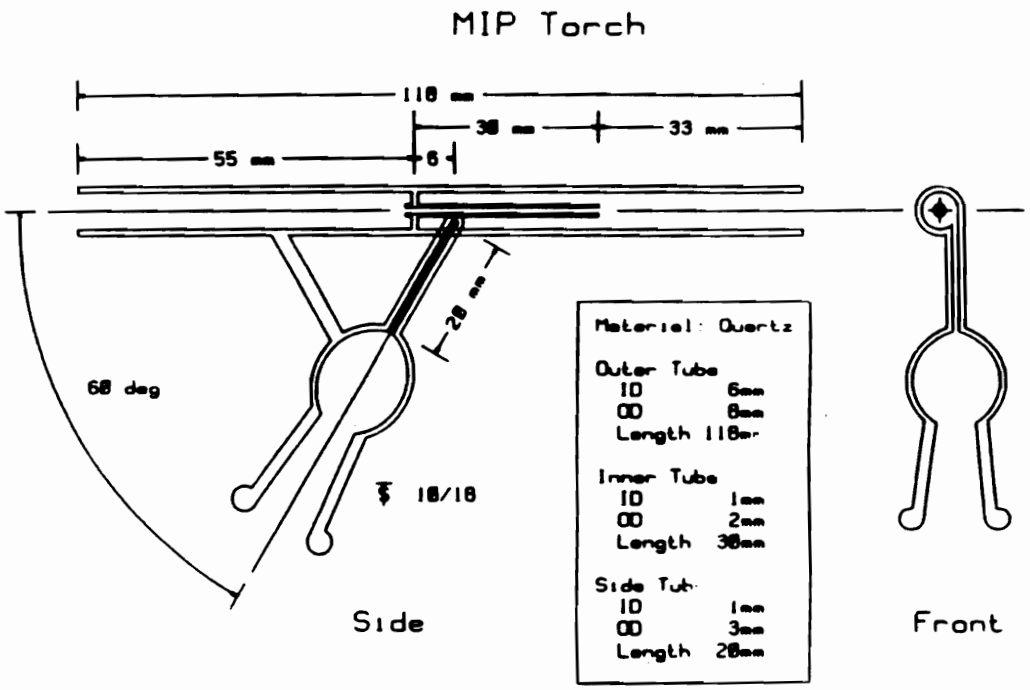

Figure 4 : MIP Discharge Tube

(Graphics courtesy of Mark Wingerd.)

concept was from a design proposed by Hieftje and Deutsch [26], but has since been heavily modified. This torch allows a stable, centered plasma to be generated at low flows. As the plasma discharge is constrained from touching the walls of the torch in normal operation, torch lifetime is prolonged.

This torch is constructed from quartz and consists of two concentric tubes, with dimensions as shown in Figure 4. The inner tube was initially used to deliver sample to the discharge (as with ICP designs), but, due to a high back pressure, which interfered with the operation of the nebulizer, this method of sample introduction is no longer done. However, the center tube does serve to aid in the preservation of the helical gas flow, and is still employed in the present design. It should be noted that the back of the torch is sealed to avoid entrainment of air into the discharge.

The plasma gas and analyte aerosol is introduced into the sidearm of the torch. This tube is set at a 60^{o} angle to the torch and is tangentially connected to the body. This geometry is critical because these angles define the helical flow pattern of the gas / sample mixture, which allows for stable discharge generation. If this union is not correct, a stable, centered discharge will only be formed at excessively increased flow rates, an undesirable situation.

Most commonly the sample introduction gas flow is connected to the torch via one arm of a T interface. This T is constructed of glass and connects to the sidearm of the torch via a ball and cup joint. The other arm of the T is connected to an auxiliary gas flow which is used to stabilize the plasma during ignition and high solvent flow situations.

It should be noted that during the period in which this research was completed, more than one torch was used. While this may cause minor variations in results, it is considered that the torches were selected to most closely match the original torches operating conditions. Any variance due to changes in torches is considered to be insignificant.

Plasma Ignition and Operation. In preparation for ignition of the plasma discharge, the total (sample plus auxiliary) gas flow into the torch is increased to approximately 2 L/min. The end of the discharge tube is extended 1 cm beyond the face of the plasma to ensure no interference or entrainment of atmospheric gases in the discharge region. The microwave generator is set to the desired power, turned on, and a length of tungsten wire inserted into the discharge tube.

The wire is inductively heated by the oscillating energy field, causing thermionic emission of electrons from the surface of the wire. These electrons "seed" the plasma and initiate the chain reaction of collisional excitation

between the support gas and electrons which generates the plasma. As soon as the plasma has been ignited, the wire is removed, the auxiliary gas flow is reduced and the cavity is tuned so that reflected power, measured by a power isolator, is minimized. The torch is then drawn back into the cavity so that only 2-3 mm extends from the face of the cavity.

Spectrometer and Signal Electronics. Figure 5 shows the two different viewing geometries which are employed in this type of work. The radial, or "line-of-sight" viewing position is preferred in this work as there is less noise involved as the high energy plasma discharge is not imaged on the slits of the monochromator. However, under certain conditions this view is not useful as there is not a discharge plume which extends from the cavity. Also, when species with high excitation energies (such as nonmetals) are analyzed, the axial mode must be used.

The analyte emission, whether axial or radial, is projected onto the slits of a 0.35 m monochromator by a f/3 lens at a magnification ratio of one. The HEMIP cavity is mounted on an optical rail and two micrometer translation stages which allow translational motion adjustments in all three axes. This allows reproducible focusing and the ability to precisely scan or profile different areas of the plasma discharge.

The incident image is modulated at 137 Hz via an optical chopper to reduce 1/f noise. Signals created by

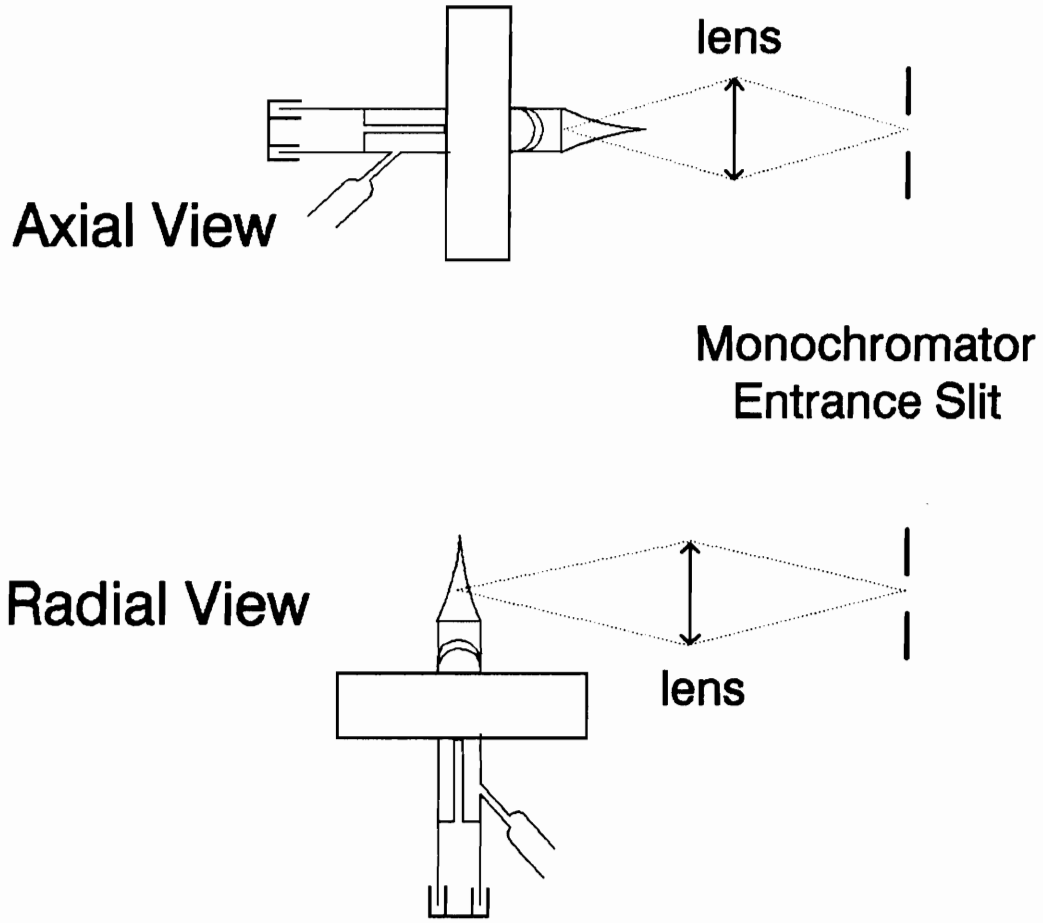

Figure 5: Axial and Radial
Viewing Geometries

analyte emission were collected by the photomultiplier and the resultant current directed into a current to voltage converter. The output voltage is fed to a lock-in amplifier which processes and measures the signal. The output is then directed to an analog-to-digital converter. A block diagram of the entire experimental system is shown in Figure 6.

Data Acquisition. Two different data acquisition systems were employed in this work. Initially, a combination of a strip chart recorder and an Apple IIe computer were used to acquire data. The Apple IIe was equipped with a 12-bit analog-to-digital converter. Programs were available on the Apple IIe to obtain integrated signal measurements and to compile data for axial profile scans. This data was then printed out and could be processed further. Also strip chart recordings were analyzed by hand to yield other measurements.

Subsequently, an MS-DOS computer was obtained and a data acquisition system purchased to replace the Apple system. This system employs a 16-bit analog to digital converter combined with a software data analysis package. When connected to the output of the lock-in amplifier, This system allows for wavelength scans to be stored on disk, similar to an electronic strip chart recording. On-screen data manipulation and processing, as well as direct output was possible.

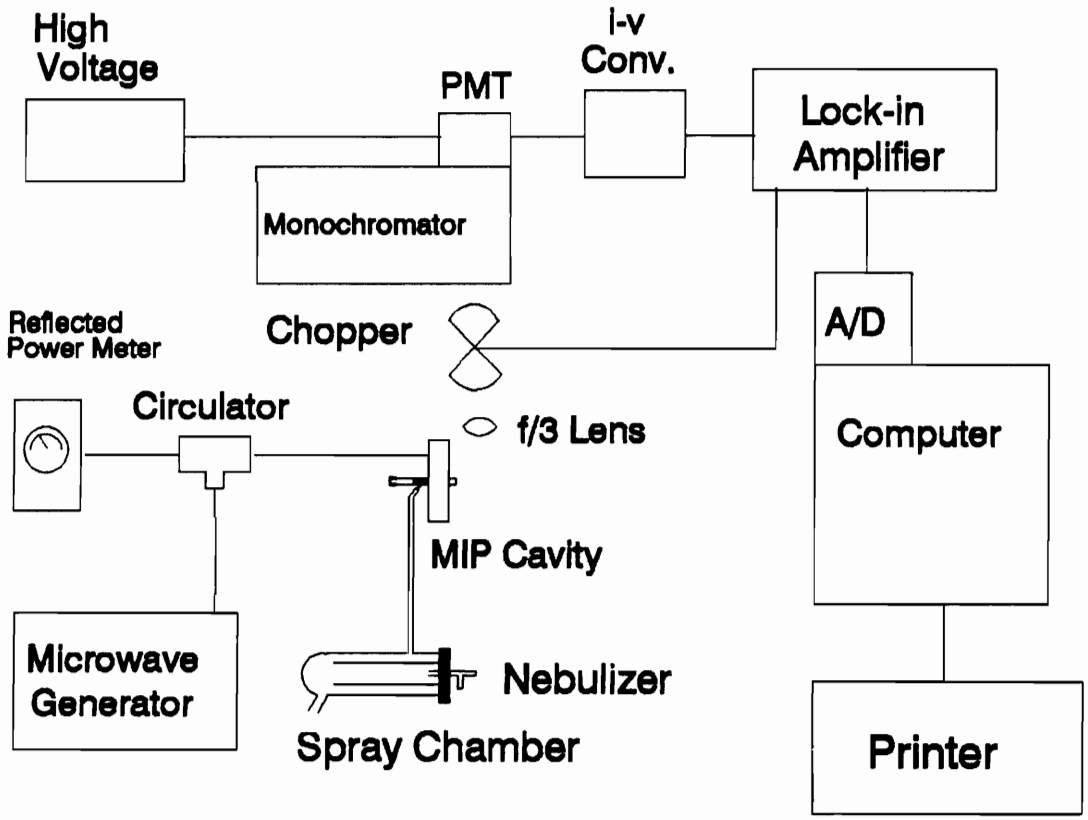

Figure 6 : Diagram of
Experimental Apparatus

Sample Introduction. Several sample introduction systems were employed in order to study the effect of solvent loading on the HEMIP. These systems allowed for comparisons made under different solvent loading conditions, to be performed while maintaining the normal operating conditions of each sample introduction system.

Standard Pneumatic Sample Introduction. The most commonly used method of sample introduction is shown in Figure 7. This system consists of a pneumatic nebulizer and a Scott-type spray chamber. Rotameters are used to obtain accurate measurement of flow rates. The support gas (argon or helium) flows through the nebulizer over the sample nozzle creating, via the Venturi effect, a low pressure zone. This effect results in sample being drawn into the flowing gas stream. The liquid flow interacts with the supersonic jet stream of gas creating an aerosol. This primary aerosol has a wide distribution of droplet sizes. The spray chamber serves to discriminate against the larger droplets by secondary and tertiary impaction, to produce an aerosol stream that is greatly reduced in size from the primary aerosol. The tertiary aerosol stream is then entrained into the plasma discharge tube via a length of tubing, usually 10 mm i.d. Tygon.

Cooled Pneumatic Sample Introduction. The cooled sample introduction system is shown in Figure 8. It is similar in appearance to the standard system and shares many

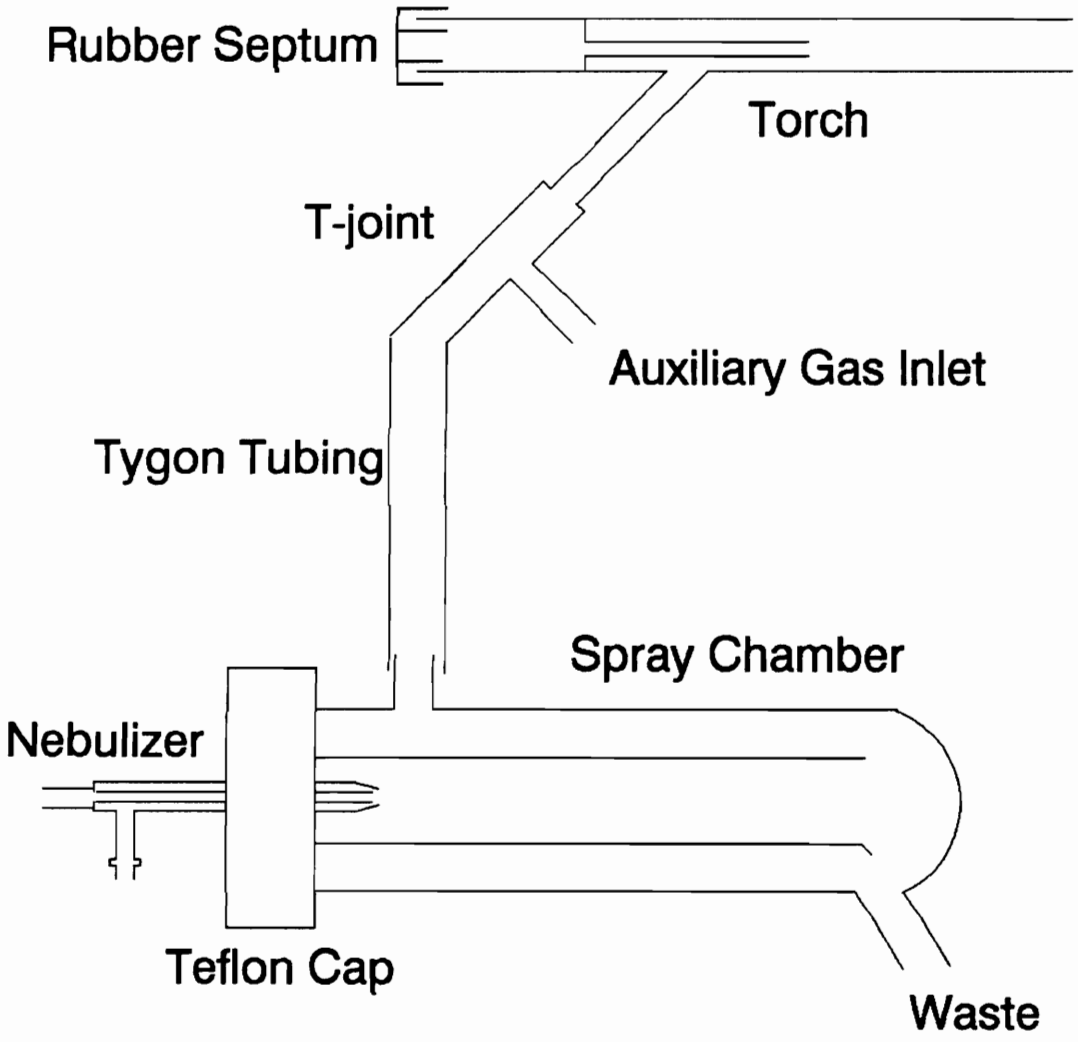

Figure 7: Standard Pneumatic
Sample Introduction

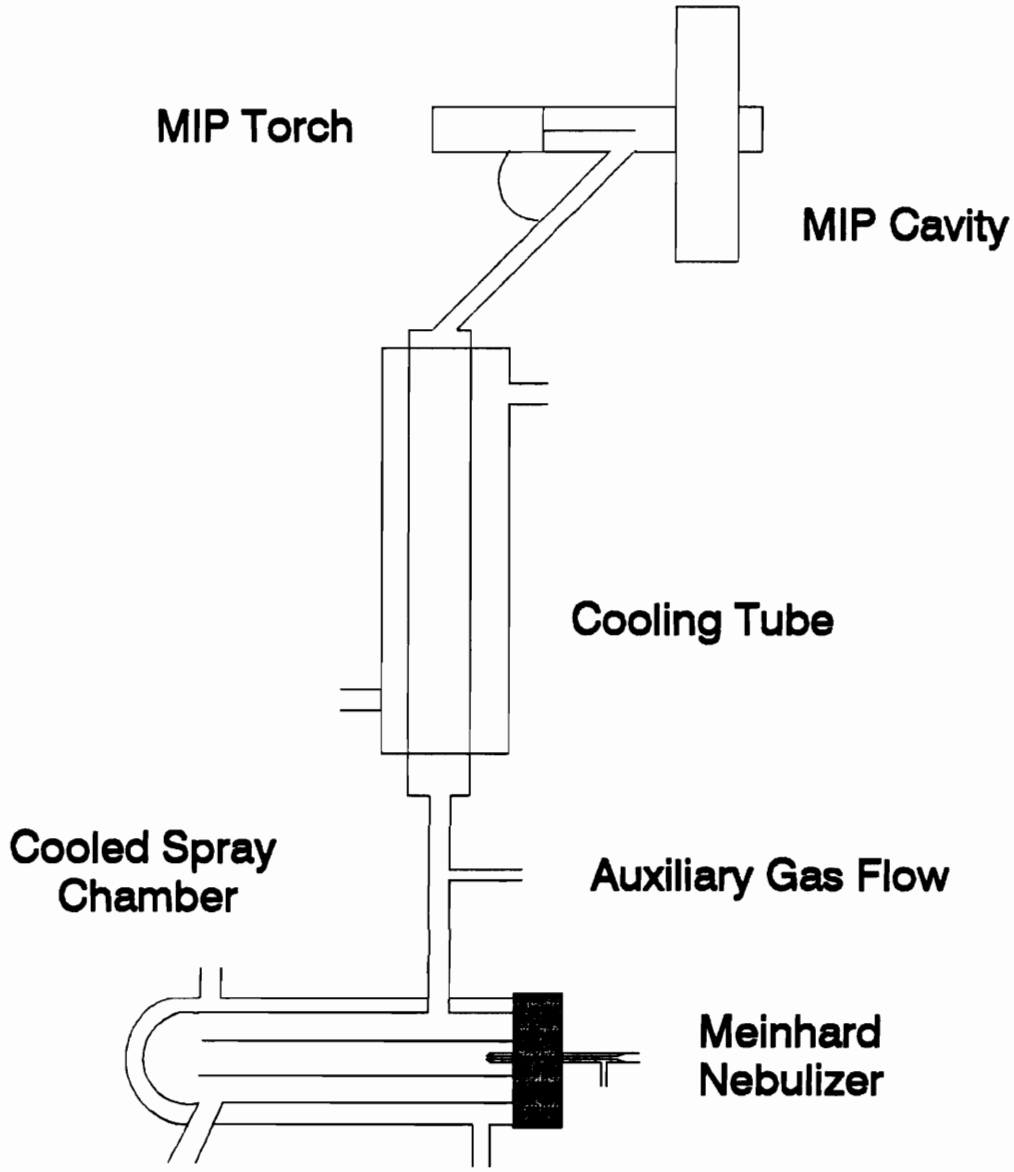

Figure 8: Cooled Pneumatic Sample Introduction

of the same components. The major change to this setup is the ability to be temperature controlled. A water jacketed spray chamber and cooled transfer tube are connected to a coolant recirculating bath, which is filled with a mixture of water and ethylene glycol. This cooled spray chamber, along with the insulated connector and transfer tube allows for the entire sample introduction pathway to be thermostated.

Ultrasonic Nebulization. The ultrasonic nebulizer sample introduction device is shown in Figure 9. The design and operation of this system is somewhat more complex than a standard nebulizer/spray chamber system. A water cooled piezoelectric crystal is connected to the output of a free running 1.4 MHz generator. Sample is introduced via a peristaltic pump over the exposed surface of the vibrating crystal, thus creating a dense fog of fine aerosol. This aerosol is swept from the spray chamber by the inert plasma gas and into a heated J-tube. This tube is heated to approximately 105^{o} C and serves to vaporize the solvent and to create a stream of dried analyte particles and solvent vapor. This binary mixture enters a water cooled condenser where the solvent condenses along the walls and the analyte particles remain suspended in the plasma gas. These particles are transported to the plasma torch via a short length of tubing. Waste solvent condenses on the trap walls

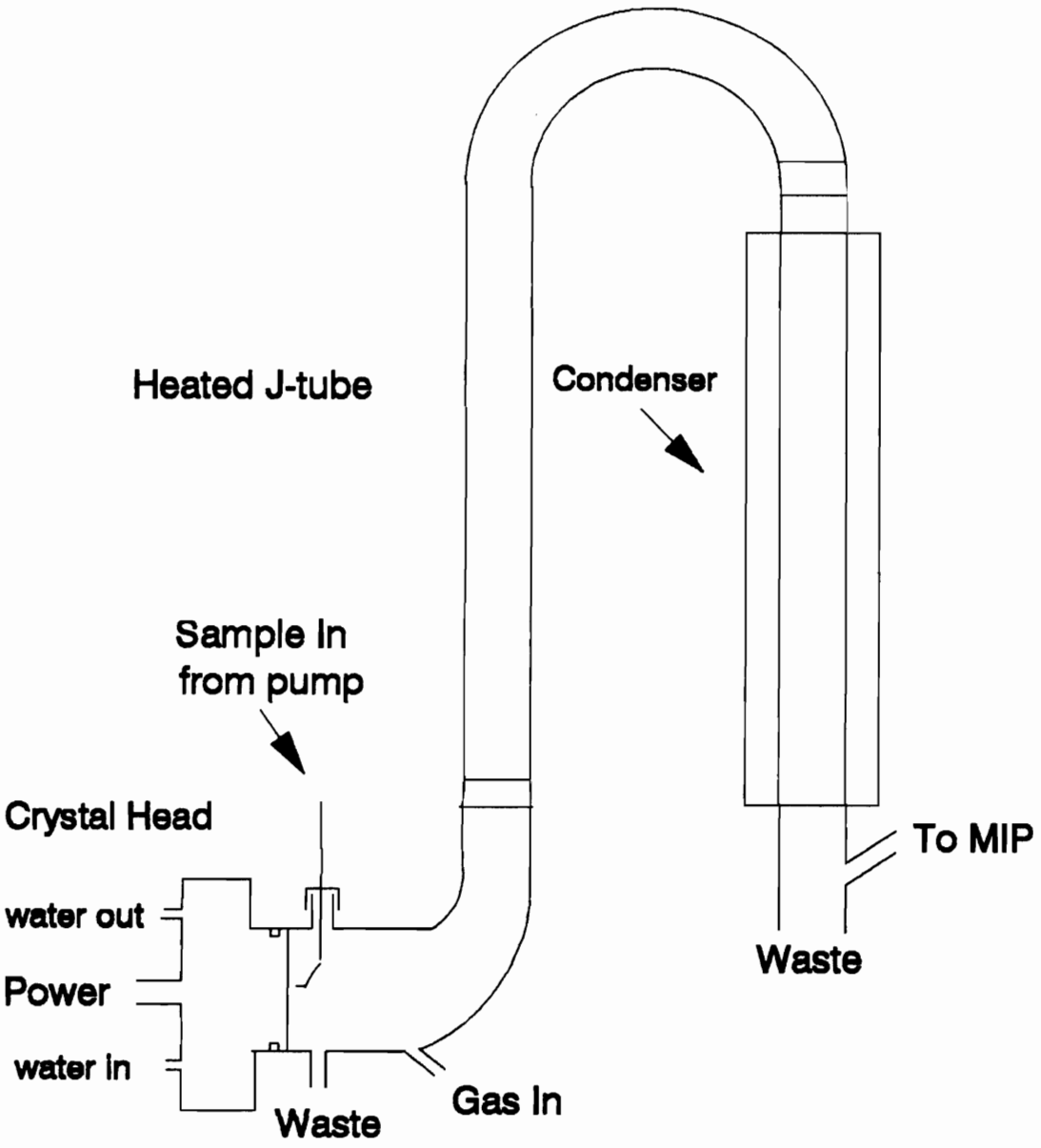

Figure 9: Ultrasonic Nebulizer

and is collected into a small length of tubing at the bottom of the condenser.

Desolvation Apparatus. The desolvation apparatus shown in Figure 10 is very similar to the desolvation mechanism in the ultrasonic nebulizer system. Because of the smaller amount of solvent introduced with the pneumatic nebulization system, this setup is somewhat reduced in size. The long end of the J-tube is connected to the outlet of the Scott-type spray chamber. This system is a modification of one used by Galante *et al* [27].

Cryogenic Desolvation. The apparatus for cryogenic desolvation is shown in Figure 11. The central feature of this system is the cryogenic flask. Measuring 27 cm long and 7.6 cm in diameter, this flask has four rows of conical indentations along the length of the chamber, which increase the inner surface area. This chamber can either be connected to the outlet of the desolvation apparatus, or directly to the exit of the spray chamber.

The sample/gas mixture flows down the central tube of the flask, which is submerged in a mixture of dry ice and acetone, keeping the flask at approximately -50^{o} C. Any residual solvent is frozen to the sides of the chamber. The dry sample particles, mixed with the support gas, exit the chamber and enter the plasma torch.

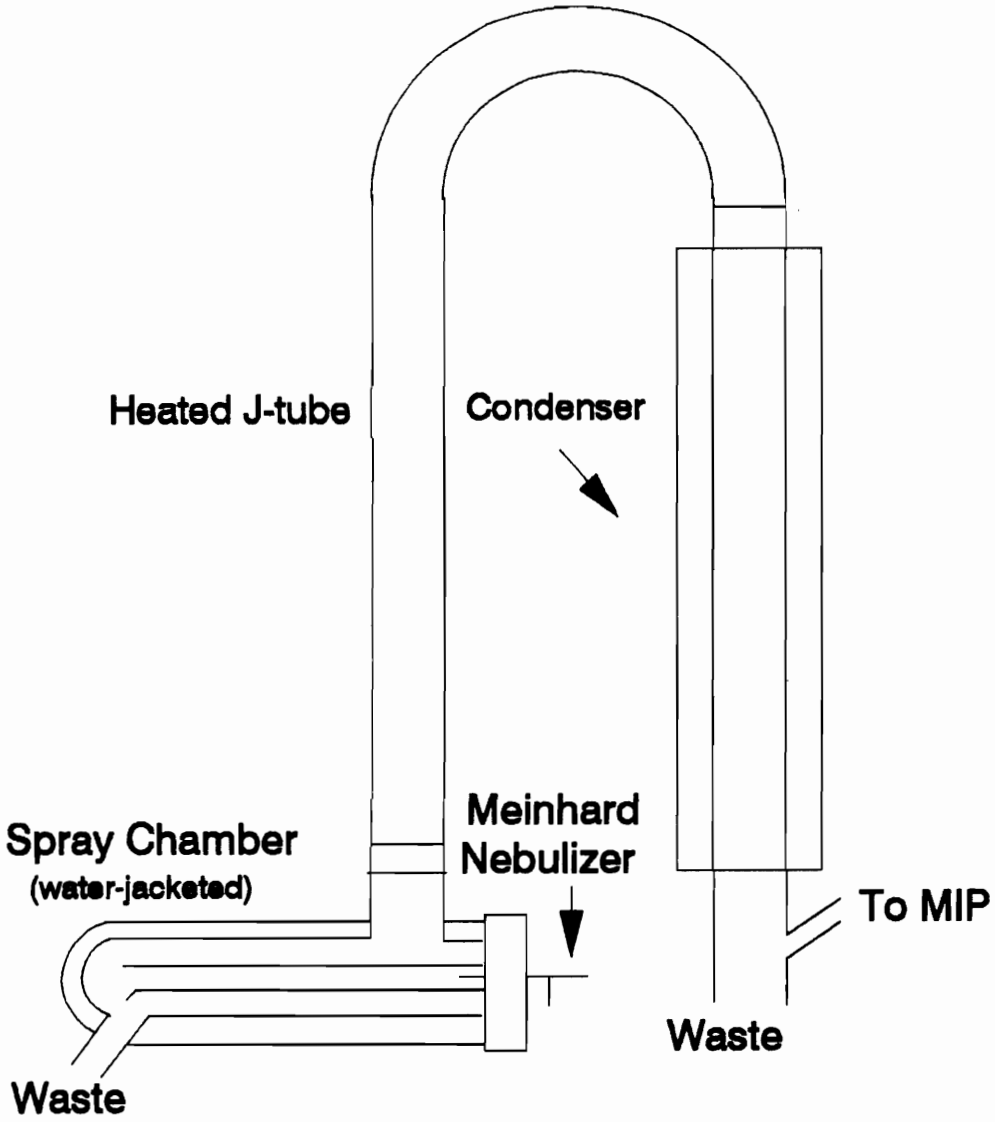

Figure 10 : Pneumatic Desolvation Apparatus

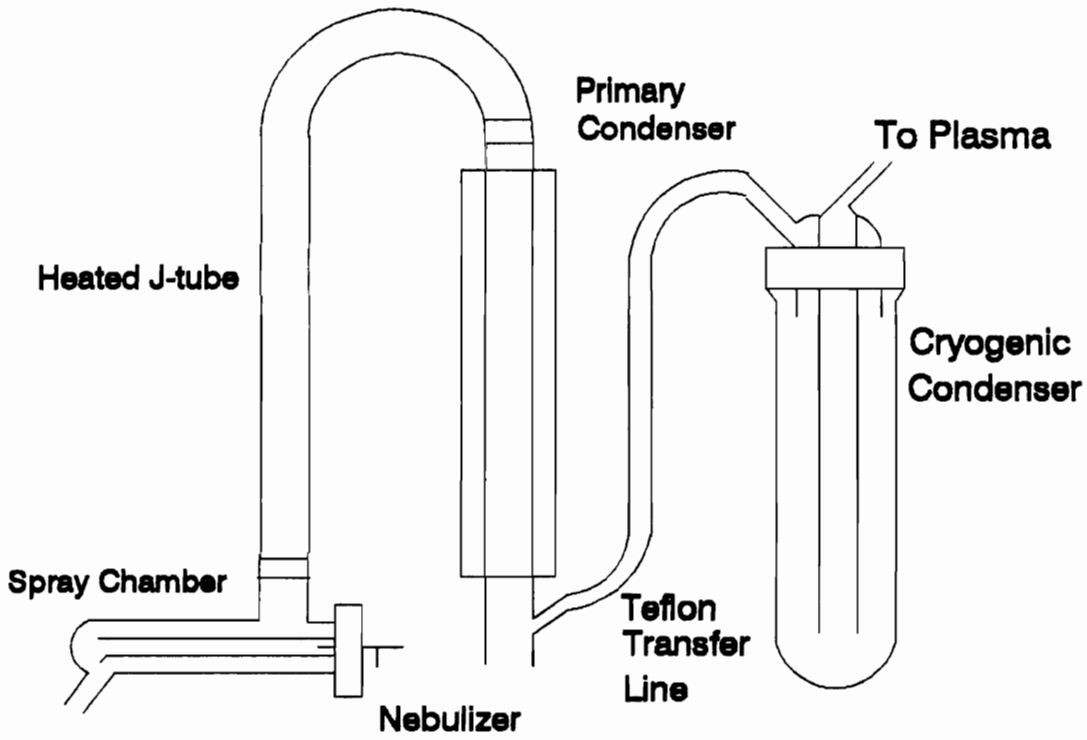

Figure 11 : Cryogenic Desolvation

Chapter 3

Description of Spectrometric Measurements

Introduction. There are several spectrometric measurements employed in this research to evaluate the effect of solvent loading on the operation and performance of the HEMIP. These measurements, such as emission profiles, limits of detection, excitation temperatures, and electron number densities, are used routinely to characterize new sources for use in atomic emission spectrometry. Additionally, changes within an excitation system can be carefully monitored with these spectroscopic measurements. These values can be used as a basis for the comparison of changes to the excitation source as the magnitude of solvent loading is altered. This chapter summarizes these spectrometric measurements, describes how they are obtained, and explains their physical significance.

Emission Profiles

An emission profile of a plasma incorporates the measurement of emission intensity in a plasma discharge at precisely incremented steps along an axis of the discharge. This profile is corrected for the contribution of background emission by first collecting a background profile on the analytical line of interest and then subtracting this measurement from an emission profile in which the analyte is

introduced into the plasma. This can be done in one, two, or all three dimensions, providing a detailed "map" of the distribution of emission intensity.

In this series of studies, one dimensional vertical profiles are used to determine the optimum observation distance from the faceplate of the HEMIP cavity. By using micrometer controlled translation stages, precise and repeatable distances can be obtained.

A diagram of the cavity geometry and sample profile are shown in Figure 12. In part A, this figure shows the monochromator slits perpendicular to the discharge tube axis and vertical with respect to the optical table. This positioning gives an averaged side to side measurement of the plasma discharge intensity. The width of this slice is governed by the entrance slit width of the monochromator, in this case 40 micrometers.

Part B shows the axes of movement available in this system. By moving the cavity along the "profiling" axis (translating the assembly laterally with respect to the entrance slits), a series of these "slices" can be obtained. The other axes are used to position the cavity assembly vertically ("height adjust"), and into focus.

Profiles are generally taken over an area ranging from the face of the cavity through the end of the discharge plume, with a maximum range of 50 mm. A sample profile is

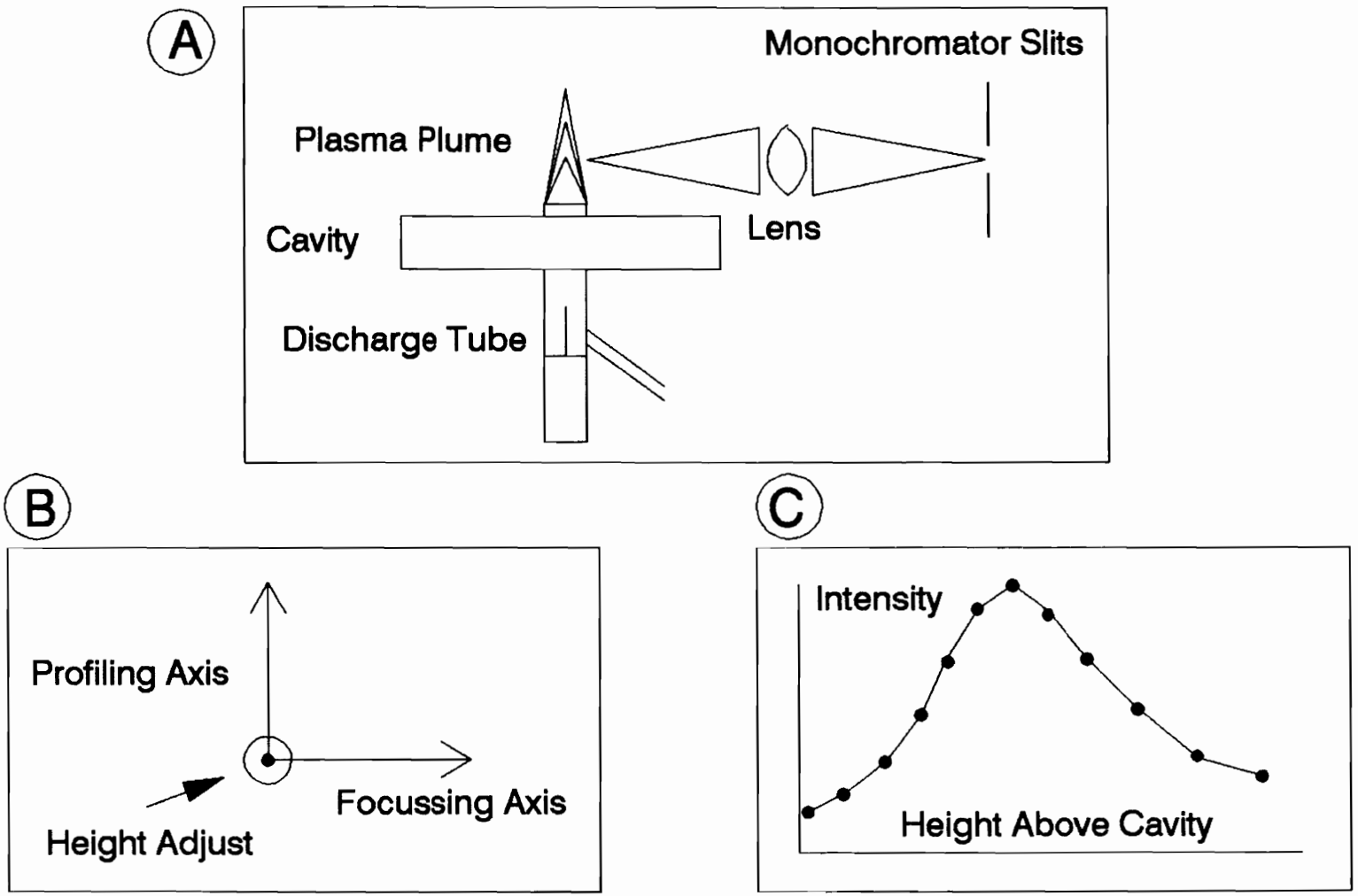

Figure 12 : Cavity Geometry and Sample Profile

displayed in part C of Figure 12 showing how the data is represented graphically.

The interpretation of these profiles yield the height of maximum analyte emission intensity in the plasma. Shifts in these maxima occur under different operating conditions, and are generally indicative of a change in the excitation ability of the plasma, or the varying refractory natures of the analyte species. The height of maximum intensity for various elements is different, and depends greatly upon the energy required to promote the vaporization, dissociation, and excitation of the refractory species.

Limit of Detection. The limit of detection for a given analysis is defined as the amount of an analyte that gives the smallest signal response that can be determined to be statistically different from an analytical blank [28]. This IUPAC value is calculated from the following equation [29]:

$$c_L = (k * s_B) / m$$

where:

c_L = the limit of detection (concentration)

k = confidence level factor

s_B = standard deviation of the background

m = analytical sensitivity

In this work c_L is determined as described below. A working curve is constructed using at least 3 points (2

analyte concentrations plus blank). The s_B is the standard deviation of twenty blank measurements, the minimal amount determined to give a reasonable estimation of the true standard deviation [29]. Five measurements of each analytical sample are taken, and the average of these measurements is corrected for the background by subtracting the mean background intensity from this reading. The working curve is constructed using the mean data points. Linear regression provides the slope of the curve, m, the analytical sensitivity, as well as the y-axis intercept, b.

The confidence level factor, k, that is used in this work is 3, following the IUPAC recommendation. This choice of k implies that the limit of detection has to be at least 3 standard deviations away from the average background value. For a normal distribution of noise, the use of k=3 implies that there is a probability of no less than 99.86% that the observed sample signal at this prescribed value is not a random fluctuation of the baseline.

Plasma Diagnostics. The knowledge of the physical state of a plasma discharge is most important to an analytical spectroscopist because it is the plasma discharge which is solely responsible for the demanding processes of analyte vaporization, dissociation, and excitation. The efficiency with which the discharge is operating will have a direct effect upon the production of the characteristic line spectra that is used for qualitative and quantitative

analysis. In order to gain insight into the fundamental processes occurring in an analytical plasma, diagnostic measurements must be made. These include the excitation temperature, the ionization temperature, and the electron number density, and form the basis for describing the way in which plasma species and analytes interact.

Many of the analytical plasmas used today are of significantly different designs and operate under widely varying conditions. This dissimilarity makes any comparisons between analyses and laboratories somewhat difficult to perform. For two plasmas to best be compared, diagnostic tests should be run under normal operating conditions and used as a basis for evaluation. Similarly, diagnostic measurements are often performed to characterize a single plasma device under different operating conditions. It is in this fashion that the diagnostics will be employed to study the effects of solvent loading on the HEMIP.

Atomic spectroscopists, by convention, describe a plasma's energy in terms of temperature. Ideally, a spectrochemical plasma could be described by a single temperature. This statement would be true only if every energy exchange process in the plasma were balanced by its reverse process. This balance would have to be true not only for collisional (excitation and ionization) interactions, but also radiative (emission and absorption)

processes. The achievement of such a state is called complete thermodynamic equilibrium (CTE) [30].

In a standard laboratory plasma, CTE is never reached. The radiative processes are out of balance, with emission dominating absorption. The physical constraints of a gaseous plasma discharge allow for radiation to escape the plasmas boundaries, thereby violating Planck's Law. This is manifested physically as areas of the plasma which are termed "optically transparent". Hence, the only known source that follows Planck's distribution is the radiation field in a blackbody emitter.

In cases where Planck's Law is not obeyed, the previously mentioned relationships may be valid. Plasmas that satisfy these conditions are said to be in local thermodynamic equilibrium (LTE)[31]. This construct has been extended for situations where equilibrium is established at every point in the plasma, but allows for the prospect of different temperatures at different spatial locations in the plasma.

Excitation Temperature. The excitation temperature of a plasma is a measure of the population distribution of bound state (energy) levels in the plasma discharge. This partitioning between energy levels is described by the Boltzmann distribution. Emission line intensities can be derived from the Boltzmann equilibrium. Given a set of emission lines from a single element, along with such

information as transition probabilities, statistical weights, and frequencies of transition, the excitation temperature can be determined from the following equation [32].

$$\ln[(I_{pq} / g_p)/(A_{pq} * v_{pq})] = E_p / (k * T_{exc})$$

where:
- I_{pq} = measured relative line intensity
- g_p = statistical weight of state p
- A_{pq} = transition probability
- v_{pq} = frequency of transition pq
- E_p = energy of state p
- k = Boltzmann's constant
- T_{exc} = excitation temperature

For a series of atomic line intensities, the left side of the equation is plotted against the energy of the upper state (E_p) of the emitting analyte species. The resulting plot should be linear with a slope inversely proportional to the excitation temperature. This measurement is commonly made using the emission line intensities of helium or iron, as the transition probabilities and energy levels for these species are well known [33]. If the plasma is in LTE, T_{exc} will be the temperature which describes each type of particle in the plasma at every energy level. If not, T_{exc} holds only for the energy levels of the species used to make the measurement.

Table II shows wavelengths and constants for selected iron and helium emission lines used in the T_{exc} measurement

Table II

Wavelengths and Constants used for Excitation Temperature Measurements (from reference 33).

Iron			
Wavelength	Ep (cm^{-1})	g_p	A_{pq}
367.99	27167	9	0.138
370.56	27395	7	0.328
371.99	26875	11	0.163
372.26	27560	5	0.505
373.49	33695	11	0.886
373.71	27167	9	0.143
374.83	27560	5	0.090
374.95	34040	9	0.744
375.82	34329	7	0.611
376.38	34547	5	0.523

Helium			
Wavelength	Ep (cm^{-1})	g_p	A_{pq}
388.87	185565	9	0.98
447.15	191445	15	0.246
471.31	190298	3	0.095
492.19	191447	5	0.198
501.57	186210	3	0.134

[33]. When Fe is used to measure T_{exc}, a 1000 ppm aqueous Fe solution is aspirated and introduced into the discharge, and the intensities of two or more of these emission lines are measured. Similarly, for a He T_{exc} measurement the He emission lines are monitored. It should be noted that water is aspirated in order to assure that the cooling effect of the water on the plasma (as with aqueous Fe solutions) is kept constant. The intensity vs. wavelength data is then entered into a computer program whereby T_{exc} is calculated via linear regression [34]. For the two line measurement, a simple ratio is used. Figure 13 shows a wavelength scan of the ten Fe emission lines represented in Table II. The error associated with this measurement is estimated to be 3% overall, due to the uncertainties in the spectroscopic constants [32].

Ionization Temperature. The ionization temperature is a measure of the equilibrium between successive ionization states in the plasma. This distribution is governed by the Saha-Eggert relationship [35]. This temperature measurement is usually performed in conjunction with T_{exc}, such that these two temperatures can be compared with each other, as well as for different plasma systems or different operating conditions. The difference in magnitude between T_{exc} and T_{ion} is a suggestion of how far a plasma discharge deviates from the conditions of LTE. If the difference is large (on the order of several hundred degrees K), this is an

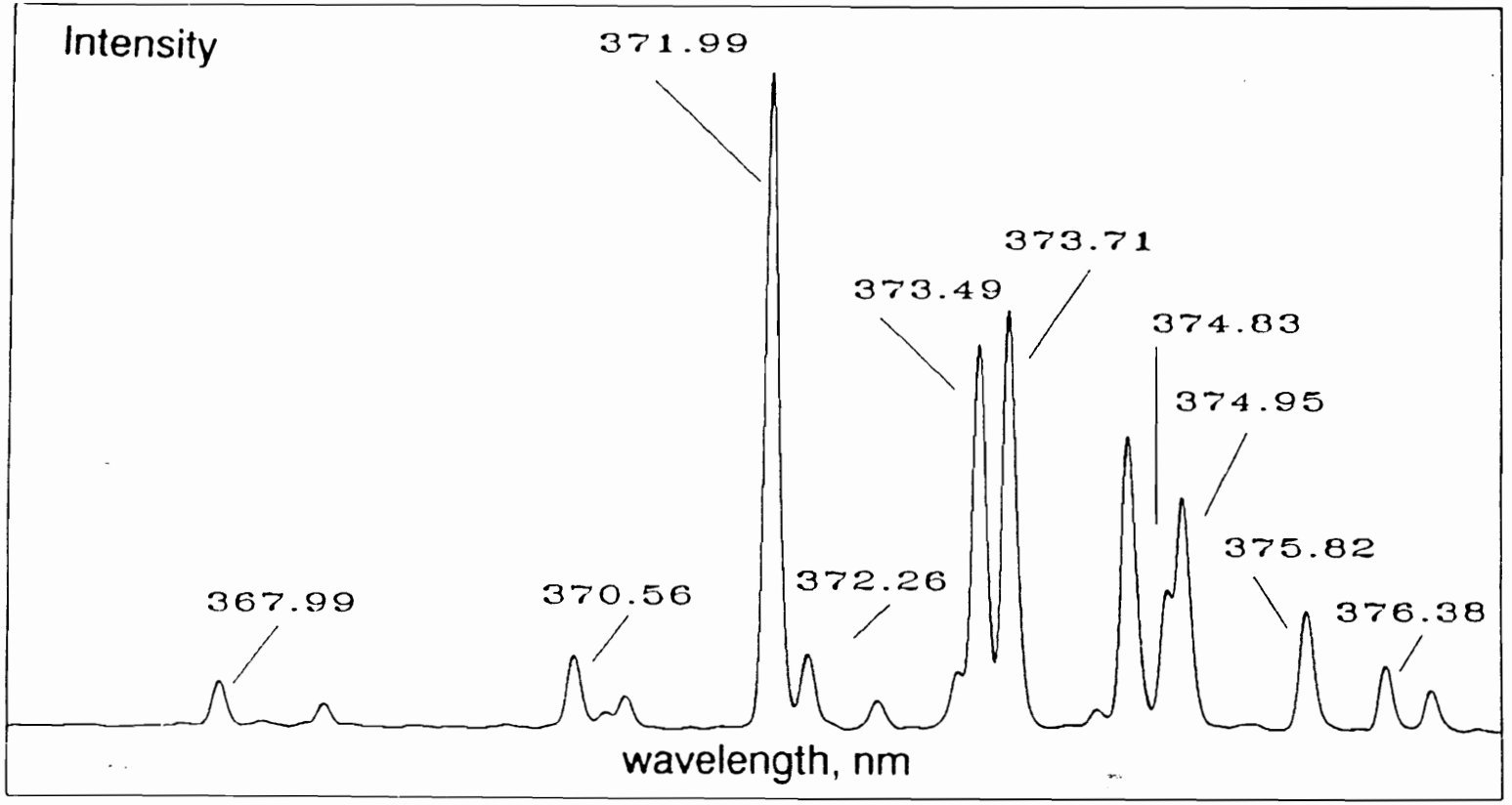

Figure 13 : Fe Emission Lines for T_{exc} Measurement

indication that the discharge is not near LTE conditions. A negligible difference is not conclusive evidence of the existence of LTE, but an indication that further study is necessary.

The ionization temperature calculation requires a measure of the relative intensities of both atomic and ionic emission lines for a single element. The ratio of these intensities is the basis for the T_{ion} calculation. The form of the Saha-Eggert equation used to determine T_{ion} is given below [35].

$$(I_i/I_a) = [4.83 \times 10^{15}/n_{e-}](g_p A_{pq}/\ pq)_i(\ pq/g_p A_{pq})_a \times T^{3/2} \times \exp[(-E_i - E_{pi} + E_{pa})/kT]$$

where:

Ii	=	ion line intensity
Ia	=	atom line intensity
n_{e-}	=	electron number density (electrons*cm^{-3})
g_p	=	statistical weight of level p (upper level)
A_{pq}	=	transition probability of the p-q transition (s^{-1})
	=	wavelength of transition (nm)
E_i^{pq}	=	ionization energy (eV)
E_{pi}	=	excitation energy of level p (ion) (eV)
E_{pa}	=	excitation energy of level p (atom) (eV)
k	=	Boltzmann's constant
T	=	ionization temperature (K)

This equation is employed in a laboratory written computer program [36] to iteratively determine T_{ion}, given T_{exc}, n_{e-}, and the ion to atom ratio of a given element. T_{exc} is used as the first temperature for a calculated ratio. This

T value is incremented within the program and the calculated ratio redetermined until an acceptable level of agreement (< 10% difference) between the two ratios (calculated and experimental) is reached. Elements commonly used for this experiment are: Ca, Sr, Mg, Cd, Zn, and Fe. However, any element can be used as long as the above parameters are available. Table III shows wavelength and constant information for some atom / ion pairs generally used [35].

Electron Number Density. Another way of describing the energetics of a plasma is the electron number density (n_{e-}). This is a measure of the concentration of electrons in the plasma discharge. This is often used in conjunction with temperature measurements as a means of comparing dissimilar plasmas. The n_{e-} is an important parameter as the free electron seems to be the most likely candidate causing analyte excitation (and ionization) in a plasma [35].

There are several ways of determining the number density, but the preferred method makes use of the Stark broadening of spectral lines. Electrons in the plasma create an electric field. This E field polarizes hydrogen (present in the plasma from water aspiration) removing energy level degeneracy and causing splitting of excited state levels (Stark Effect) to occur. This effect is manifested physically as broadening of the hydrogen emission line. The magnitude of broadening can be related to the

Table III

Wavelengths and Constants used for Ionization Temperature Measurements. (From Reference 35)

Element	(nm)	E_p(eV)	E_i(eV)	$g_pA_{pq}(10^8 s^{-1})$
Ca (I)	422.7	2.936	6.111	6.54
Ca (II)	393.6	3.152		5.88
Sr (I)	460.7	2.692	5.692	6.03
Sr (II)	407.8	3.042		5.68
Mg (I)	285.2	4.35	7.644	14.4
Mg (II)	279.5	4.43		10.4
Cd (I)	228.8	5.42	8.991	15.9
Cd (II)	226.5	5.47		6.0
Zn (I)	213.9	5.80	9.391	21.27
Zn (II)	202.5	6.13		13.2

concentration of electrons in the plasma (electron number density).

Densities measured in this fashion are relatively independent of plasma temperature and assumptions regarding LTE. Stark broadening theory is well developed and an extensive broadening data base is available, especially for hydrogen, as the theory is more accurate than for multi-electron species.

Of the several hydrogen emission lines available, the most often used is the H-beta line at 486.13 nm. This line is a strong, distinctive line in a spectral region relatively free of interference. This allows for a greater ease of accurate measurements.

The full width at half-maximum (FWHM) of the H-beta line can be related to electron number density via the following equation [37].

$$n_{e-} = C(n_{e-},T) \times (FWHM)^{3/2}$$

where: $C(n_{e-},T)$ = constant (function of n_{e-} and T)
FWHM = full width @ half-maximum of H-beta

The constant in the above equation is a function of the temperature and the magnitude of n_{e-}. It has one of two values, 3.84×10^{14} for a plasma greater than 5000K in T_{exc}, 3.68×10^{14} if the plasma temperature is less [37]. The

difference in the constants takes into account the likelihood of self reversal of the emission line at higher temperatures.

Electron number density is measured by slowly scanning across the 486 nm region of the spectra, obtaining a easily measurable trace. The FWHM is measured as either time or width in cm, and converted to angstroms knowing the scan rate and chart speed. The resultant width is then entered into a computer program which determines n_{e-}.

Chapter 4

Effect of Water on a Microwave Plasma

Introduction

The effect of solvent vapor loading on the Ar and He HEMIP is evaluated by examining the effect of spray chamber/condenser temperature, and hence solvent vapor loading, on transport process, the excitation and ionization temperatures, the electron number density, emission profiles and the limits of detection. The results of these experiments as well as an assessment of the effect of solvent vapor loading on the low power HEMIP is found below.

Experimental

Operating Conditions. The operating conditions used in this study are listed in Table IV. The applied forward power to the cavity was maintained at 130 W. The reflected power from the cavity was less than 3 W. The flow rate of argon gas was approximately 1.5 L/min, and the helium flow was maintained at 3 L/min. The range of temperatures used in this study was from 0^{o}C to 40^{o}C and was controlled to within 0.1^{o}C by the cooled circulating pump. The flow rate of the pump was 2 L/min. Temperatures below 0^{o}C resulted in the freezing of the aerosol in the spray chamber. Temperatures above 40^{o}C resulted in extreme condensation in the sample introduction system.

Table IV. Operating Conditions

Forward Power	130 W
Reflected Power	<3 W
Ar flow, total	1.5 L/min
He flow, total	3.0 L/min
Probe Penetration	96 %
Temperature Range	0½ - 40½ C
Uptake Rate, Ar	1.4 - 1.6 mL/min
Uptake Rate, He	0.5 mL/min
Coolant Flow	2 L/min

Total Solvent Load. The total solvent load was measured for this system by introducing a known volume of sample through the system, and measuring the amount of gas that was required for this introduction. The solvent that entered the discharge tube was collected with a cylinder containing silica gel, and measured gravimetrically. The mass of solvent collected divided by the volume of gas is a measure of the total solvent load (aerosol and vapor).

Aerosol Load. To differentiate between the aerosol and vapor loads it was necessary to determine the amount of solvent vapor that would be transported to the discharge tube in the course of a normal experiment. This was accomplished by passing a known amount of support gas through a thermostated chamber containing water. This flask was weighed before and after the experiment to determine the amount of vapor picked up by the flowing gas stream. The measurements were made for two different configurations of the gas flow. In the first case the gas was simply flowed over the surface of the water, so that minimal gas/water contact was obtained. For the second case, the tube from which the gas entered the flask was submerged in the water and the gas was allowed to bubble through the water on its path through the flask. The average of these measurements at each spray chamber temperature was used.

Solvent Efficiency / Analyte Efficiency. The efficiency with which the solvent and analyte passed through

the sample introduction system were measured in a manner similar to that of the total solvent load. The fraction of solvent that passed through the system to the discharge tube area was measured and divided by the total amount of solvent introduced to the system.

For the determination of the analyte efficiency, a known volume of a standard spectrometric solution was aspirated into the system. The fraction that passed to the discharge tube area was trapped in a flask filled with glass beads and a 5 % nitric acid solution. The glass beads ensured thorough contact between the bubbling gas and the acid solution. This solution and a fraction from the waste trap of the spray chamber were submitted for analysis by either ICP-AES or flame AAS. Mass balances performed on the results of the spectrometric determination yielded the percentage of analyte that exited the system at the torch.

Laser Scattering. The laser scattering experiments employed a 0.5 mW He-Ne laser. The laser beam was focused onto the aerosol stream which exited from the plasma torch (the plasma discharge was not ignited for these experiments). The scattered laser light was monitored at a right angle to the laser beam by the emission monochromator.

Results and Discussion

Effect of System Temperature on Solvent Load. Figures 14 and 15 show the effect of the spray chamber / condenser

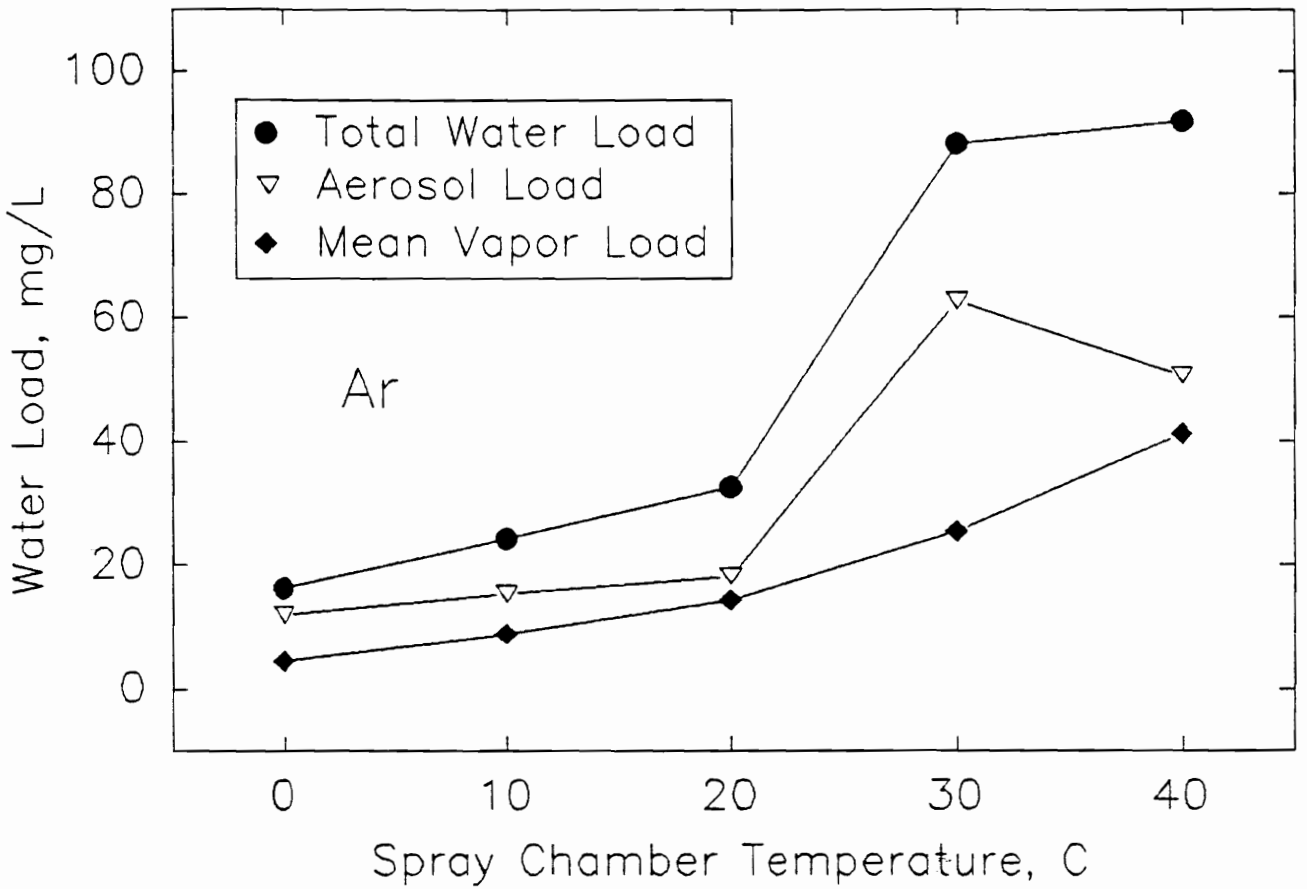

Figure 14. Water Load vs. Spray Chamber Temperature (Ar)

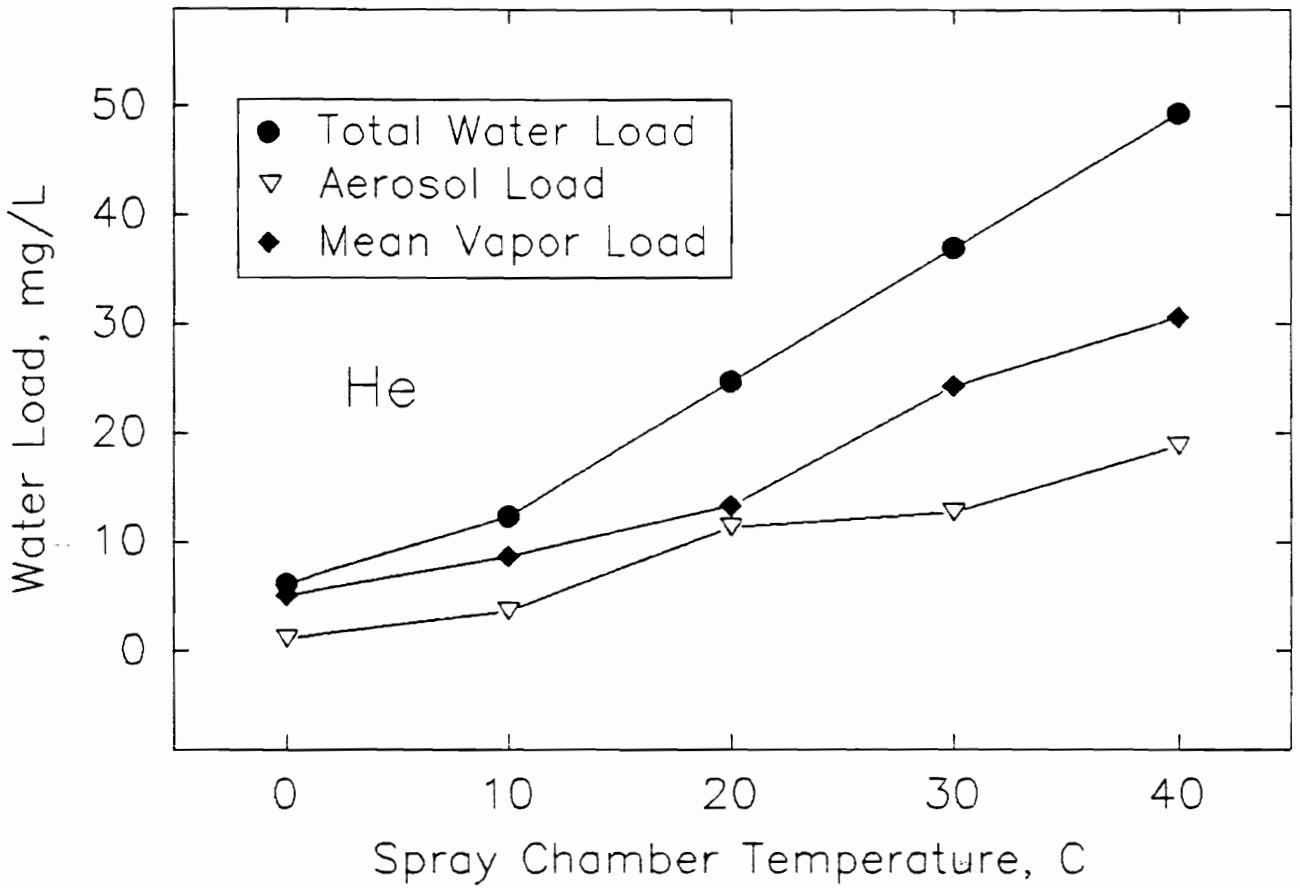

Figure 15. Water Load vs. Spray Chamber Temperature (He)

temperature on the solvent load in the plasma for Ar and He respectively. The total solvent load graph shows an increase for both gases up to 30^{o} where the curve begins to level off for Ar. The He curve still maintains the same slope beyond this value. At this point it may be theorized that for Ar the onset of saturation is occurring. The vapor load curves for both gases (average of the two vapor measurements) show a steady increase. The aerosol curve for Ar decreases between 30^{o} and 40^{o} C, again indicative of saturation occurring and an increase in the vaporization of water.

Effect of Cooling System on Sample Transport. The effect of the cooled temperature spray chamber/condenser system on the sample transport process is monitored by measuring the intensity of scattered laser light by the aerosol as a function of water loading.

The effect of temperature on the relative size and number of droplets entering the plasma can be assessed through the use of laser scattering measurements. The intensity of the scattered laser light can be related to the mean particle size and relative number of aerosol particles generated. It should be pointed out that in these experiments no attempt was made to employ light scattering theory to determine the size of the analyte droplets produced by the sample introduction system. Rather, the intensity of the signal was used to determine empirically

the combined number of aerosol droplets introduced into the plasma discharge. The intensity measurements in the middle of the temperature range are statistically the same. At the extremes of 0°C and 40°C, a decrease in the scatter signal is seen. The smaller decrease at 0°C is most likely a result of a small decrease in the uptake rate of the nebulizer.

The decrease in scatter signal at 40°½C is partially a result of a lower uptake rate (1.4 vs 1.6 mL/min) measured at this point. More importantly, it can be attributed to a reduction in the droplet size as a result of the evaporation of the droplets. The droplets generated by the pneumatic nebulizer are calculated to have an approximate residence time of 3 s in the cooling system. At 40°C significant evaporation should occur in this time interval. This evaporation would reduce the mean droplet diameter, resulting in a decreased scatter signal, and contributing to a greater quantity of solvent vapor being present in the plasma gas. In contrast, the effect of solvent vapor loading on the plasma should be diminished at temperature in the 0°C range due to the small amount of evaporation that would occur under these conditions.

For He, similar results were observed. In this set of experiments a peristaltic pump was used to control uptake rate and remove this variability. Again, a decrease in scatter signal is obtained at 40 degrees.

Solvent and Analyte Efficiencies. The solvent and analyte efficiencies for Ar and He are plotted in Figures 16 and 17. In the case of argon the analyte efficiency remains statistically the same while the increase in system temperature causes a large rise in the solvent efficiency. It would be expected from this data that the resulting analyte emission signals would be diminished at high temperatures / solvent loading conditions. For helium the result is slightly different. The analyte efficiency increases with temperature, as does the solvent efficiency. In this plot however, it can be observed that the slope of the solvent curve is greater than that of the analyte, such that the solvent load is increasing faster than the analyte. This should also result in decreased emission signals.

Excitation Temperature. The excitation temperature for the plasma was determined by employing the Fe slope method [32]. The excitation temperature was determined for the various water loading conditions in order to assess the effect of solvent loading on the Ar and He plasma.

The plasma excitation temperatures vs. water load are plotted in Figure 18 and 19. Two plots are shown in each figure. The shaded data points correspond to a plot of the aerosol load, while the open triangles show the plot vs. the vapor load. The error associated with each measurement is 3% and is illustrated with error bars on each figure point.

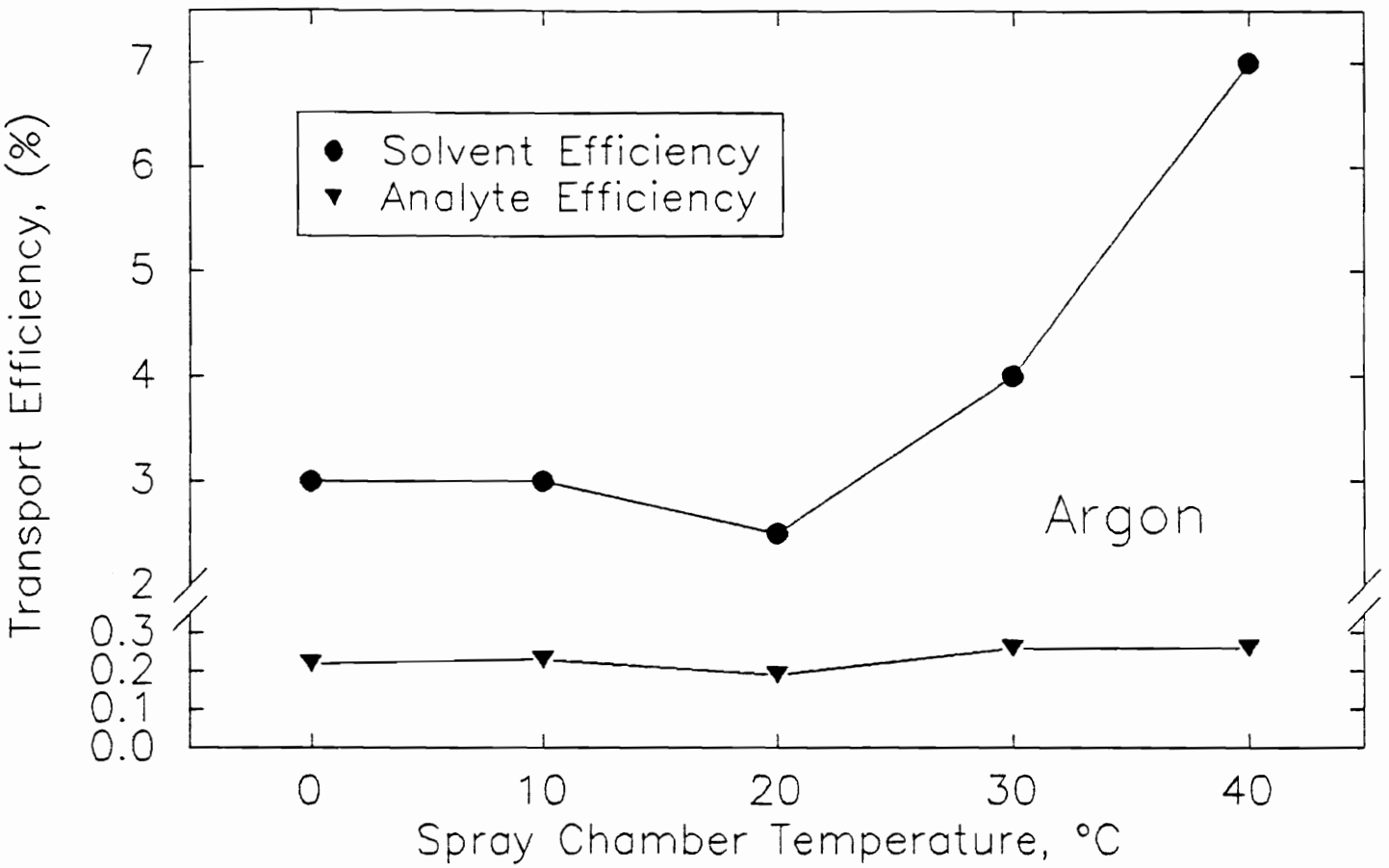

Figure 16. Transport Efficiency (Ar)

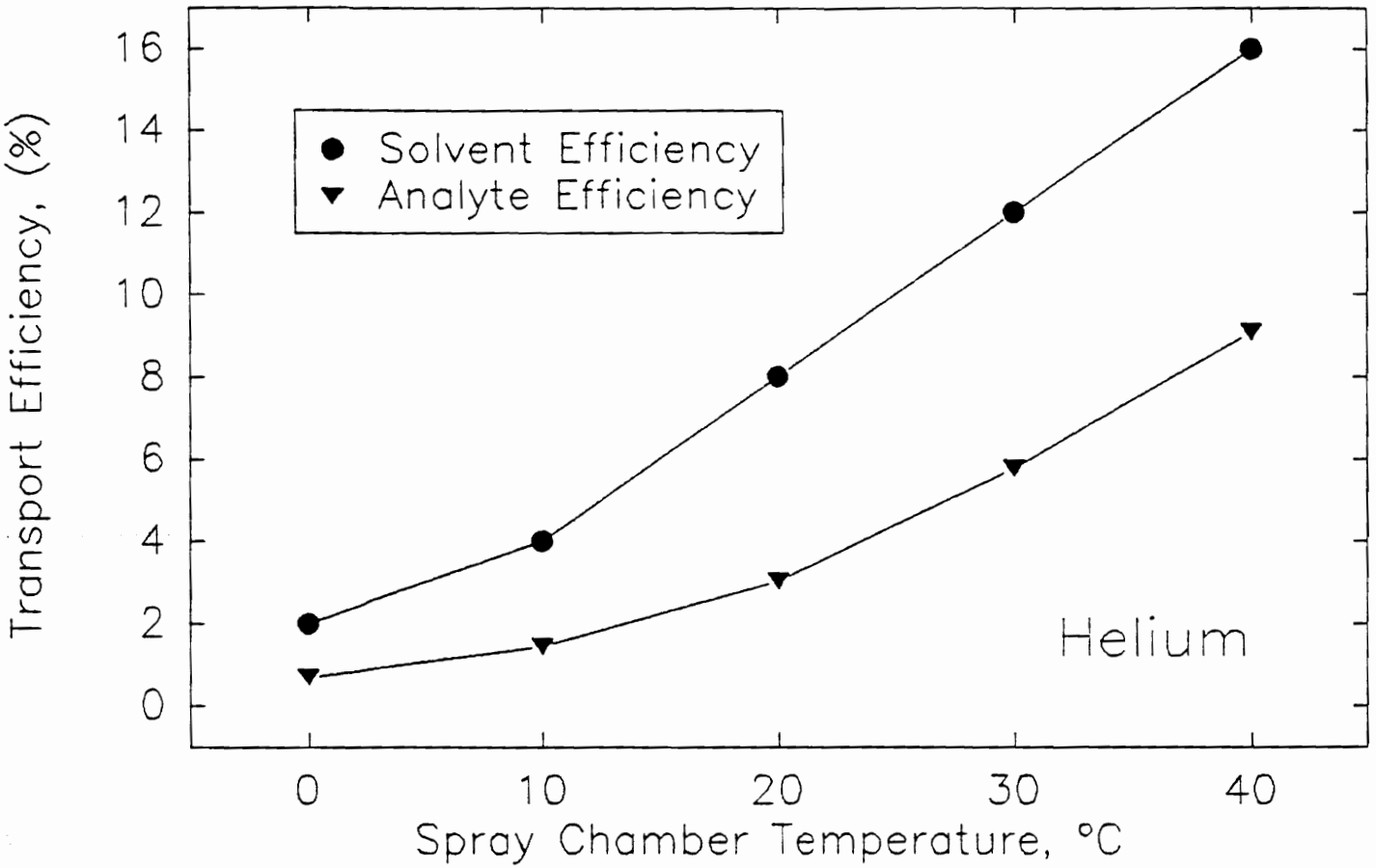

Figure 17. Transport Efficiency (He)

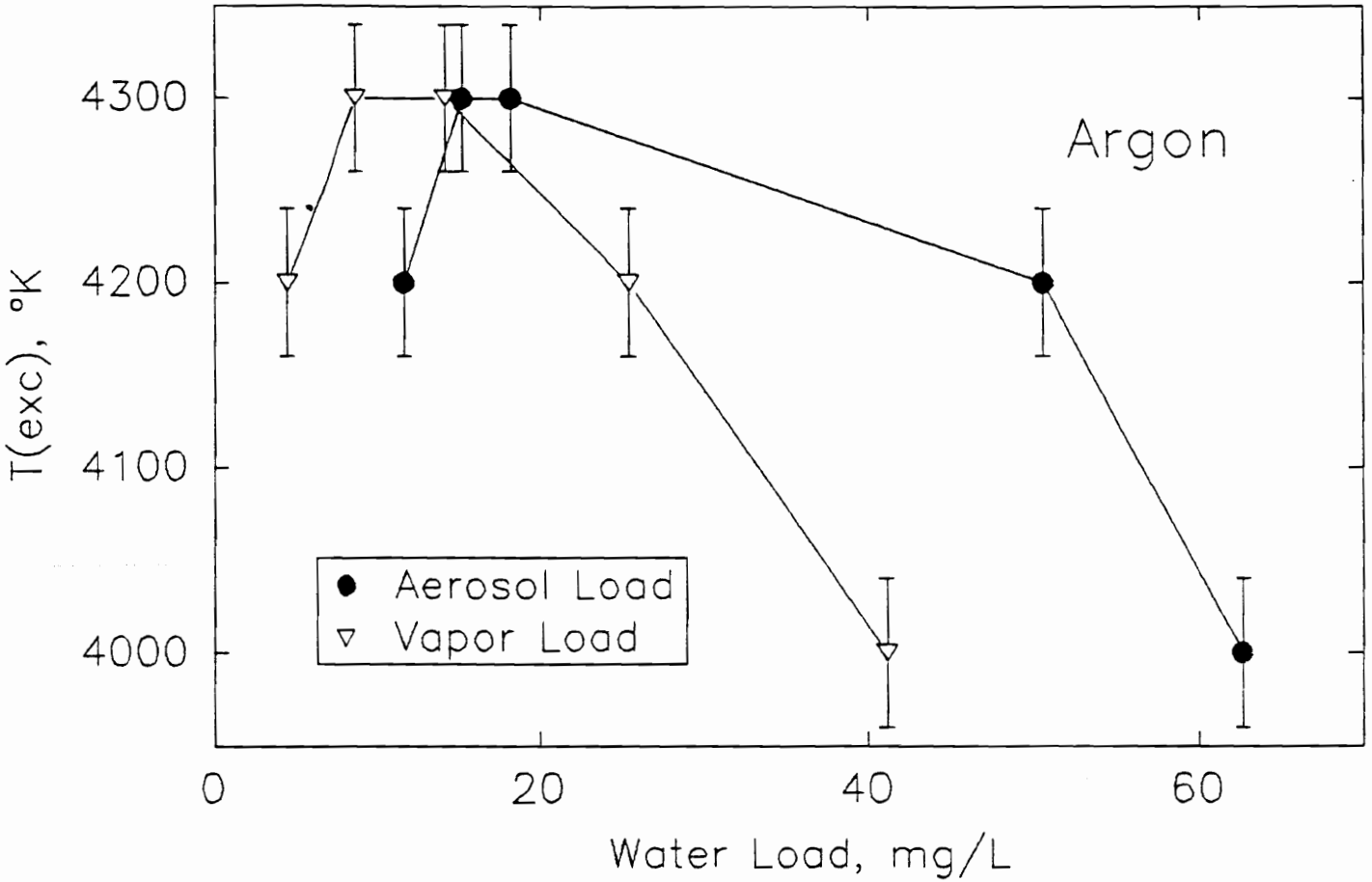

Figure 18. Excitation Temperature vs. Water Load (Ar))

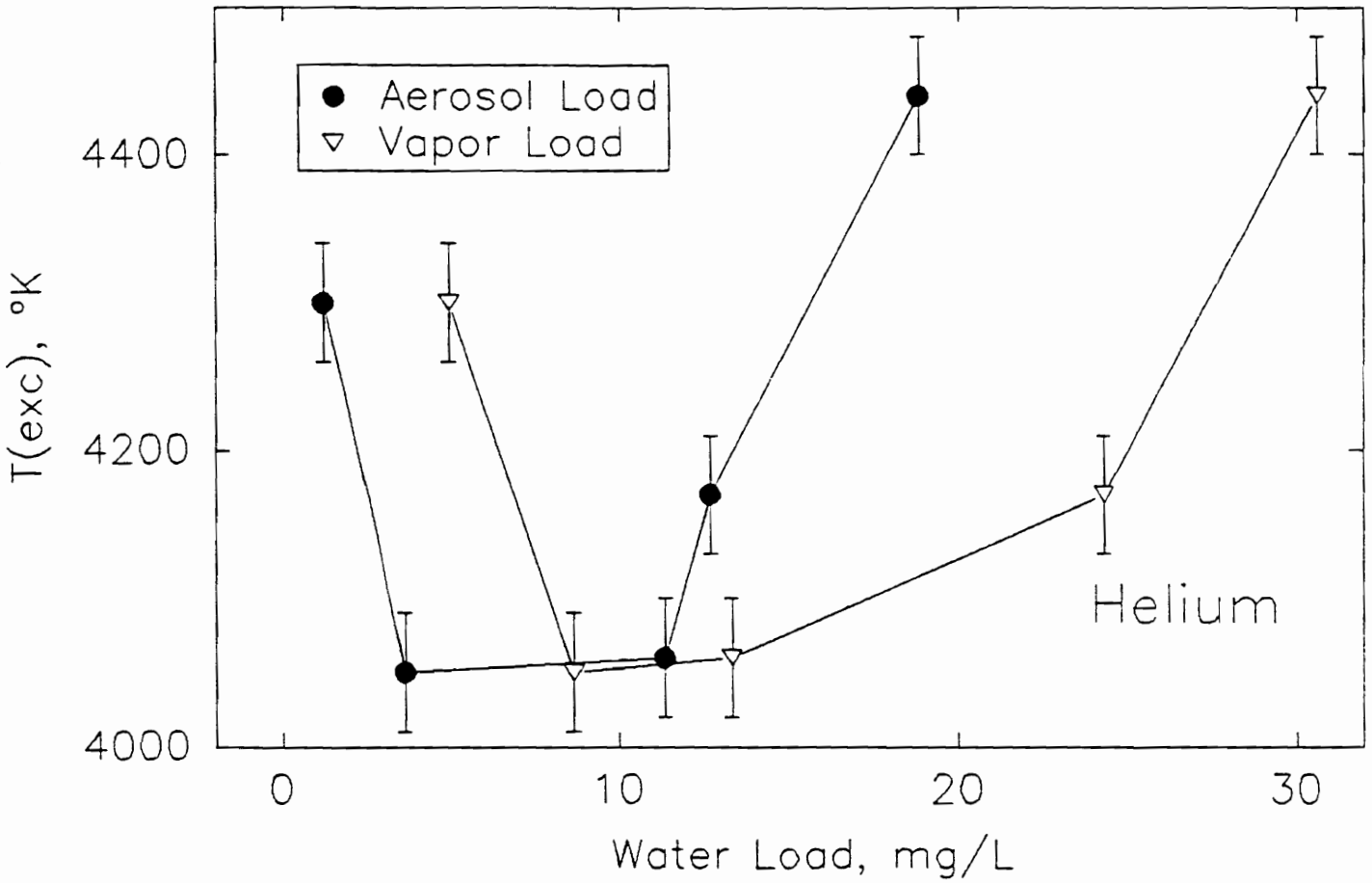

Figure 19. Excitation Temperature vs. Water Load (He)

By constructing the plots in this manner it is possible to assess which form of the solvent (vapor or condensed phase aerosol) has the greater effect on the plasma temperature. This can be done by examining the change in temperature as a function of each form. It should be stressed that this interpretation does not attempt to separate the interactions of the two forms of solvent in the plasma. Rather, this data analysis is used to learn which form has the greater influence on the analytical properties of the discharge.

Generally, for argon, a decrease in excitation temperature is noted for an increase in water load. Between the two plots, there is a better correlation of T_{exc} to the vapor load.

The data for He though is somewhat unusual. There is a definite U shape to the curve, with local maxima at the highest and lowest water loads. These data are the average of five repeat measurements and are reproducible. The trend in the raw data show a decrease in intensity of the lines used in this measurement with respect to increasing water load / spray chamber temperature, but the T_{exc} values are scattered.

Ionization Temperature. To further explore the effect of solvent loading on the HEMIP, ionization temperatures were measured employing the Saha-Eggert relationship [35]. The results of these measurements are shown in Figures 20

and 21. The argon results show a slight decrease in T_{ion} for both Ca and Mg, with increasing solvent load. The results for He are somewhat more noticeable. There is a 800 degree drop in the Mg T_{ion} from the lowest to highest water load situation. Again, for both Ar and He, there is a more direct correlation with respect to vapor loading.

Electron Number Density. The effect of system temperature / water load on the electron number density, ne- was also investigated. Plots of n_e-, determined using the method of Griem [36], versus water load are shown in Figures 22 and 23 for the Ar and He plasmas.

For argon the trends hold as with excitation temperature. The use of a 40½C system temperature causes a significant decrease in n_e- over the middle range. The highest n_e- value is obtained where solvent loading of the plasma is the least. Again there is a better correlation of n_e- to the vapor load.

The data for helium show wide scatter for the electron number densities. The error bar in the plot indicates that there is no significant change in n_e- with changing water load.

Emission Profiles. The effect of solvent vapor loading on the analytical emission signals can be shown by constructing emission profiles (signal vs. observation height) for the various spray chamber/condenser temperatures. The elements that were studied for both He and

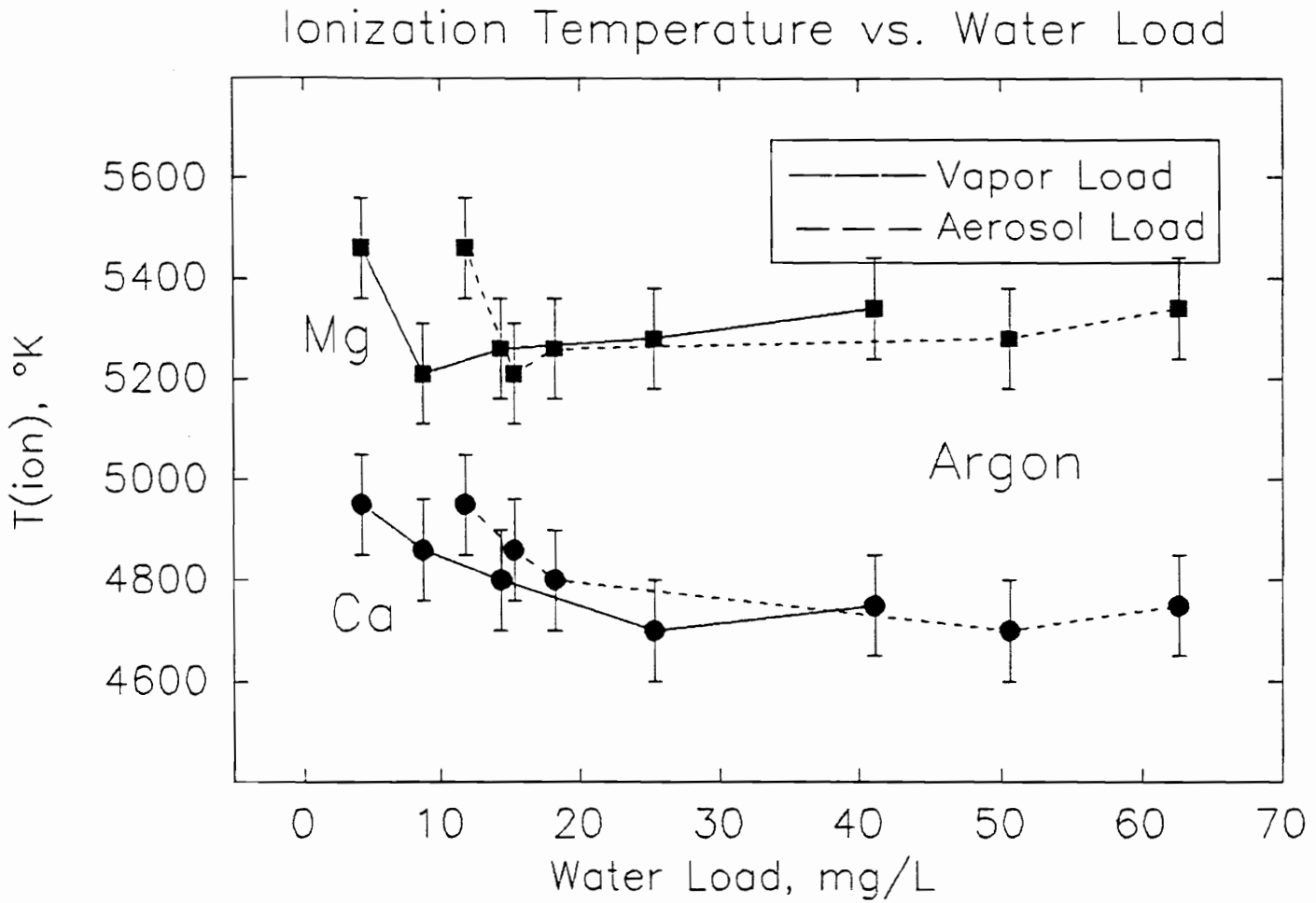

Figure 20. Ionization Temperature vs. Water Load (Ar)

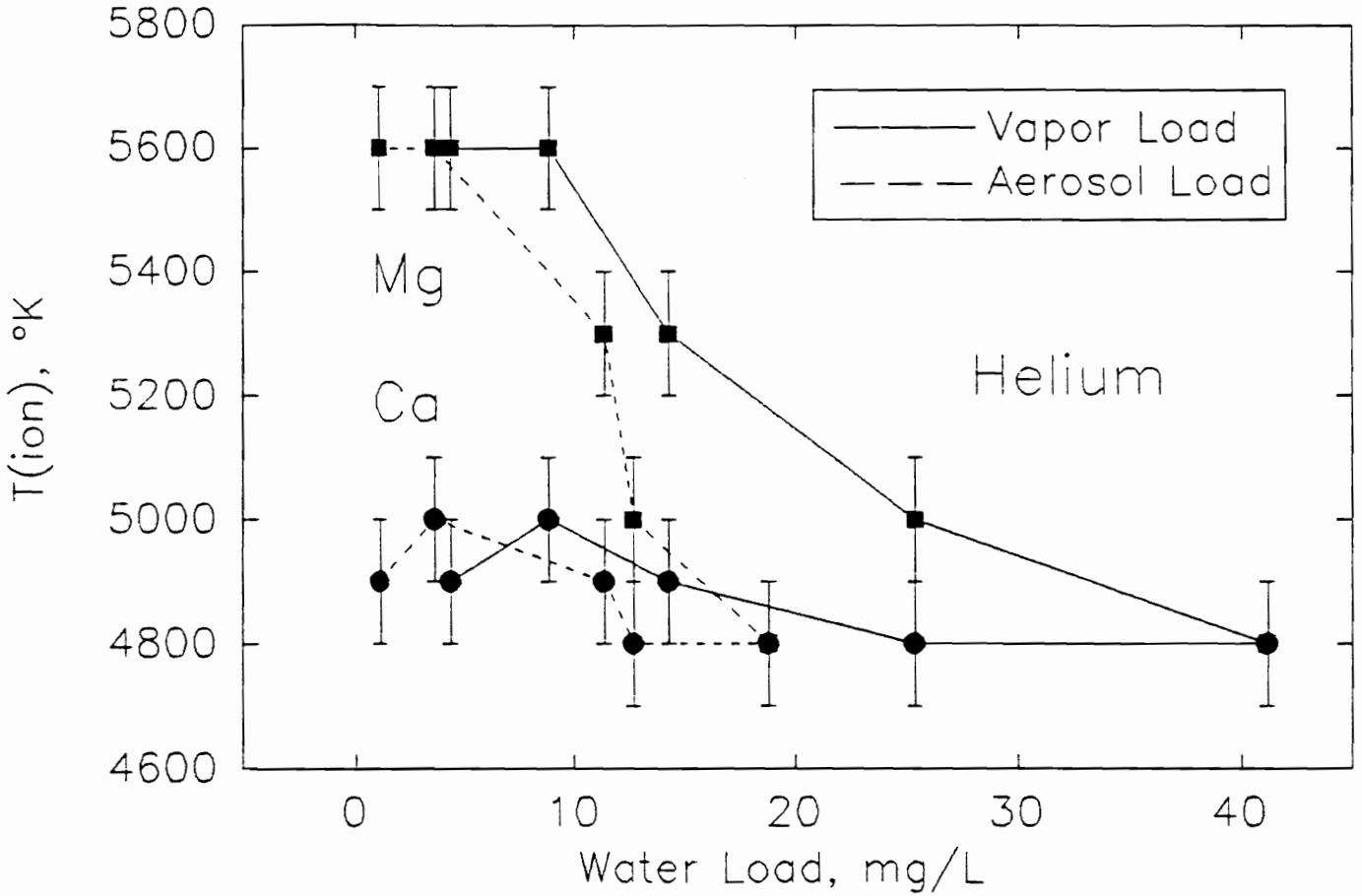

Figure 21. Ionization Temperature vs. Water Load (He)

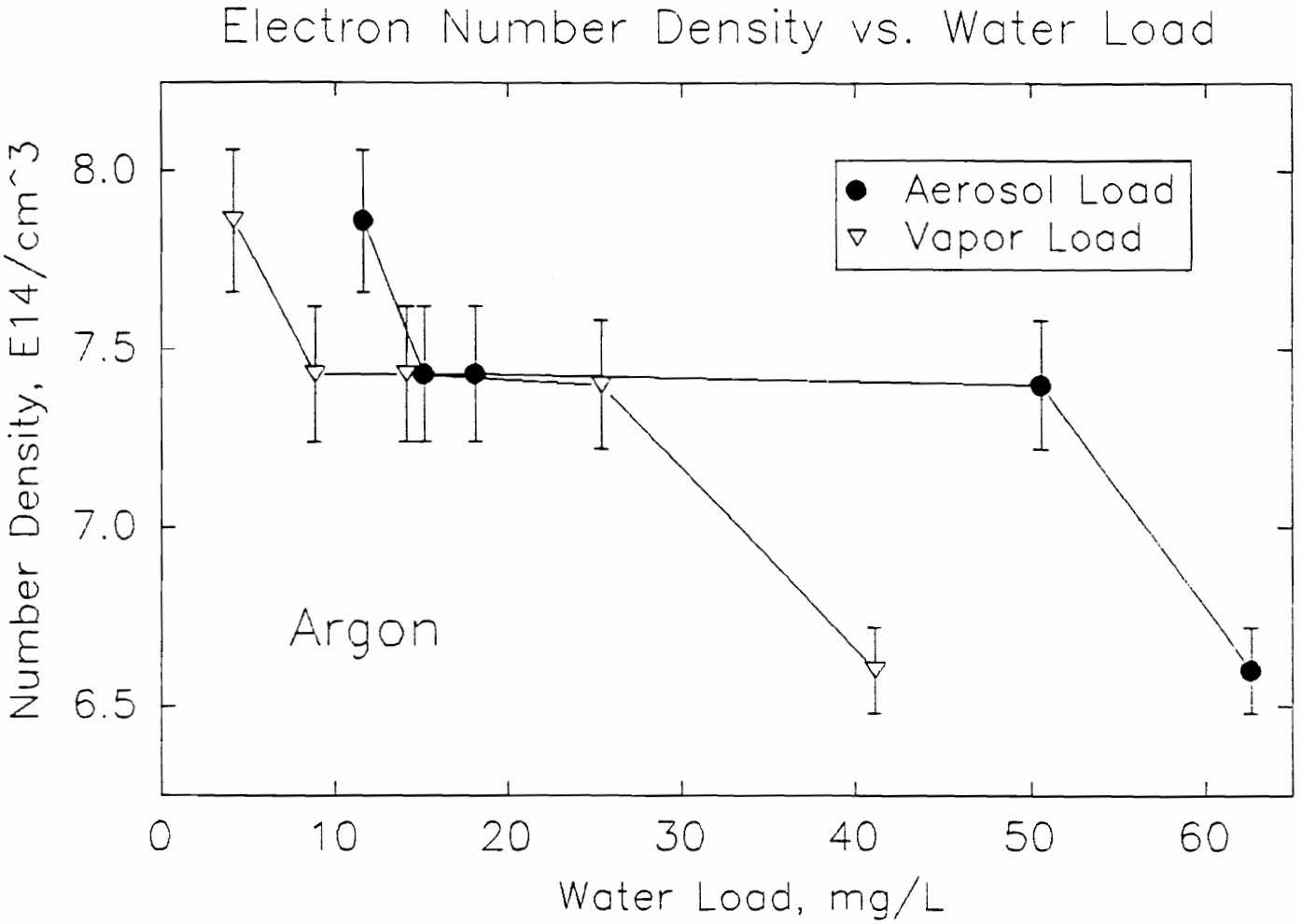

Figure 22. Electron Number Density vs. Water Load (Ar)

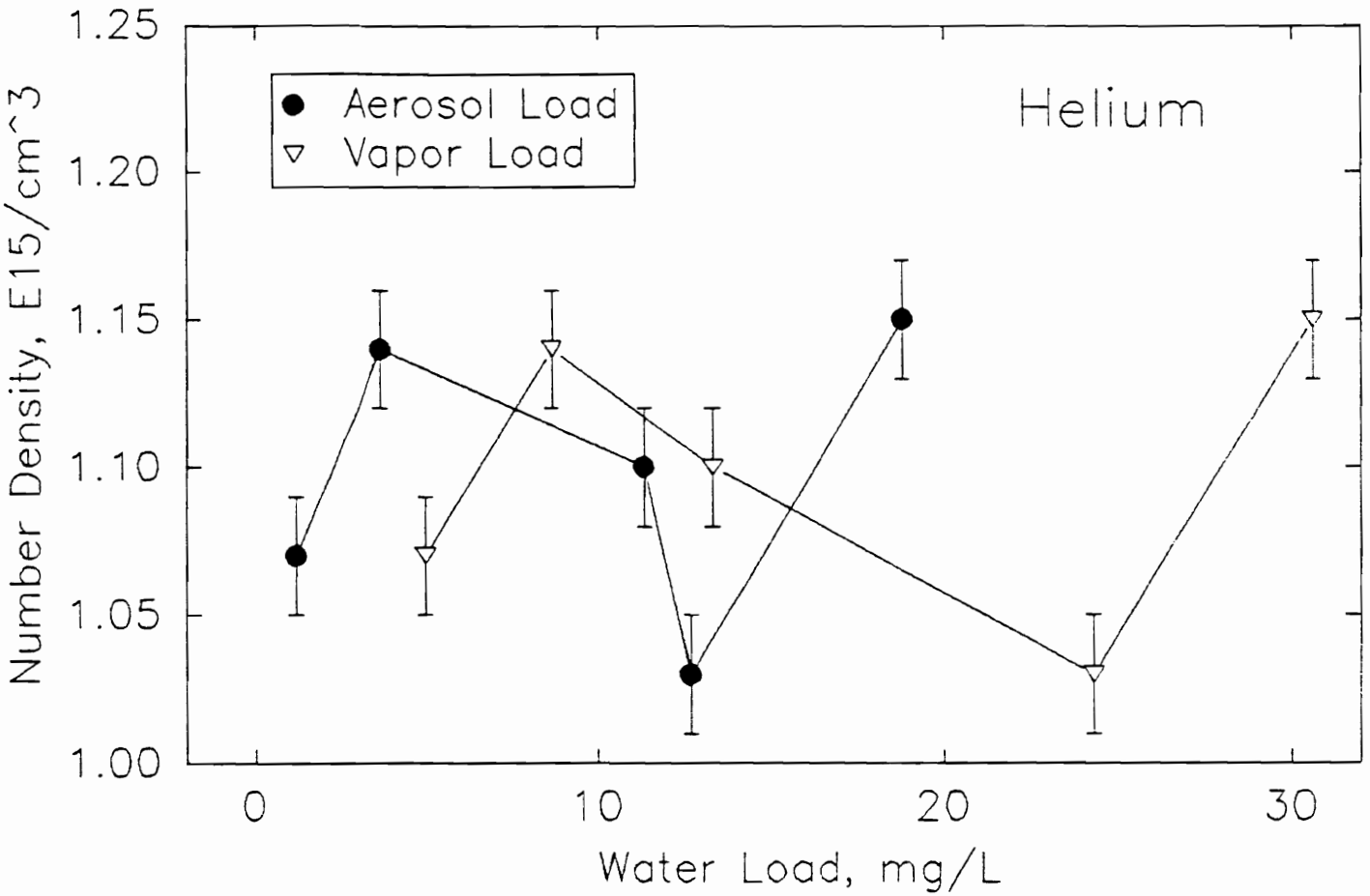

Figure 23. Electron Number Density vs. Water Load (He)

Ar are Co, Mg, Ca, and Na and were chosen because of their differing refractory natures. Profiles from a 100 ppm aqueous Mg and Na solution are illustrated in Figures 24-27 for the temperatures from $0^{o}C$ to $40^{o}C$ for Ar and $0^{o}C$ to $30^{o}C$ for He. He was not studied at 40^{o} as the emission had degraded so drastically. The emission units are in millivolts for Ar, volts for He, while the zero position of the observation height is flush with the surface of the cavity. The use of higher spray chamber/condenser temperature results in a decreased emission signal at all observation positions. At $40^{o}C$ the profile is barely discernible from the background emission for the solutions.

At lower temperatures a large enhancement of the signal is noted. This large increase in signal in attributed to a more energetic plasma discharge, which is the result of a lesser amount of water vapor being present in the plasma gas. A second feature in this profile that should be noted is a shifting of the emission maximum to higher observation heights for the lower spray/chamber condenser temperatures. This increase can be attributed to the production of larger diameter droplets by the sample introduction system (from reduced evaporation). Because analyte desolvation and vaporization is related to droplet diameter, the larger droplets should result an emission maximum later in the plasma tail plume. Similar trends were observed for Ca and Co.

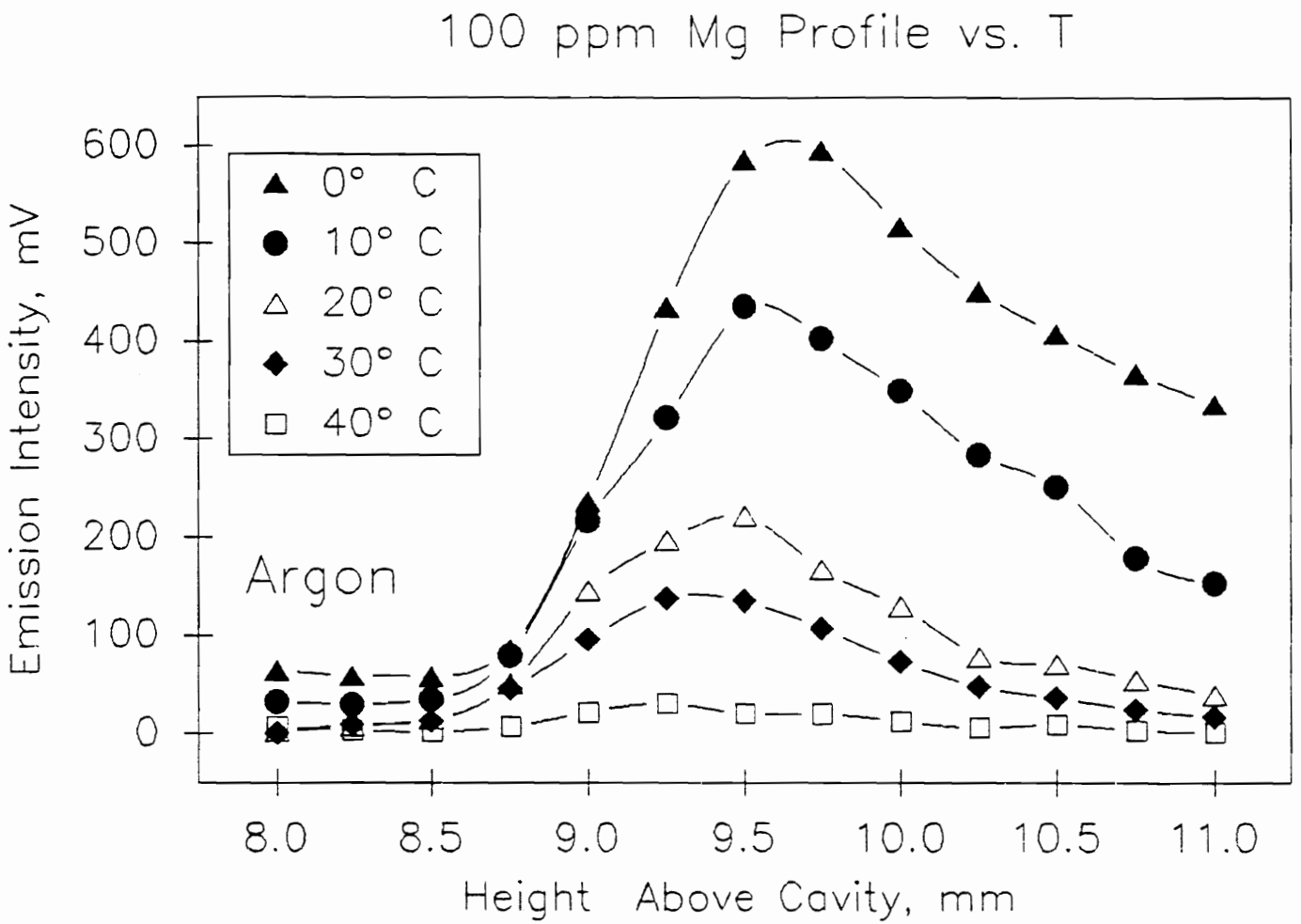

Figure 24. Mg Emission Profile vs. Temperature (Ar)

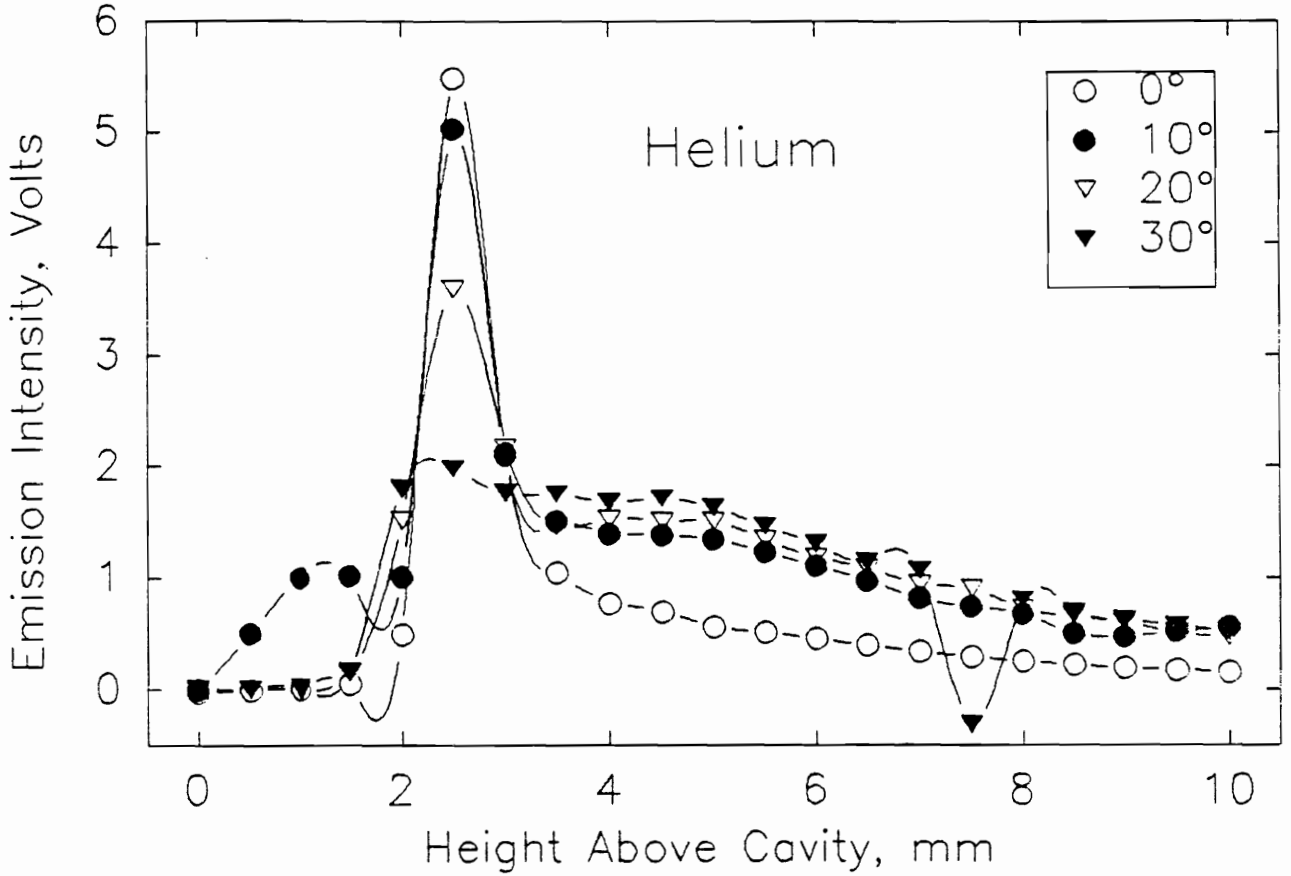

Figure 25. Mg Emission Profile vs. Temperature (He)

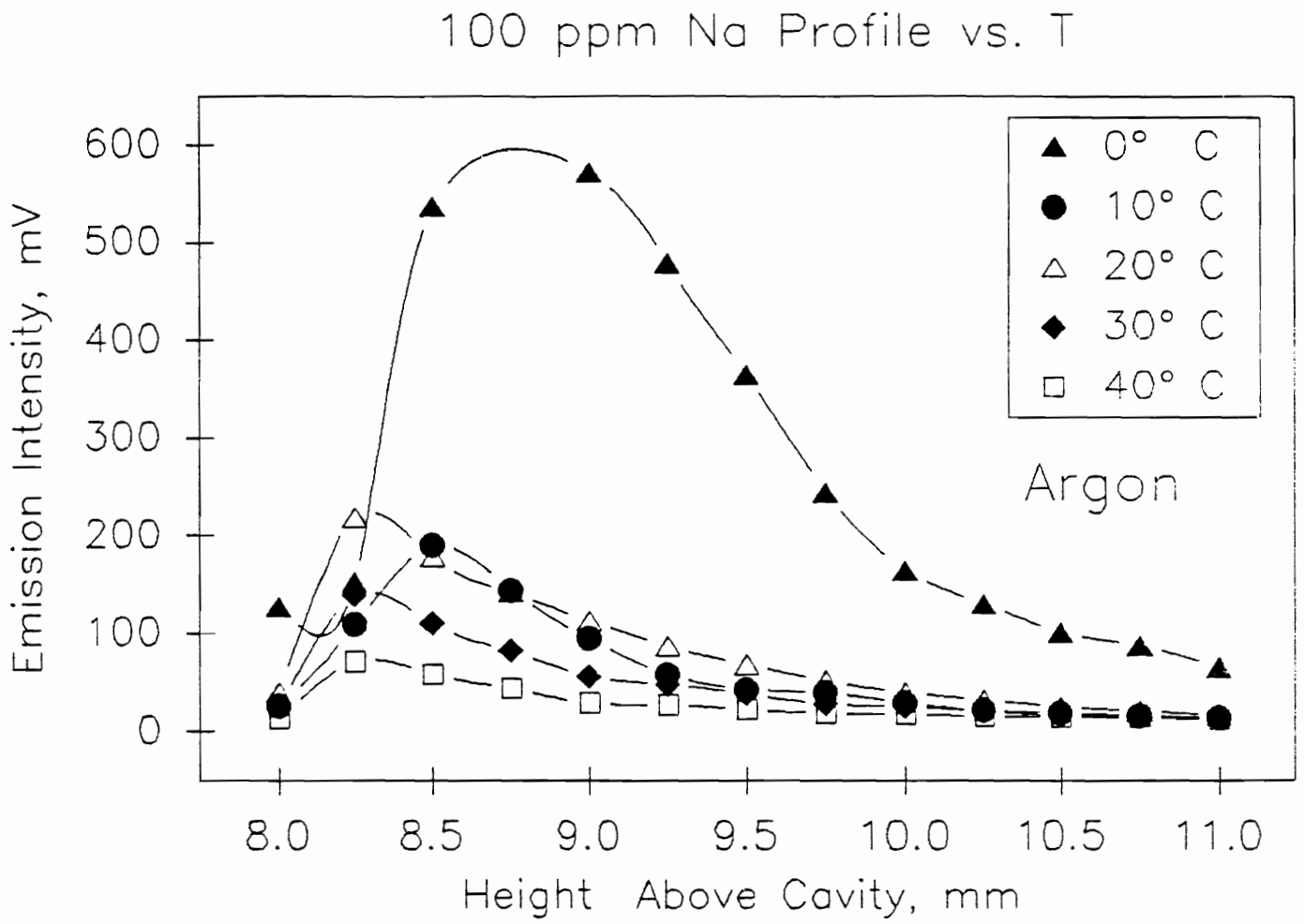

Figure 26. Na Emission Profile vs. Temperature (Ar)

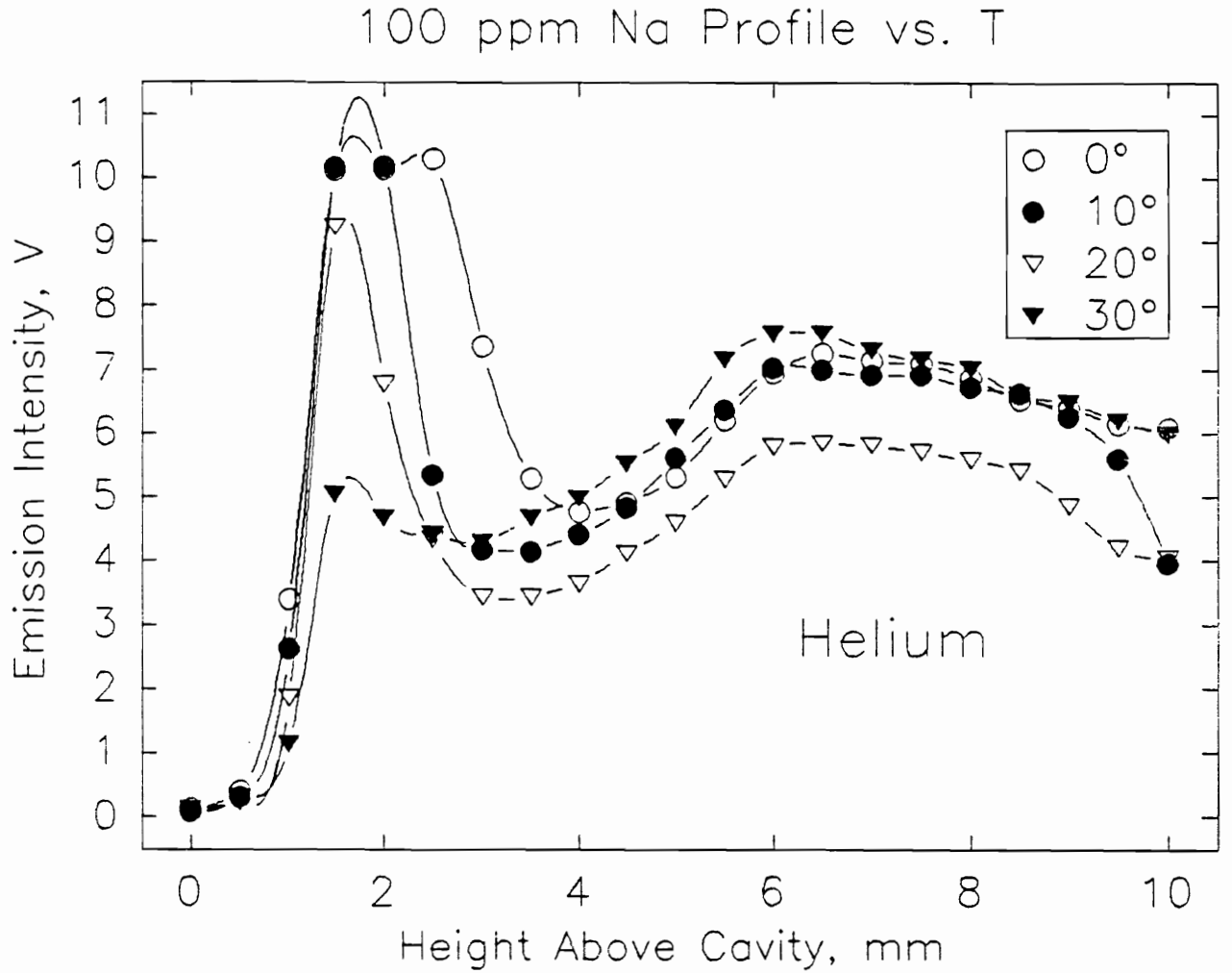

Figure 27. Na Emission Profile vs. Temperature (He)

The helium profiles show similar trends, except for the fact that the profiles have much sharper maxima. This is the result of the He discharge being physically smaller than the Ar discharge. Hence, the zone that can be used for the viewing of the emission signal is reduced. The lateral shifting of profiles here is less evident due to the increased maxima.

Limits of Detection. The effect of solvent loading on the Ar and He plasmas may also be observed by evaluating the limit of detection as a function of system temperature / water load. The values for several elements are presented in Table 5 for argon and Table 6 for He. A value of k=3 was used in these calculations. For the purpose of comparison, ICP limits are presented. For some of the elements, the limits of detection were only calculated for the optimum and ambient conditions. The degradation in the limit of detection can be attributed to the loss of energy in the plasma discharge from the presence of high levels of water vapor in the plasma gas. The limit of detection is noted to greatly improve with the use of lower temperatures. The effect on limit of detection of the change in water load is most noted for those elements of a more refractory nature. Those elements that are more easily ionized show less change with respect to water load.

One observation that does not seem to make sense upon initial consideration is the result that helium's limits of

Table V. Limits of Detection, k=3, Argon

All values are in parts per billion (ng/mL)

Element	Temperature					
	0	10	20	30	40	ICP[31]
Ca(I)	10	10	10	6	6	10
Ca(II)	9	9	8	9	8	1
Na	200	200	200	200	220	69
Co	150	170	280	150	200	20
Mg(I)	60	20	160	80	210	20
Mn	20			220		50
Fe	180			210		15
Zn	20			170		230
K	130			220		425
Sr	10			100		68

Table VI. Limits of Detection, k=3, Helium

All values are in parts per billion (ng/mL)

Element	Temperature				
	0	10	20	30	ICP[31]
Ca(I)	90	340	340	4400	10
Ca(II)	150	700	1000	8300	1
Na	20	50	40	40	69
Mg	80	180	130	250	20
Fe	140	420	850	2800	15
Mg(II)	360	320	9000	3400	65
Mg(I)	80		120		20
Mn	800		1400		50
Zn	1800		3200		230
K	630		2000		425
Sr	620		2200		68

detection are inferior to those of argon. As helium has a higher excitation energy, it would be expected that the He values for the limits of detection would be smaller. The solvent loading data also shows that He has a lesser solvent load per unit volume of gas. Again, it would be expected that this would cause an improvement in the He sensitivity.

It is only when the flow rate of gas is taken into account that it can be understood why He showed poorer results. The gas flow required to sustain the He plasma at the powers used is a factor of 2 greater than that of the Ar plasma. As equal powers were used for each case, the decrease in residence time that the analytes have in the plasma accounts for part of the discrepancy. Also, when consideration is given to amount of water in the plasma per unit time, as opposed to unit gas volume, the water load in the He plasma is actually greater in all cases. These considerations tend to support the observation that the He plasma is less sensitive under the given conditions.

Assessment of Solvent Vapor Loading. In the previous sections, The use of high solvent loads is shown to have a detrimental effect on the analytical performance of the HEMIP. The degradation in the excitation and ionization temperatures, electron number density and limits of detection is an indication that the water loading causes a reduction in the plasma energy. The solvent load is demonstrated to be composed of two separate parts, aerosol

and vapor. Experiments were performed to ascertain if one component of the total load had a more pronounced effect on the discharge. The vapor component of the solvent loading had more of a direct effect on the excitation conditions of the plasma discharge. This was determined to be the case by examining the plots of the excitation temperatures, ionization temperatures and electron number density vs. the solvent load. The graphs showed a more direct linear correlation when the diagnostic parameters were plotted against the vapor load.

Previous work, done on radio-frequency plasmas, shows the same detrimental effect of water on the plasma's energy and sensitivity [9,11,12,,22,23]. However, in these cases, the more direct negative effect was determined to be due to aerosol as opposed to vapor. Under these conditions, the aerosol droplets that enter the plasma have a greater effect on the discharge.

This observation is hypothesized to be due to a cooling effect. The large droplets must be desolvated and vaporized before emission can occur and it is believed that water droplets significantly cool the discharge. The vapor load, gaseous water, has little effect on the ICP. This theory is supported by the fact that under higher solvent loading conditions, there is a shift in the area of maximum emission in the ICP to areas further away from the core of the

discharge. The sample species must spend a longer time in the discharge to be sufficiently excited.

The effect of water loading on the HEMIP is hypothesized to be two fold. There is a decrease in energy due to the thermal cooling effect similar to the ICP. However, the main decrease in energy is due to the vapor loading. This effect may be explained by taking into account the difference in the frequency of the radiation employed to sustain the two plasmas.

In the case of the ICP, this radiation is in the radio frequency range, and there is no significant absorption of rf energy by water. This is not the case for the microwave radiation in the MIP. It is believed that significant absorption of the microwave field necessary for the sustenance of the discharge is being absorbed by the water vapor. To simplify, not only is the energy of the plasma being taken by a cooling effect in the discharge, but the vapor is absorbing the field energy and decreasing the amount of energy available for the plasma to maintain the discharge. This dual effect results in a greatly diminished plasma, one that becomes less useful as an atom cell for emission studies, as is evidenced by the increase in limits of detection with higher solvent load. These trends are consistent between the two support gases. Argon and helium both have the most energetic discharges under the minimal solvent loading conditions.

The partial pressure of water, which controls the evaporation, changes with temperature. The partial pressure of water in air is a factor of 2 higher at 40°C than at 20°C, and a factor of 11 higher at 40°C than at 0°C [38]. The percentage of water vapor in the plasma gas should greatly increase along these guidelines as the spray chamber/condenser system temperature increases. At 40°C, this percentage of water vapor in the plasma gas should be approximately 7% (based on partial pressures and assuming saturation).

The use of 0°C to 10°C results in an improved performance over ambient conditions. A more energetic discharge is produced, presumably from a smaller percentage of water vapor being contained in the plasma gas. An analysis of these data indicate that the cooling of a spray chamber results in a lesser quantity of water vapor entering the plasma discharge, hence, providing an enhanced analytical sensitivity for an argon microwave induced plasma.

Summary

Solvent vapor loading is shown to greatly affect the operational characteristics and analytical sensitivity of low powered Ar and He microwave induced plasmas. Though the use of a thermostated spray chamber/condenser system, solvent vapor loading was seen to have a detrimental effect

on the excitation and electron number density when high temperatures are used. At ambient temperatures, a lesser effect is seen on these parameters. However, the best sensitivity and detection limits were obtained when the aerosol was cooled to $0^{o}C$. It is presumed that at these conditions, the evaporation of the droplets is retarded and, coupled with a lower partial pressure of water vapor in the plasma gas, a lesser amount of water vapor is capable of entering and affecting the discharge. Since the uptake rate of the nebulizer and the relative scatter intensity of the aerosol is not statistically different at $0^{o}C$, as compared to ambient conditions, the presence of water vapor in the plasma gas is attributed to the observed reduction in temperature and degradation in detection limits.

Chapter 5

Ultrasonic Nebulization and the MIP

Introduction

To further study the effect of solvent loading on the HEMIP, studies were performed using an ultrasonic nebulization (USN) system. Although studies exist for the use of an ultrasonic nebulizer with Ar [39-41], these have been limited to using the ICP as an excitation source. The use of He as a support gas for ultrasonic nebulization has been studied [42], again using an ICP. It was noted that using He as a support gas for USN was limited as He was limited in its capacity to intermix with the nebulized sample to transport the analyte to the excitation source.

Only one study to date has been published using the ultrasonic nebulizer with a MIP [43]. This report was focussed on determining limits of detection, and no mention was made of solvent interactions.

This is the first documented study of the effects of solvent loading on the MIP using both Ar and He as a support gas. The USN lends itself well to this study in that the only solvent interactions that can take place are vapor phase as the heated desolvation chamber removes all aerosol from the gas stream.

Experimental

The apparatus for these studies has been listed in Chapter 2. The diagnostics performed have been described in

Chapter 3. The solvent loading measurements have been described in Chapter 4.

Operating Conditions. The optimized operating conditions for the evaluation of the ultrasonic nebulization system with the Ar and He HEMIP are listed in Table VII.

Results and Discussion.

Solvent Loading. The solvent loading measurements were performed as described previously. In the case of the ultrasonic nebulizer, as it employs a heated tube to completely desolvate the analyte stream, any solvent that reaches the plasma discharge is in the form of vapor. For argon, the plasma is loaded at the rate of 3.9 mg/L of gas and for helium the value is 7.5 mg/L.

Solvent Efficiency. The solvent efficiency data, measured by introducing a known amount of solvent through the system and collecting the fraction passed through the discharge tube was collected to determine any difference that existed between Ar and He as support gases for the UDX/HEMIP system. The experiments yielded results of 1 % for Ar and 3 % for He.

Analyte Efficiency. Analyte efficiencies were determined by introducing 50 mL of a 200 ppm Ca solution through the UDX system and analyzing the collected fractions by flame atomic absorption spectrometry (FAAS). The data yield efficiencies of 2.5 % by weight for Ar and 6.6 % for He.

Table VII. Ultrasonic Studies Operating Conditions

Forward Power	(Ar)	130 W
	(He)	130 W
Reflected Power	(Ar)	<3 W
	(He)	<1 W
Gas Flow	(Ar)	1.5 L/min
	(He)	3.0 L/min
Probe Pentration		96 %
Sample Flow Rate		0.85 mL/min
Heater Temperature		95 degrees C
Condenser Temperature		0 degrees C
Condenser Flow Rate		2 L/min

Excitation Temperature. The excitation temperatures, measured for the ultrasonic nebulizer are as follows. Replicate analysis for Ar yields a T_{exc} value of 4100 degrees. The helium value is statistically the same.

Ionization Temperature. The ionization temperatures for the UDX were measured for both Ar and He using two different thermometric species. Calcium and magnesium ion to atom ratios were collected and the T_{ion} values determined. For argon, the Ca T_{ion} was 5100 degrees K and the Mg T_{ion} equaled 5800 degrees K. For helium, the Ca value was 5000K and Mg was 5800K.

There is no significant difference between the respective values for Ar or He for either species. The difference between the Ca and Mg values is an indication that the plasma, for either gas, is not near local thermodynamic equilibrium.

Electron Number Density. Electron number densities, n_e^-, were determined by evaluating the Stark broadening of the H-Beta line. The values reported for each gas are the average of ten replicate measurements. For Ar, the number density was determined to be 7.5×10^{14} electrons per cubic cm. For He the value is 1.2×10^{15} e^-/cm^3.

Emission Profiles. Emission profiles for Ca(I), Ca(II), Co, and Mg are presented in Figures 28-31. These graphs show the argon and helium data are somewhat different. Overall two features distinguish the profiles. It can be noted that the overall sensitivity of the Ar

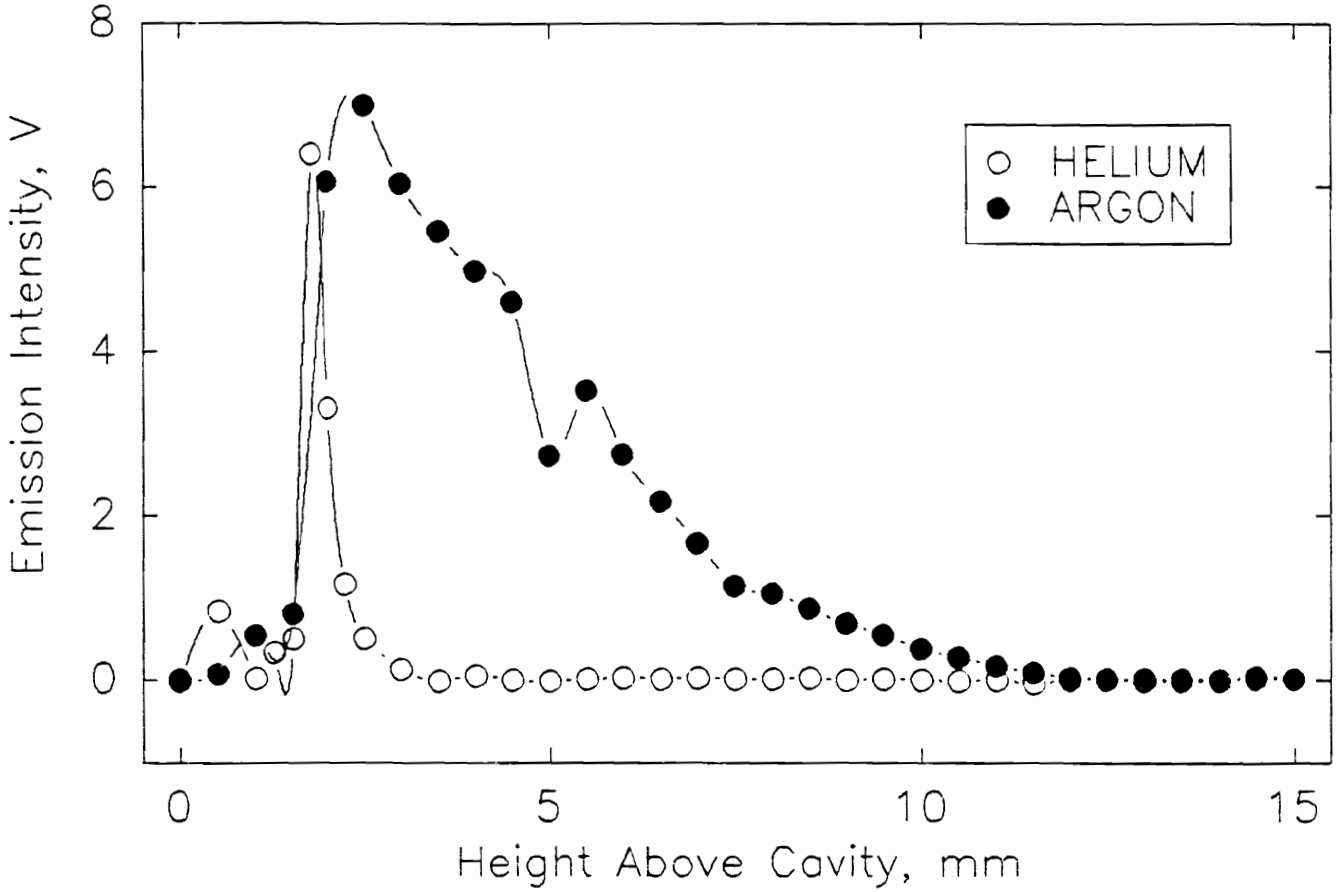

Figure 28. Ca(I) Ultrasonic Emission Profies

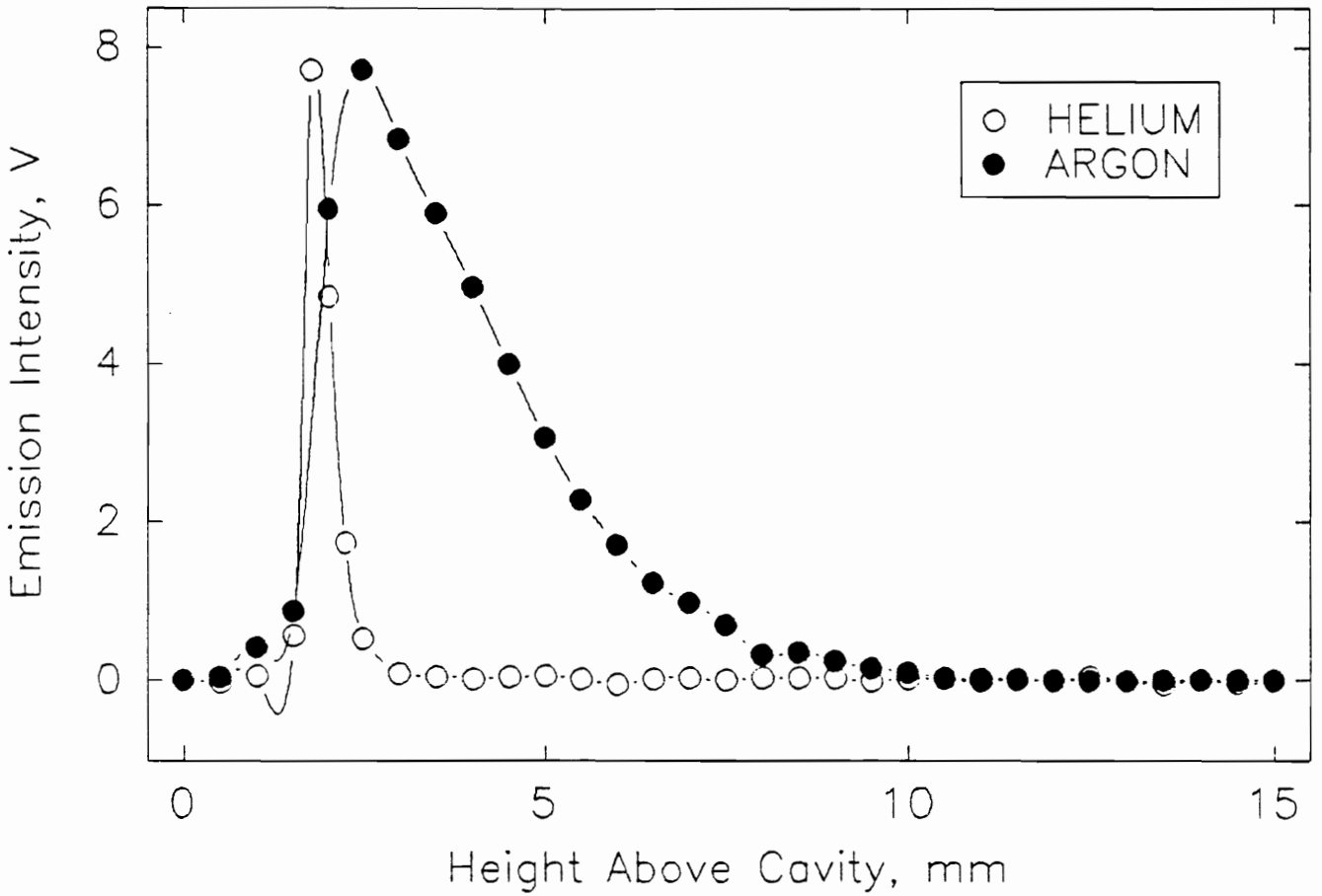

Figure 29. Ca(II) Ultrasonic Emission Profiles

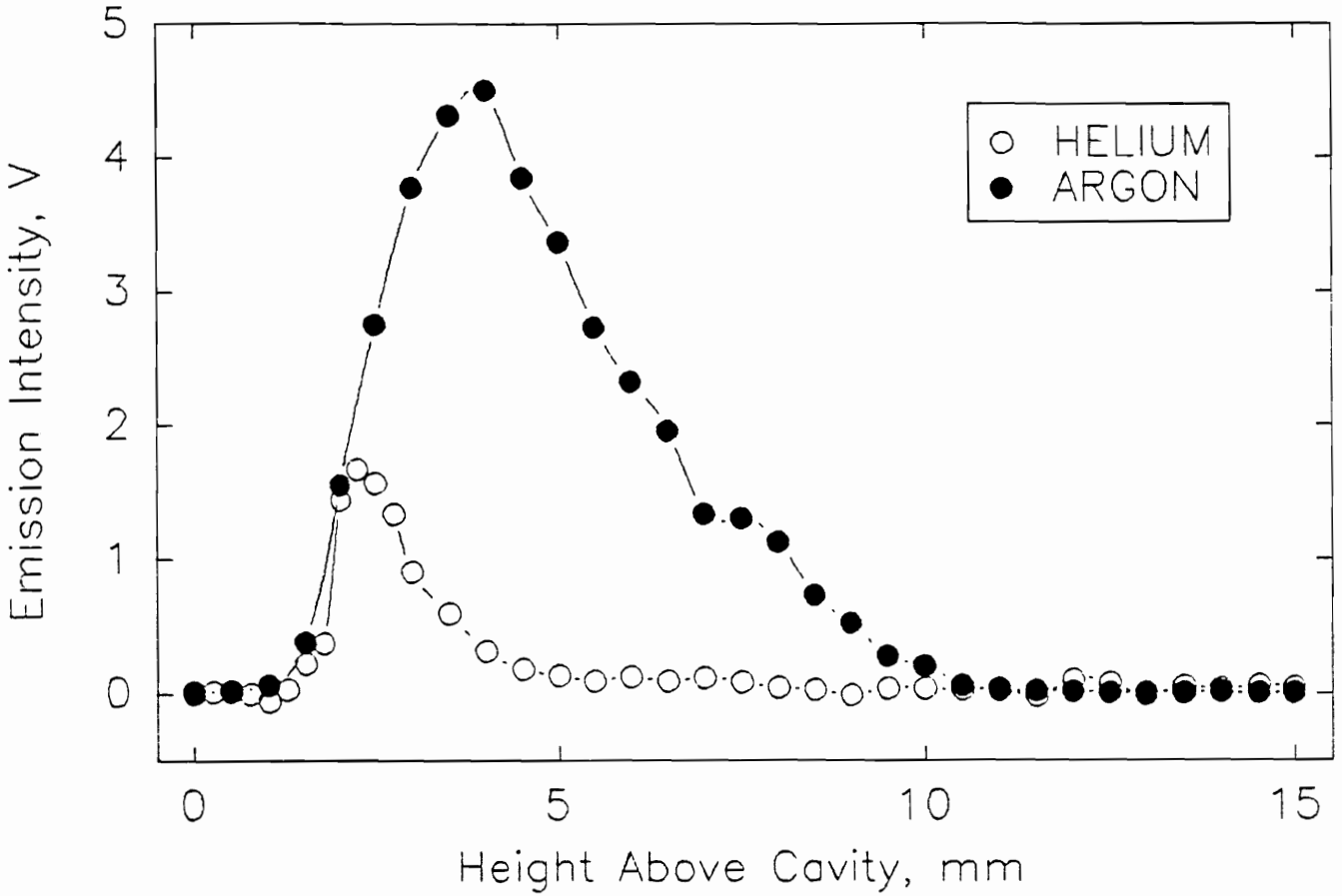

Figure 30. Co Ultrasonic Emission Profiles

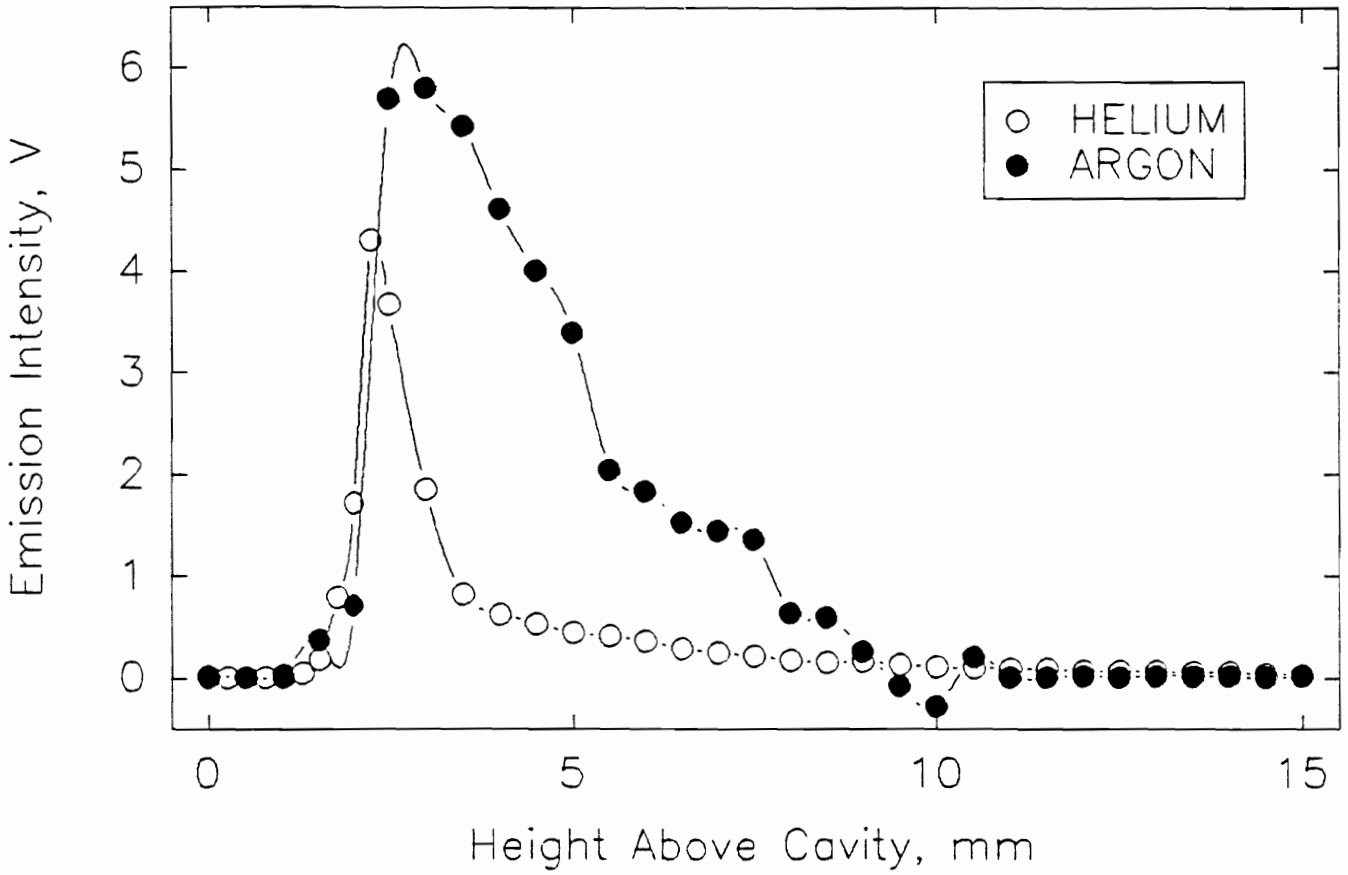

Figure 31. Mg Ultrasonic Emission Profiles,

plasma, as depicted by the maximum emission, is greater than that of the He plasma. The profiles were recorded under the same measurement sensitivities so any difference is indeed real. Secondly, the width of the profiles are widely different. For argon, the maxima slowly tail off to baseline values after 5 or more millimeters. The helium "peaks" are much narrower, again due to the smaller nature of the discharge.

Limits of Detection. The limit of detection data for both Ar and He are presented in Table VIII. Overall it can be observed that there is a slight sensitivity difference between the two gases with Ar being more sensitive in many cases. For some of the elements there is no significant difference between the values (i.e. Mn, Sr, Cr, and Zn). Analyzing the raw data shows that in general the analytical sensitivities for Ar are greater, and the standard deviations for the background are smaller. Comparative data is shown for the ICP. This data was provided by the manufacturer of the USN.

Summary. Overall, the diagnostics studies show that there is little, if any, difference between using the two support gases. The profiles and limits of detection indicate an increase in sensitivity when using argon. This may be due to two factors. The solvent loading for He is greater than that of Ar. Also the flow rate of gas required to maintain a stable He plasma is a factor of two greater. This will increase the amount of solvent per unit time in

Table VIII. Ultrasonic Limits of Detection

All detection limits are for k=3 and reported in parts per billion (ng/mL).

Element	Ar	He	ICP/USN
Ca(I)	1	30	0.04
Ca(II)	1	10	
Co	20	80	0.2
Cr	150	190	0.3
Fe	60	20	0.2
K	10	10	5
Mg(I)	2	10	0.2
Mn	10	30	0.1
Sr	20	20	0.1
Zn	20	50	0.3

the He plasma and decrease the time analyte resides in the excitation area. This helps to explain the sensitivity difference.

There is a difference in the shapes of the emission profiles. The argon emissions were much broader than those of He. This is due to the fact that the Argon plasma discharge is approximately two times larger than that of He. The Ar plasma extends outside of the confines of the plasma cavity and actually extends about 1 centimeter above the faceplate of the cavity. The He plasma does not escape the boundaries of the cavity. Thus the normal analytical viewing zone of the Ar plasma is larger, and the emission profile expected to be longer.

The sensitivity of the ultrasonic nebulizer is shown to be on the order of 10 to 25 times more sensitive than the pneumatic nebulization. The smaller droplet that the USN forms and the total aerosol removal in the desolvation chamber help to explain this difference.

Chapter 6

CONCLUSIONS

The primary objective of the research presented in this dissertation was to determine the effect of solvent (aerosol and vapor) loading on the Highly Efficient Microwave Induced Plasma. The total solvent load, defined as the amount of water that was introduced into the plasma discharge per liter of support gas was measured under a range of operating conditions.

Water was determined to have a detrimental effect on the plasma. The higher the solvent load, the less energetic the plasma became. As the fraction of water that entered the plasma increased, the analyte emission signal decreased. The plasma must desolvate and vaporize the species that enter it for radiative emission to occur. As the solvent to analyte ratio increased, it was only reasonable to assume that less energy would be available for analyte emission. Plasma diagnostic measurements, as well as limits of detection and emission profiles showed this to be the case.

The solvent load, measured for two different sample introduction systems was demonstrated to be composed of two separate parts, aerosol and vapor. Experiments were performed to ascertain if one component of the total load had a more pronounced effect on the discharge. The vapor component of the solvent loading had more of a direct effect

on the excitation conditions of the plasma discharge. This was determined to be the case by examining the plots of the excitation temperatures, ionization temperatures and electron number density vs. the solvent load. The graphs showed a more direct correlation when the diagnostic parameters were plotted against the vapor load.

Previous work, done on radio-frequency plasmas, showed the same detrimental effect of water on the energy and sensitivity of the plasma. In this case the aerosol is proposed to have the major effect. It is the thermal cooling of the plasma by large aerosol droplets that causes this decrease.

The effect of water loading on the HEMIP is hypothesized to be two fold. There is a decrease in energy due to the thermal cooling effect similar to the ICP. However, the main decrease in energy is due to the vapor loading. This effect may be explained by taking into account the difference in the frequency of the radiation employed to sustain the two plasmas. The radio frequency signal required to sustain an ICP is not attenuated by the presence of water. The microwave radiation of the HEMIP does. This is in essence the main difference between the effect of solvent on the ICP and MIPs in general and the HEMIP in particular.

When comparing the cooled pneumatic sample introduction system to the ultrasonic nebulizer with respect

to solvent load several factors must be taken into account. With the ultrasonic nebulizer, the only solvent that enters the plasma is in the form of vapor due to the heated desolvation chamber. This removes one step of the energy draining processes otherwise required of the plasma. Hence the discharge is more energetic to start with under equal power and gas flow conditions.

Ultrasonic nebulization also generates smaller analyte droplets. This leads to a greater number of smaller dried analyte particles per unit time, which are more easily excited in the plasma, leading to higher emission levels and higher analytical sensitivities. Overall, it is easy to see why the results for the ultrasonic nebulizer showed an improvement over the pneumatic case.

The difference in the performance between argon and helium as support gases is unusual. It is expected that He would provide a more sensitive source under all circumstances owing to the fact that He has a greater excitation energy (24 eV as opposed to 11 eV) than does Ar.

In this work, this is not shown to be the case. In every case the Ar plasma is shown to be more sensitive. Factors such as flow rate and the absolute magnitude of the solvent load help to explain the difference. Also when using radial profiles as opposed to axial, there is a hindrance to using He. The He plasma does not extend beyond the confines of the cavity, making radial profiles less

sensitive. The major reason axial profiles were not chosen to be the normal mode of measurement was due to the increased noise present when observing the full plasma discharge. The limitations in our experimental apparatus preclude these measurements.

The volume of the argon discharge was shown to be almost twice that of the helium. Taking this into account with the solvent load and the flow rate helps to explain the sensitivity difference.

The data presented in this dissertation provide a reasonable explanation as to why the amount of solvent loading in a microwave plasma has the effect that it does. Attempts should be made in all further work to minimize solvent loading to ensure maximum sensitivity. This will help to improve the already powerful capabilities of the HEMIP as a source for atomic emission spectrometry.

References

1. R. F. Browner and A. W. Boorn, Anal. Chem., **56**, 787A (1984).

2. L. G. Matus, C. B. Boss, and A. N. Riddle, Rev. Sci. Instrum., **54**, 1667, (1983).

3. C. I. M. Beenakker, Spectrochim. Acta., **32B**, 173 (1977).

4. L. D. Perkins and G. L. Long, Appl. Spectrosc., **42**, 1285, (1988).

5. L. D. Perkins and G. L. Long, Appl. Spectrosc., **43**, 297, (1989).

6. L. D. Perkins, C. B. Motley, K. A. McCleary, and G. L. Long, "A Helium High Efficiency Microwave Induced Plasma for the Atomic Spectrometric Determination of Metals and Nonmetals", Virginia Water Resources Research Center Bulletin 168, February, 1991.

7. C. B. Motley, M. Ashraf-Khorassani, and G. L. Long, Appl. Spectrosc., **43**, 737 (1989).

8. G. D. Christian, "Analytical Chemistry", Wiley and Sons, New York, (1986).

9. S. E. Long and R. F. Browner, Spectrochim. Acta., **43B**, 1461, (1988).

10. P. Schramel, Fresenius Z. Anal. Chem., **58**, 320, (1988).

11. B. L. Caughlin and M. W. Blades, Spectrochim. Acta., **42B**, 353, (1987).

12. S. E. Long and R. F. Browner, Spectrochim. Acta., **41B**, 639, (1986).

13. M. S. Cresser, and R. F. Browner, Spectrochim. Acta., **35B**, 73 (1980).

14. R. S. Houk, V. A. Fassel, G. D. Flesch, H. J. Svec, A. L. Gray, and C. E. Taylor, Anal. Chem., **52**, 2283, (1980).

15. J. W. Lam and J. W. McLaren, J. Anal. Atom. Spec., **5**, 419, (1990).

16. R. Tsukahara, M. Kubota, Spectrochim. Acta., **45B**, 581, (1990).

17. K. W. Olson, W. J. Haas, and V. A. Fassel, Anal. Chem., **49**, 632, (1977).

18. D. W. Hausler and L. T. Taylor, Anal. Chem., 53, 1223, (1981).

19. D. W. Hausler and L. T. Taylor, Anal. Chem., 53, 1227, (1981).

20. G. Kreuning and F. J. M. J. Maessen, Spectrochim. Acta., **44B**, 367, (1989).

21. T. Brotherton, B. Barnes, N. Vela, and J. Caruso, J. Anal. Atom. Spec., **2**, 389, (1987).

22. J. W. Olesik and S. Den, Spectrochim. Acta., **45B**, 731, (1990).

23. J. W. Olesik, L. J. Smith, and E. J. Williamsen, Anal. Chem., **61**, 2002, (1989).

24. G. L. Long and L. D. Perkins, Appl. Spectrosc., **41**, 980, (1987).

25. B. W. Smith and M. L. Parsons, J. Chem. Ed., **50**, 679, (1973).

26. R. D. Deutsch and G. M. Hieftje, Appl. Spectrosc., **39**, 214 (1985).

27. L. J. Galante, M. Selby, and G. M. Hieftje, Appl. Spectrosc., **42**, 559 (1988).

28. "Nomenclature, Symbols, Units, and their Usage in Spectrochemical Analysis II," Spectrochim. Acta., **33B**, 242, (1978).

29. G. L. Long and J. D. Winefordner, Anal. Chem., **55**, 713A, (1983).

30. P. W. J. M. Boumans, "Theory of Spectrochemical Excitation", Hilger and Watts, London, (1966).

31. A. Montaser and D. W. Golightly, eds., "Inductively Coupled Plasmas in Analytical Atomic Spectrometry", VCH Pubs., New York, (1987).

32. D. J. Kalnickly, V. A. Fassel, and R. N. Knisely, Appl. Spectrosc., **31**, 137 (1977).

33. W. L. Wiese and G. A. Martin, Wavelengths and Transition Probabilities for Atoms and Atomic Spectrometry, Part II, NSRDS-NBS 68, Washington, (1980).

34. J. S. Bolton, "The Effects of Organic Gases on Atomic Spectrometric Signals in the ICP", Ph.D. Dissertation, VPI-SU, Blacksburg, (1988).

35. M. W. Blades, B. L. Caughlin, Z. H. Walker, and L. L. Burton, Prog. Analyt. Spectrosc., **10**, 57 (1987).

36. H. R. Griem, "Spectral Line Broadening by Plasmas", Academic Press, New York, (1974).

37. L. D. Perkins, "Development and Characterization of a Low Power Helium Microwave Induced Plasma for Spectrometric Determinations of Metals and Nonmetals", Ph.D. Dissertation, VPI-SU, Blacksburg, (1989).

38. C. D. Hodgman, ed. "CRC Handbook of Chemistry", 38th edition, CRC press, Cleveland, Ohio (1956).

39. P. D. Goulden and D. H. Anthony, Anal. Chem., **56**, 2327 (1984).

40. C. E. Taylor and T. L. Floyd, Appl. Spectrosc., **35**, 408 (1981).

41. M. A. Floyd, V. A. Fassel, and A. P. D'Silva, Anal. Chem., **52**, 2168 (1980).

42. K. G. Michlewicz and J. W. Carnahan, Anal. Chem., **58**, 3122 (1986).

43. S. Chan and A. Montaser, Spectrochim. Acta., **40B**, 1467 (1985).

Appendix 1

Evaluation of a Demountable Tangential Flow Torch for Microwave Induced Plasma Atomic Emission Spectrometry

Introduction

The design of a tangential flow microwave induced plasma discharge tube is presented. Comparisons between this demountable torch and the conventional single-piece quartz design were performed. Factors that were used in this comparison were: excitation and ionization temperatures, electron number densities, emission profiles, and limits of detection. Both torches were evaluated using aqueous and supercritical fluid chromatographic sample introduction. Flow pattern testing shows that a helical flow of gas exists for both torches well above and below normal operating levels. The analytical performance of the new torch is shown to be statistically equivalent to the quartz design, while maintaining the advantages of greater reproducibility and ease of construction.

Literature Review

Much effort has been expended on the design attributes of the apparatus used in the field of plasma atomic spectrometry. A new commercially available system has been introduced [1,2], and many permutations of sources have been documented [3]. However, one critical component of these

systems remains underdeveloped. Discharge tubes, which define the plasmas geometry, continue to be a problem.

The plasma discharge tube, or torch, is a critical part of the plasma emission apparatus. It is in the torch where the support gas and analyte are combined and introduced to the plasma discharge. It is necessary that the discharge tube be capable of supporting a stable, centered plasma.

Several torch designs have been proposed in previous work on microwave plasmas. The most simple consist of a single quartz tube [4], one to six millimeters in inner diameter. Other torches, such as the laminar flow [5], tangential flow [6], and annular flow [7] are less simple, consisting of flow direction devices and complex glasswork.

Much success has been obtained in our laboratory using a modified tangential flow device, which is an adaptation of an earlier design by Hieftje and Deutsch [8]. The tangential flow design is beneficial in that the plasma discharge is constrained from touching the side walls of the torch by a helical flow of gas. This flow keeps the walls cool and prolongs torch lifetime, especially when He is used as a carrier gas. One drawback to this design is that the entire discharge tube is constructed as a single quartz unit. This requires expert glassblowing, and the end result is somewhat fragile. Indeed, the main cause of discharge tube failure is operator breakage. Also, as each torch is handmade, minor variations in the manufacture can cause a

torch to have differences in operation, causing an external source of deviation in an experiment. While the success rate for torches constructed in our glassblowing facility is greater than 60%, minor differences in operation are a fact of life.

One way to solve this problem would be to construct a mechanical torch. Such a design would be inherently more sturdy, and if the gas flow direction portion of the torch were permanent, and increase in reproducibility would be gained. Other advantages that could be attained with such a demountable torch would include the ability to quickly replace worn or broken quartz tubes, as well as vary the inner diameter or length of the tube, without changing the critical gas flow patterns.

Previous work in this laboratory has shown that such a design will indeed support an ignited plasma [9]. Early designs consisted of quartz bases joined to discharge tube sections by ground glass joints. While plasma operation was feasible with such a torch, the design was deemed even more fragile than the original torch, and also less stable.

A new design has recently been completed in our laboratory. This demountable discharge tube consists of a Teflon^{TM} base and flow director, Swagelok^{TM} gas fittings, and a simple quartz tube. This design allows for the quick change of damaged quartz tubes, and also gains the added mechanical resistance to breakage. This mechanical torch

shows much promise for use in MIP-AES. In order to fully evaluate this torches performance, a series of comparative studies were performed comparing this torch to the existing design for both aqueous and SFC eluent sample introduction.

EXPERIMENTAL

Diagnostics. Much of the relevant experimental information is listed in Chapters 2 and 3. That which has not been covered is listed below.

Quartz Torch Design. The single piece quartz torch (referred to as the "quartz" torch) is shown in Figure 1. This consists of a 6mm i.d. tube and a inner tube of 1mm i.d.. This inner tube serves to help promote a helical flow, and can be used as a means of introducing a sample flow, much like standard ICP torches. The sidearm is set at an angle with respect to the discharge tube axis and enters the main tube at a tangent. The plasma support gas and sample enter the discharge tube at this point and generate a helical flow.

Demountable Torch Design. The demountable torch design is shown in Figure 2. The body of the torch is machined from a Teflon^{TM} cylinder. This design has the capability to use a center tube for sample introduction, but this tube is not necessary for a helical flow of gas to be generated. A Teflon^{TM} plug seals the center tube hole when not in use. The inner diameter of the body is drilled so that the outer

Figure 1

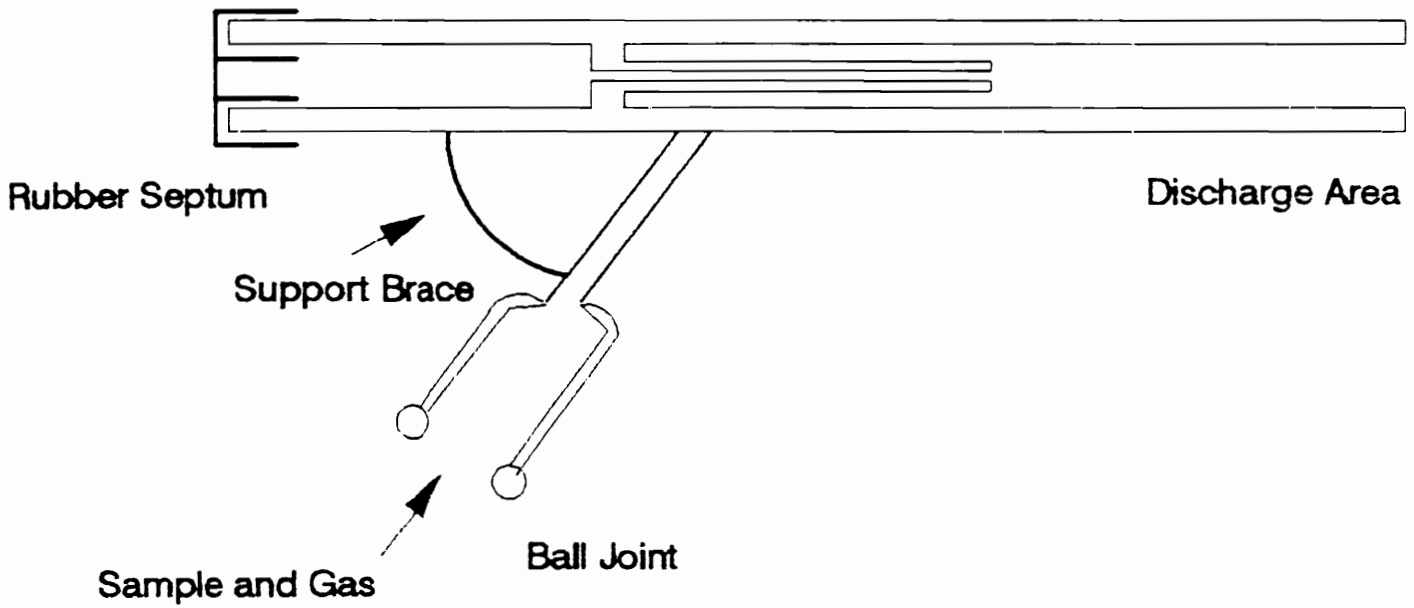

Figure 1. Quartz Torch Design

Figure 2

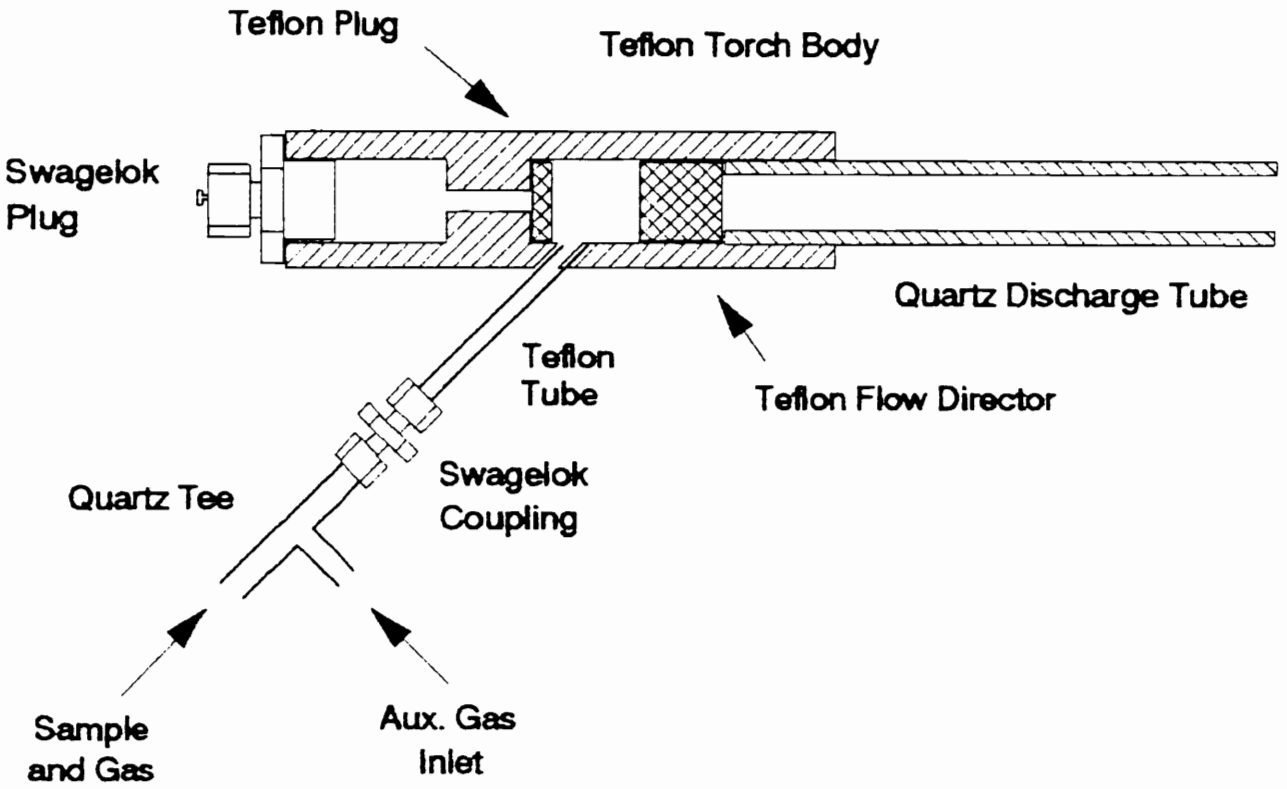

Figure 2. Demountable Torch Design

diameter of the quartz discharge tube (8mm) inserts snugly. Teflon™ tape may be wrapped around the base of the discharge tube section to insure a tight fit. The discharge tube bottoms out against the flow director. This is a tightly fit Teflon™ cylinder which has been carved with a groove circling the outer diameter. It is this groove which is responsible for the generation of the helical gas flow. The analyte/gas stream enters the torch through a Teflon™ tube which is inserted into an angled hole drilled into the side of the torch. A Swagelok™ fitting couples the Teflon™ tube to a T-union where the nebulizer gas flow and an auxiliary flow meet. A Swagelok™ plug seals the end of the body. This plug, along with the appropriate ferrule, also serves as a convenient connector for central tube sample introduction.

Reagents. SFC grade CO_2 (1500 psi He headspace and dip tube) was purchased from Scott Specialty Gases (Plumsteadville, NJ). Chromatographic iron standards were made of ferrocene (Sigma Chemical, St. Louis, MO) dissolved in HPLC grade methylene chloride (Fisher, Raleigh, NC).

Experimental Apparatus. Table 1 lists the apparatus used in this project that was not listed in Chapter 2. Figure 3 shows a block diagram of the equipment used. Inset A of Figure 3 shows the aqueous sample introduction apparatus, and inset B shows the equipment used for SFC

Figure 3

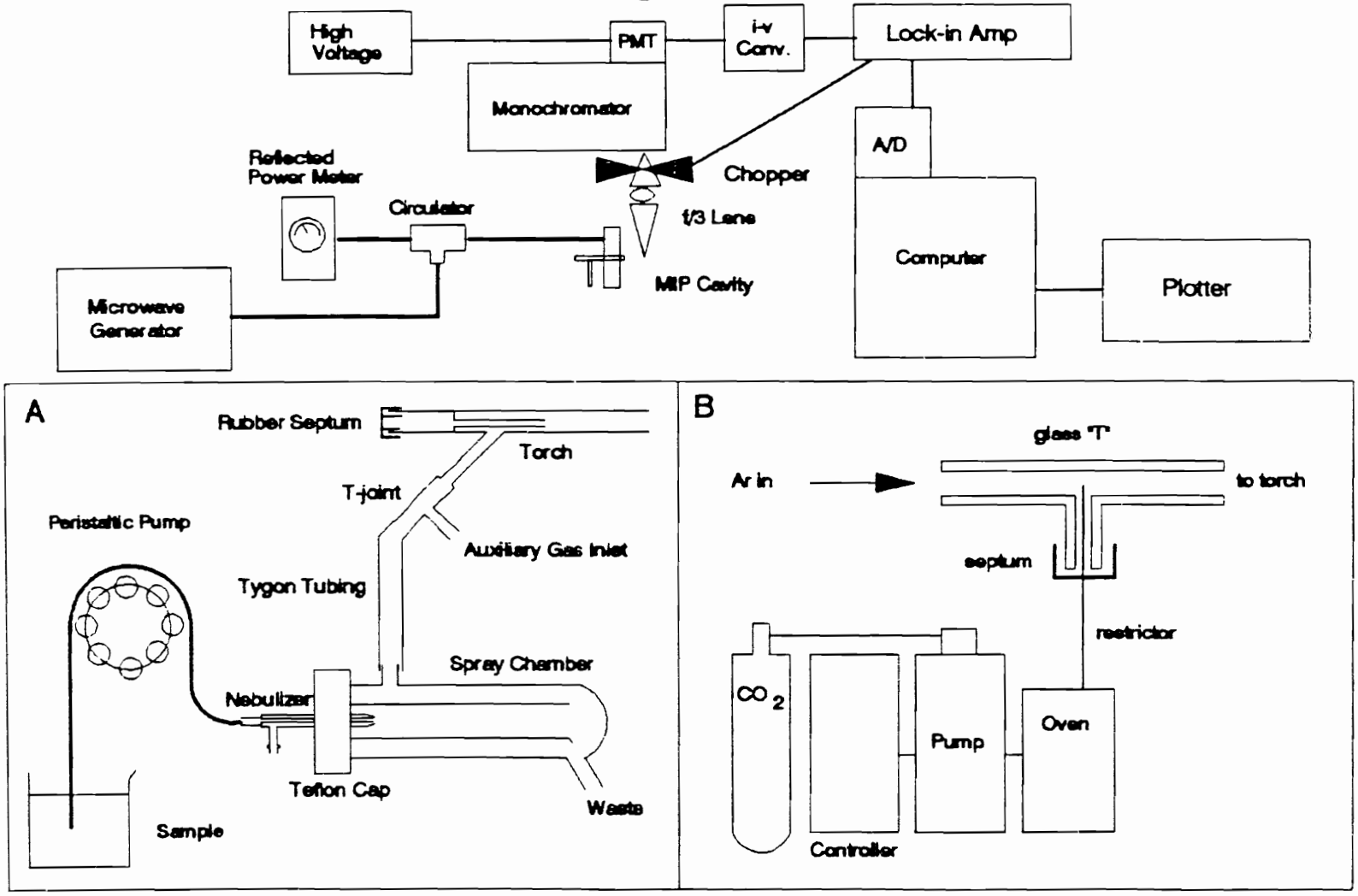

Figure 3. Sample Introduction Apparatus

coupled MIP-AES. Table 2 lists the optimized operating conditions used in this study.

Flow Pattern Measurements. To determine if there was a difference in flow dynamics of the two torches, flow pattern measurements were made. Using a hydrodynamic flow method first proposed by Hieftje [10] water was introduced into the plasma torch to observe the path that the support gas would take. The rate of water, in L/min, was recorded at the onset of helical flow (least operable flow) and at the point of disruption of the helix (maximum flow rate).

Limits of Detection. For aqueous sample introduction, the limit of detection (c_L) is reported as described in Chapter 2. For SFC coupled MIP-AES the limit of detection was determined using the method employed by Foley and Dorsey [11]. For this method the standard deviation of the background was measured as 0.2 times the peak to peak noise. A four point calibration curve was constructed with the peak heights of three iron injections and the null point. This c_L was also measured using k=2.

RESULTS AND DISCUSSION

Operating Characteristics. The two torches were capable of stable centered plasmas under identical conditions. There was no visible difference in the appearance of the plasma discharge. It was observed that both discharge tubes operated optimally under the same set

of equipment settings. The demountable torch was observed to be somewhat more amenable to SFC-MIP-AES in that there was less difficulty in maintaining a stable plasma with the introduction of the CO_2 effluent. With CO_2 entering the plasma at 72 mL/min, the demountable torch maintained a stable plasma for longer periods of time. With aqueous sample introduction, the long-term stability of the discharge was not observed to be different. One drawback of the demountable design was observed: the washout time for an aqueous sample introduced into this torch was increased by approximately 15% over the quartz torch. This was found not to be the case for gaseous (SFC) samples however.

Electron Number Density. The n_e- was measured for both plasma torches under optimum operating conditions. The calculated n_e- for the quartz torch was 1.3×10^{15} electrons / cm^3. The demountable torch also elicited a n_e- of 1.3×10^{15} electrons / cm^3. Any difference between the two torches is well within experimental error limits. The number densities observed here compare well to previous measurements with this system, and indicate that the discharge is quite energetic.

Temperature Measurements. T_{exc} for the two torches were measure to be 4850K for the quartz torch and 4870K for the demountable. It should be noted that the T_{exc} measurement is accurate to the nearest 2-3%. Ionization temperatures were also measured. T_{ion} values for the quartz

torch were measured to be 4950K (Ca) and 5870K (Mg). The demountable torch yielded T_{ion} values of 4990K and 5760K for Ca and Mg respectively. Again, any differences between the measured values are within experimental error. It is interesting to note the difference between the Ca and Mg ionization temperatures. The difference between the T_{ion} values for the same torch with different elements is an indication that the discharge in not under Local Thermodynamic Equilibrium (LTE) conditions.

Emission Profiles. The emission profiles for the two torches are presented in Figures 4 (Mg) and 5 (Ca). It is of interest to note that although the profiles both show maximum emission at 3 mm above the face of the cavity, that the maximum relative intensities are indeed different. This is indicative of a slight loss in sensitivity with the demountable torch. Generally, such a loss in sensitivity occurs along with either a loss in analyte or a shift in the sample's aerosol size. If this had happened, it would be expected that the emission maxima be shifted to one side of that of the quartz torch. This did not occur, and the direct cause of the sensitivity loss is unknown.

Flow Pattern Measurements. The quartz and demountable discharge tubes were tested for the existence of a helical flow path using the hydrodynamic method [10]. Both torches show similar helical flows under the normal gas flow region of 0.5 L/min to 2.0 L/min. However, the demountable torch

Figure 4

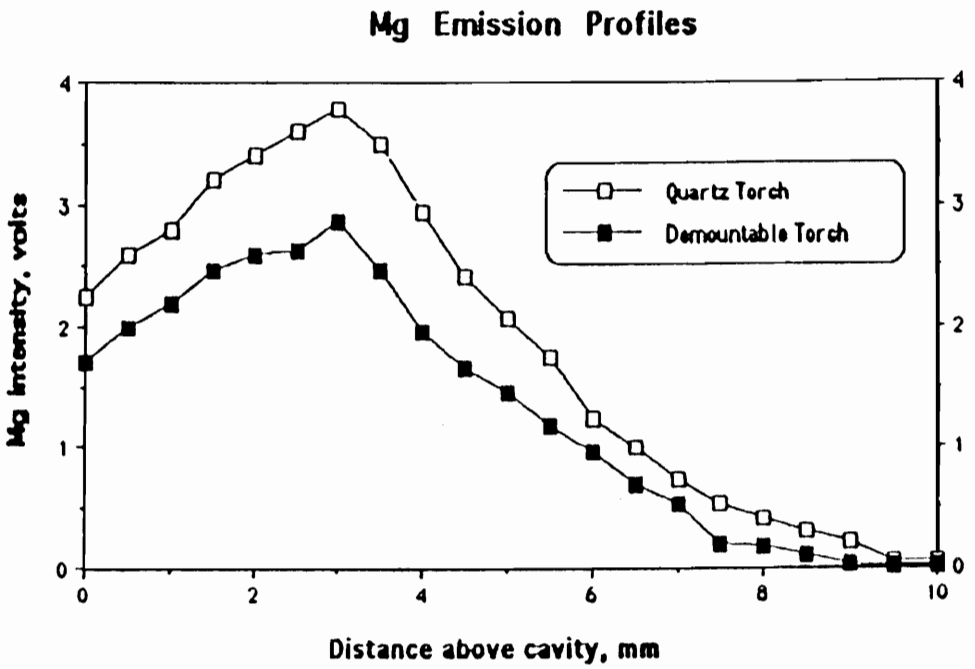

Figure 4. Emission Profiles for Mg.

Figure 5

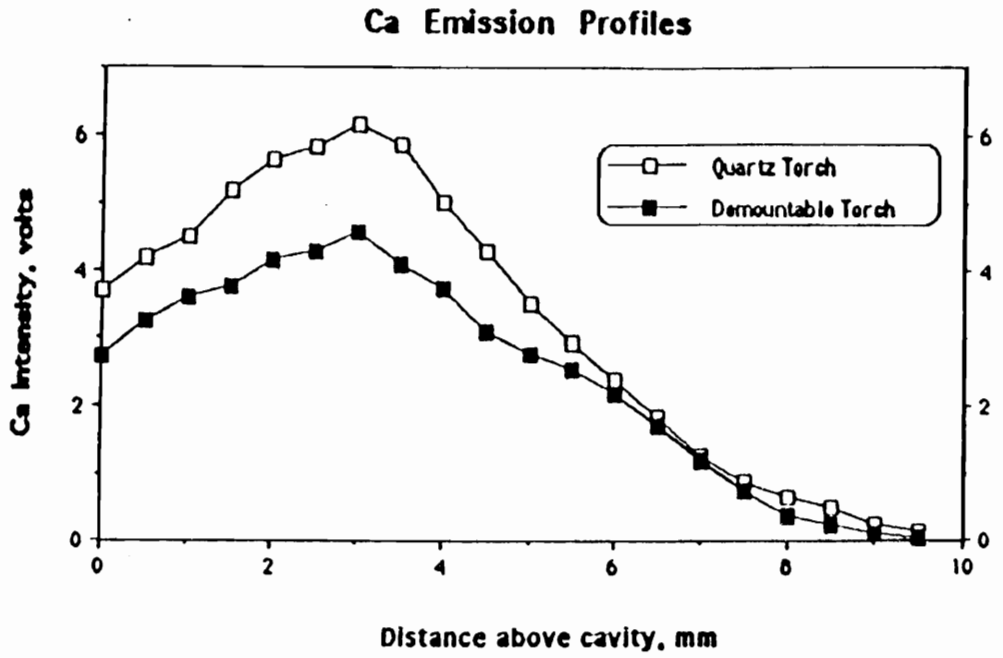

Figure 5. Emission Profiles for Ca.

showed a wider range on both sides of this region, maintaining a helical flow at a low of 0.39 L/min and continuing at flows greater than 5 L/min. The quartz torch first generated a helical flow at 0.48 L/min and continued only up to 2.2 L/min.

Limits of Detection. The limits of detection determined in this study are presented in Table 3. Overall, the c_L values are lower for the quartz torch. However, except for the case of Mg(II), these differences are insignificant. It may be possible to explain the differences in c_L if the calibration curves are examined, as well as the profiles.

The profiles showed a decrease in the maximum emission intensity for the demountable torch. The calibration curves show a similar trend. Although all of the working curves are linear to a minimum correlation factor of 0.999, the slopes of the curves, and hence the analytical sensitivity is decreased.

If the sensitivity difference were the only change occurring, the difference in the c_L values would be greater than what is listed. There is also a change in the standard deviation of the background. This decrease in s_B for the demountable torch compensates for the decrease in analytical sensitivity, causing the c_L values to be similar.

The nature of this difference is proposed to be due to an impaction effect that occurs at the point where the gas

mixtrue enters the flow director. As this is a flat surface some loss of analyte will occur. This is supported by the fact that for aqueous introduction the decrease in emission is worse than that for gaseous (SFC) introduction. Further designs will try to minimize this effect.

At this juncture, the point that needs to be stressed is that there is no significant difference in the c_L values and that these values show good overall sensitivity. The c_L values reported here compare well to previously reported measurements using this system.

CONCLUSIONS

The suitability of a newly designed demountable torch for MIP-AES and SFC-MIP-AES has been demonstrated. Diagnostic comparisons as well as analytical sensitivity measurements show no statistical difference between the two designs. The demountable design has the added benefits of: intrinsically greater reproducibility due to a fixed gas flow system; much greater flexibility as the section in which the plasma resides can be readily modified with respect to length or inner diameter; and greater ease of use in that damaged or broken discharge tube ends can be rapidly replaced, without the need for expensive glassblowing. The new torch also shows an improved long-term stability when used with SFC coupled MIP-AES. This factor becomes critical during prolonged chromatographic separations.

There is a need for further study to be done with this design to test its utility with a He plasma. Also, a question remains regarding the decreased slope of the working curves as compared to the all quartz torch.

References

1. B. D. Quimby and J. J. Sullivan, Anal. Chem., **62**, 1027 (1990).

2. J. J. Sullivan and B. D. Quimby, Anal. Chem., **62**, 1034 (1990).

3. K. A. Forbes, E. E. Reszke, P. C. Uden, and R. M. Barnes, J. Anal. Atom. Spec., **6**, 57 (1991).

4. C. I. M. Beenakker, Spectrochim. Acta., **32B**, 173 (1977).

5. M. L. Bruce, J. M. Workman, J. A. Caruso, and D. J. Lahti, Appl. Spectrosc., **39**, 935 (1985).

6. S. R. Goode, B. Chambers, and N. P. Buddin, Spectrochim. Acta., **40B**, 329 (1985).

7. T. Nakahara, K. Kawakami, and T. Wasa, Chem. Express, **4**, 73 (1989).

8. R. D. Deutsch and G. M. Hieftje, Appl. Specrosc., **39**, 214 (1985).

9. L. D. Perkins, unpublished results.

10. E. Sexton, R. N. Savage, and G.M. Hieftje, Appl. Spectrosc., **33**, 643 (1979).

11. J. P. Foley and J. G. Dorsey, Chromatographia, **18**, 503 (1984).

Appendix 2

Cryogenic Desolvation

The use of cryogenic desolvation for sample introduction into a plasma atomic emission system was first employed by Wiederin, Houk, Winge, and D'Silva in 1990 [1]. In this work, a 10mm i.d. tube, formed into a double loop was packed in dry ice and employed as the cryocondensing chamber. This chamber, when used as a secondary condenser in an ultrasonic nebulization system, allowed the researchers to introduce organic solvents into an ICP with the common problems of plasma instability, cooling and spectral interferences reduced or eliminated. Ultrasonic nebulization without this system was not possible as the plasma would not stay ignited for any period of time.

Several solvents were tested and improvements were realized in all cases. Spectral interferences were reduced by as much as 25 fold. Aqueous detection limits that were obtained were comparable with others reported for the same system without cryogenic desolvation. Unfortunately, there were no reports of the degree of desolvation or the decrease in solvent load.

From this report, it seemed as if this system may be useful as a desolvation unit for pneumatic nebulization and the microwave induced plasma. It would also be useful as another system in which solvent loading studies could be

made. A desolvation chamber similar to the one reported was constructed. This condenser was set up as a secondary condenser for a desolvated pneumatic system. See Chapter 2 for a description of this apparatus.

Tests showed that this system did remove solvent from the support gas / analyte stream. However, this system only worked for a short period of time until the loops became plugged, causing a back pressure of gas throughout the system and extinguishing the plasma. This system would not work for a long enough period of time to be useful.

Several other designs were constructed which would accommodate a larger amount of solvent to condense without the system plugging. Further testing resulted in a final design being chosen. This design is described in Chapter 2. This system then was connected and tests commenced to determine the extent to which solvent would be removed from the system.

Initial tests were run to determine the effect of the secondary condensing chamber on the excitation characteristics of the microwave plasma. A series of scans of the H-beta line were made from the point of immersion of the chamber into a cryogenic bath (a dry ice acetone mixture which resulted in a temperature of -55 degrees C) to equilibration. The peak heights and areas of the H line leveled to a point of lowest S/N. Electron number densities calculated from this data show an increase from 1.4×10^{15}

electrons/cm^3 to 2.6 x 10^{15}. It was obvious that the solvent was being removed from two observations: the peak heights and areas of the H emission were decreasing due to the removal of water (the only H source in the system), and that the number densities were increasing, showing the increased energy of the plasma due to the solvent reduction.

At this point enough promising results had been obtained to pursue this matter further. The determination of the extent of solvent removal was performed. By aspirating a known amount of solvent through the system and then gravimetrically determining that solvent which was collected in the various waste traps, a measure of the solvent that escaped the system (i.e. reached the plasma discharge) could be calculated. This measure of the total solvent removal efficiency was performed for several solvents.

The results of these experiments are listed in Table I. The system efficiency refers to the percentage of solvent that did not reach the plasma discharge due to the whole sample introduction system. The desolvation efficiency refers to that amount of solvent which was trapped in the cryogenic chamber. Also listed for each solvent are the boiling point, freezing point, and vapor pressure of each solvent. An attempt was made to elucidate a relationship between those parameters and the desolvation efficiency, but no clear correlation seemed to exist.

A experiment was conducted to determine to what extent the analyte was affected by this cryogenic system. A series of collected waste fractions of a multi-element standard were subjected to ICP analysis by an available outside laboratory. The results are an average of 15 elements in the standard. For aqueous samples, the desolvation system resulted in a decrease of 68% of the solvent past the spray chamber, and a 43% reduction in analyte over a non desolvated case. The analyte reduction appears significantly detrimental until taking the solvent decrease into account. Overall, there is a higher analyte to solvent ratio that reaches the plasma in the cryogenic case as opposed to the nondesolvated case. A similar experiment was run for the xylenes case, resulting in a 28% reduction in analyte and a 57% reduction in solvent. For xylene samples it seems that the cryogenic desolvation is even more beneficial.

To put this system to a practical analytical test, the cryogenic desolvation system was employed in an existing ICP analysis for metals in gasoline samples. Due to the volatility of gasoline, samples previously run on this system had to be diluted by a factor of 200 with xylenes to decrease the volatility sufficiently so that the ICP would stay ignited throughout the experiment. This, as a matter of sample preparation, precluded the analysis of trace materials in gasoline.

The existing cryogenic desolvation system was connected to the sample introduction setup on the ICP. No other desolvation apparatus was employed as concern was expressed regarding passing gasoline through a heated chamber. The ICP required gas flow adjustments to ignite a stable plasma. After ignition, xylene samples were run as a preliminary test. Limits of detection were only slightly improved, on the order of 25-30% decrease.

Neat gasoline was introduced into the ICP via the sample introduction system and the plasma promptly extinguished. With more gas flow adjustments, a stable plasma was ignited with gasoline introduction. New standards had to be prepared as the standards for the previous experiments were xylene based. A gasoline based standard was procured and run.

The limits of detection improved over the xylene dilution case by a factor of 50. This was a major success, although somewhat less than expected. It was assumed that the entire 200 fold improvement would be realized. However, once the reduction in sample due to the cryogenic desolvation trap was taken into consideration, this improvement was more realistic.

Further studies need to be conducted with the cryogenic desolvation apparatus. More solvent and analyte studies need to run to more accurately determine the extent to which normal analyses can be improved. This method may possibly

lend itself to favorable usage as an interface between plasma emission spectrometry and liquid chromatography. It shows much promise towards this end already, as it is a useful solvent removal system for a variety of organic solvents, even in high capacity loads.

Reference

1. D. R. Wiederin, R. S. Houk, R. K. Winge, and A. P. D'Silva, Anal. Chem., **62**, 1155 (1990).

Appendix 3

Summary of Water Loading Data

In order to further explain the effect of water loading on the microwave plasma, this appendix summarizes the data obtained from previous measurements and provides further calculations to support this data.

Water Loading Data

Optimum Aerosol load, Ar (mg/L)	11.8
Optimum Vapor load, Ar (mg/L)	4.4
Flow Rate, Ar (L/min)	1.5
Optimum Aerosol load, Ar (mg/min)	17.7
Optimum Vapor load, Ar (mg/min)	6.6
Plasma Length, Ar (cm)	3.8
Plasma Volume, Ar (cm^3)	1.2
Approximate Residence Time, Ar (sec)	0.048
Optimum Aerosol load, He (mg/L)	3.7
Optimum Vapor load, He (mg/L)	8.7
Flow Rate, He (L/min)	3.0
Optimum Aerosol load, He (mg/min)	11.1
Optimum Vapor load, He (mg/min)	26.1
Plasma Length, He (cm)	2.2
Plasma Volume, He (cm^3)	0.7
Approximate Residence Time, He (sec)	0.014

After examination of the data presented above, several observations can be made. Overall, it is shown that for He, there are several factors that work to the detriment of the

He plasma. There is four time greater the amount of vapor loading on the He plasma. Combined with a 42 % decrease in plasma volume and a 3.4 times decrease in residence time in the plasma, it can be understood why there is a severe decrease in limit of detection with He.

VITA

Keith Alan McCleary

Born:	July 13, 1966 Detroit, MI
High School	Ferndale High School Ferndale, MI Diploma, June 1984
Undergraduate Education	Michigan Technological University Houghton, MI Bachelor of Science, Chemistry, May 1988
Graduate Education	Virginia Polytechnic Institute and State University Blacksburg, VA Doctor of Philosophy, Chemistry, July 1992
Dissertation:	Sample Introduction and Solvent Effects in an Ar and He Microwave Induced Plasma Advisor: Dr. G. L. Long
Professional Societies	Society for Applied Spectroscopy American Chemical Society
Awards	Graduate Research Development Grant January 1990, VPI-SU
Present Employer	Du Pont Chemicals Jackson Laboratory Chambers Works Deepwater, NJ 08023

Publications

L. D. Perkins, C. B. Motley, K. A. McCleary and G. L. Long, "A Helium High Efficiency Microwave Induced Plasma for the Atomic Spectrometric Determination of Metals and Nonmetals", Virginia Water Resources Research Center Bulletin 168, February 1991.

K. A. McCleary and B. D. Quimby, "An Improved Method for the Determination of Additive-Level Oxygenates in Gasoline by Gas Chromatography-Atomic Emission Detection", submitted to HRC and CC.

K. A. McCleary and G. L. Long, "Effect of Solvent Vapor Loading on a Low Power Microwave Induced Plasma", submitted to Applied Spectroscopy.

K. A. McCleary, G. D. Ducatte, D. H. Renfro, and G. L. Long, "Evaluation of a Demountable Tangential Flow Torch for the Microwave Induced Plasma", in preparation for submission to Applied Spectroscopy.

K. A. McCleary and G. L. Long, "Sample Introduction with an Ultrasonic Nebulizer for MIP-AES using Ar and He", in preparation for submission to Applied Spectroscopy.

Presentations

K. A. McCleary and G. L. Long, "Studies of Solvent Introduction into Ar and He HEMIPs", presented at the Pittsburgh Conference on Analytical Chemistry and Applied Spectroscopy, March 1990, New York NY, paper #757.

K. A. McCleary, D. W. Hausler, G. L. Long and J. J. Sullivan, "Diagnostic Studies of a Helium Plasma Atomic Emission Detector for Gas Chromatography", presented at the 18th annual meeting of the Federation of Analytical Chemistry and Spectroscopy Societies (FACSS), October 1991, Anaheim CA.

G. L. Long and K. A. McCleary, "Influence of Water on an Ar MIP", presented at the 18th annual meeting of the Federation of Analytical Chemistry and Spectroscopy Societies (FACSS), October 1991, Anaheim CA.

K. A. McCleary and G. L. Long, "A Comparison of Desolvated Nebulization Methods and MIP Performance", presented at the Pittsburgh Conference on Analytical Chemistry and Applied Spectroscopy, March 1992, New Orleans LA, paper #92.

B. D. Quimby, V. Giarocco, J. J. Sullivan, and K. A. McCleary, "Fast Analysis of Oxygen and Sulfur Compounds in Gasoline by GC/AED", presented at the Fourteenth International Symposium on Capillary Chromatography, May 1992, Baltimore MD, poster L-8.